FGH75334

CI-06229975-6

CISTI ICIST

Document Delivery Service in partnership with the **Canadian Agriculture Library**

Service de fourniture de documents en collaboration avec la **Bibliothèque canadienne de l'agriculture**

Phone/Téléphone: 1-800-668-1222 (Canada - U.S.) (613) 993-9251 (International)
Fax/Télécopieur: (613) 993-7619 www.nrc.ca/cisti cisti.producthelp@nrc.ca

THIS IS NOT AN INVOICE / CECI N'EST PAS UNE FACTURE

SWETSCAN
MCGILL UNIVERSITY
DEPT OF MECHANICAL ENGINEERING
817 SHERBROOKE ST W
MONTREAL, QC H3A 2K6
CANADA

REQUEST NUMBER:	CI-06229975-6
Account Number:	FGH75334
Phone Number:	514/398-4767
Delivery Mode:	FTP
Delivery Address:	132.206.27.11
Reply Via:	F31
Reply Address:	514/398-7365
Submitted:	2006/05/24 10:50:42
Shipped:	2006/06/05 14:42:40
Service Level:	Link
Document Type:	Book
Mode Sent:	WWWSWET

Publication:	LANDOLT BORNSTEIN NUMERICAL DATA AN
Author(s):	B. PREDEL
Vol./Issue:	VOL.5 SUBVOL.E
Pages:	153-290
Article Title:	**PHASE EQUILIBRIA, CRYSTALLOGRAPHIC AND THERMODYNAMIC DATA OF BINARY ALLOYS - SUBVOLUME E - FE-X BINARY SYSTEMS**
Publisher:	SPRINGLER-VERLAG BERLIN AND HEIDELBERG GMBH & CO.K;
Publication Year:	1995
Series Title:	
Vol:	
ISBN:	3540584285
Source of Info:	
Note; Special Instructions:	MAMOUN; 75 Preset limit. Do not contact client.; ** Loans not allowed for this account **

29 Fe–X binary systems

Fe–Ga (Iron–Gallium)

Phase diagram

The phase equilibria have been investigated rather often and by different methods. Experimental work has been done by Dasarathy et al. [65 Das1], Meissner et al. [65 Mei1] (thermal analysis, X-ray diffractography), Lu et al. [66 Lu1] (X-ray diffractography), Wachtel et al. [67 Wac1, 67 Wac2] (thermomagnetic analysis), Couderc et al. [77 Cou1] (X-ray diffractography), Bras et al. [77 Bra1] (X-ray diffractography, differential thermal analysis), Köster et al. [77 Kös1, 77 Kös2] (differential thermal analysis, dilatometry, metallography), Tiemann et al. [78 Tie1] (Mössbauer spectroscopy), Köster et al. [78 Kös1] (dilatometry), Gödecke et al. [77 Göd1] (differential thermal analysis, dilatometry). In some cases the results are not in good agreement with each other. Reviews on the constitution of this system have been given by Kubaschewski [82 Kub1], Okamoto [90 Oka3] and Bannykh et al. [86 Ban1].

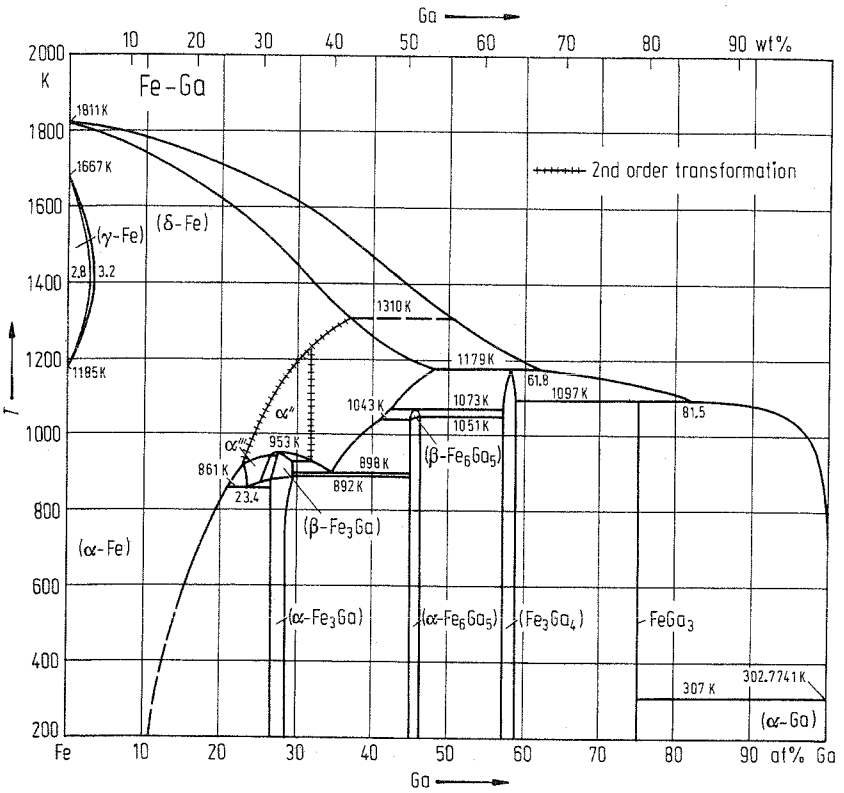

Fig. 1. Fe–Ga. Phase diagram.

Taking all information available from the literature, after thorough discussion Okamoto [90 Oka3] has proposed an assessed phase diagram, which was the basis for Fig. 1. Mainly accepted have been results published by Köster et al. [77 Kös2] (see also Kubaschewski [82 Kub1] and Bannykh et al. [86 Ban1]). Phase equilibria in the concentration range between about 20 and 30 at% Ga are given on enlarged scale in Fig. 2 (taken from [82 Kub1], see Köster et al. [77 Kös1, 77 Kös2]).

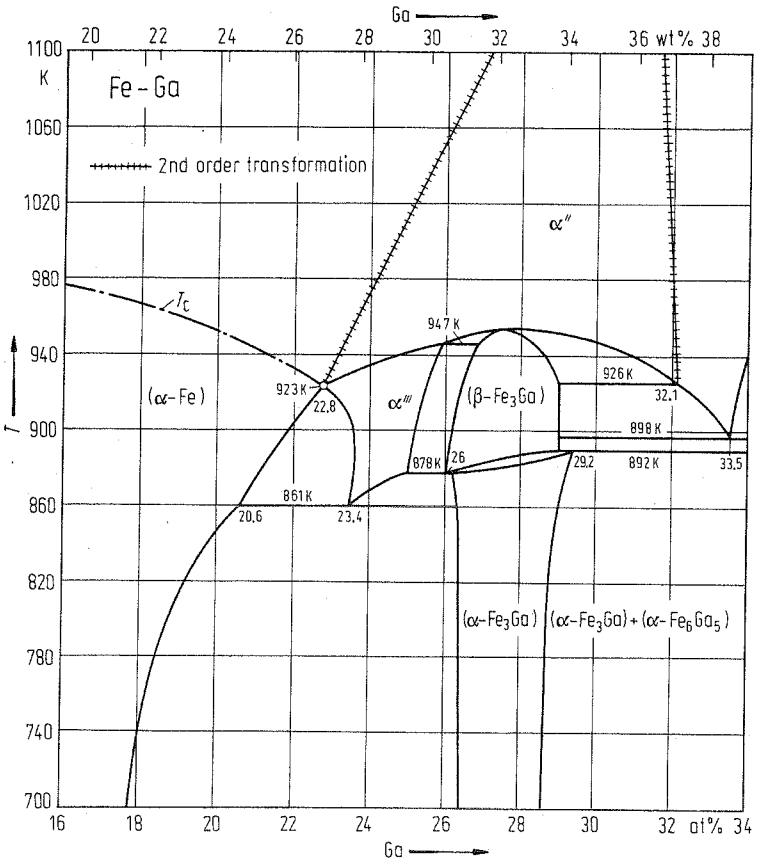

Fig. 2. Fe–Ga. Partial phase diagram (16...34 at% Ga).

Crystal structure

Crystallographic data of intermediate phases are collected in Table 1.

Dasarathy et al. [65 Das1] as well as Lu et al. [66 Lu1] have determined lattice parameters of (α-Fe) solid solutions (bcc structure). The mean of their results is plotted in Fig. 3. The lattice parameter as a function of concentration of cubic α''' ($AuCu_3$-type) is plotted in Fig. 4 (mean of results from [72 Kaw1] and [67 Luo1]).

By rapid quenching in the concentration range between 10 and 50 at% Ga metastable phases are formed. For corresponding transformations and structures (not quite well investigated) see Okamoto [90 Oka3].

Table 1. Fe–Ga. Crystal structure and lattice parameters of intermediate phases.

Phase	Structure	Type	a [nm]	b [nm]	c [nm]	Ref.
α'	cub	CsCl	see Fig. 2			67 Luo1
α''	cub					77 Kös1
α'''	cub	Cu_3Au	see Fig. 3			67 Luo1
α-Fe_3Ga	cub	Cu_3Au	0.3701			60 Sch1, 71 Cou1, 84 Suz1
β-Fe_3Ga	hex	Ni_3Sn	0.52184		0.42373	71 Cou1, 77 Cou1
α-Fe_6Ga_5	mon	Fe_6Ge_5	1.0058	0.7946 $\beta = 109.33°$	0.7477	74 Mal1, 74 Phi1
β-Fe_6Ga_5	hex	Al_8Cr_5	1.241		0.776	65 Mei1
Fe_3Ga	mon	Fe_3Ga_4	1.0091	0.7666 $\beta = 106.67°$	0.7866	74 Phi1, 75 Phi1, 65 Mei1
Fe_3Ga	tetr		0.1260		0.551	65 Das1
$FeGa_3$	tetr	$CoCa_3$	0.6260		0.6580	58 Sch1, 59 Sch1, 65 Das1, 65 Lu2
$FeGa_3$	tetr	$FeGa_3$	0.6256		0.6560	86 Kra1, 65 Lu1

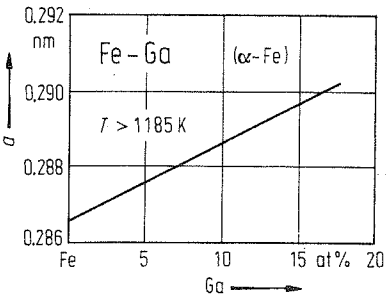

Fig. 3. Fe–Ga. Lattice parameter for bcc (α-Fe) solid solution at $T > 1185$ K.

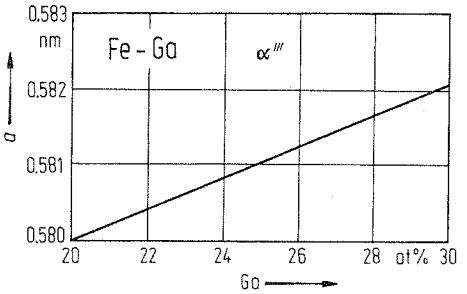

Fig. 4. Fe–Ga. Lattice parameter for cubic (Cu_3Au-type) solid solution α'''.

Thermodynamics

Predel et al. [75 Pre1] have determined calorimetrically the enthalpies of formation of two intermediate phases. They found for Fe_3Ga_4 the value of $\Delta H^S = 9.6$ kJ g-atom^{-1}, and for $FeGa_3$ the value $\Delta H^S = 11.7$ kJ g-atom^{-1}.

Fe–Gd (Iron–Gadolinium)

Phase diagram

Experimental determinations of the phase equilibria have been done by Copeland et al. [62 Cop1, 62 Cop2], Savitskii et al. [60 Sav1, 61 Sav1], Novy et al. [61 Nov1], Vickery et al. [60 Vic1], Kripyakevich et al. [61 Kri1], Baenziger et al. [61 Bae2], Hubbard et al. [62 Hub1], and Burov et al. [64 Bur1]. A review of this system and an assessed phase diagram have been given by Kubaschewski [82 Kub1] and, later on, by Okamoto [93 Oka1]. The phase diagram assessed by Kubaschewski [82 Kub1], based mainly on results published by Copeland et al. [62 Cop1, 62 Cop2] (thermal analysis, metallography, X-ray diffractography), was taken by Okamoto [93 Oka1] to construct a diagram assessed in more detail. This latter diagram was taken to draw Fig. 1.

The maximum solubility of Fe in (α-Gd) was stated by Copeland et al. [64 Cop1] to be 0.6 at% Fe.

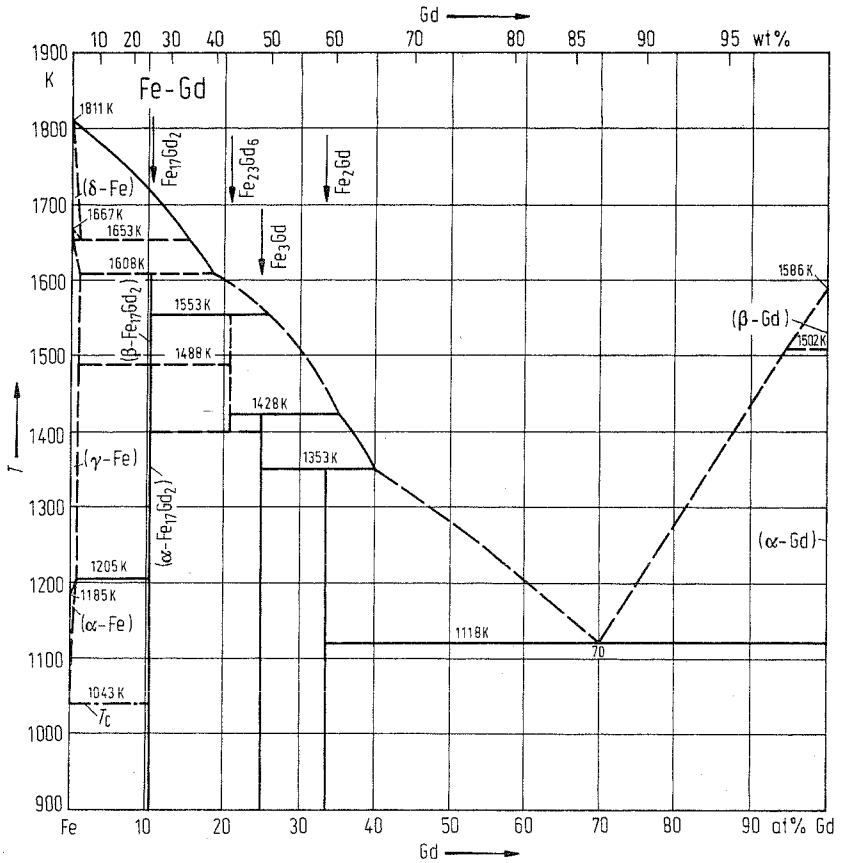

Fig. 1. Fe–Gd. Phase diagram.

Crystal structure

Crystallographic data of intermediate phases are listed in Table 1.

More intermediate phases have been found than those given in Fig. 1. These types of phases are not occurring in other Fe–rare-earth systems and therefore their existence is questionable.

Amorphous alloys have been prepared by melt quenching (Tokumitsu [91 Tok1]) in the concentration range between 16 and 70 at% Gd. The crystallization process has been investigated by X-ray diffraction method and by Mössbauer spectroscopy.

Table 1. Fe–Gd. Crystal structure and lattice parameters of intermediate phases.

Phase	Structure	Type	a [nm]	b [nm]	c [nm]	Ref.
α-$Fe_{17}Gd_2$	hex	Cu_7Tb	0.4907		0.4168	70 Giv1
β-$Fe_{17}Gd_2$	hex	$Ni_{17}Th_2$	0.8496		0.8345	70 Giv1, 61 Nov1, 63 Kri1, 66 Bus2
$Fe_{23}Gd_6$	cub	$Mn_{23}Th_6$	1.212			86 Nag1, 65 Kri2
Fe_3Gd	hex	Be_3Nb	0.51692		2.4737	65 Smi1, 85 Sei1, 66 van1
Fe_2Gd	cub	$MgCu_2$	0.7380			71 Sla1, 76 Grö1, 87 Ich1, 64 Man1
Questionable phases						
Fe_5Gd	hex	$CaCu_5$	0.492		0.411	61 Nov1, 60 Nas1
Fe_4Gd	hex		0.515		0.664	61 Nov1
Fe_7Gd_2	orth		0.571	0.678	0.715	61 Nov1
Fe_3Gd_2	cub		0.825			61 Nov1

Thermodynamics

By solution calorimetry using liquid Al as the solvent, Collinet et al. [87 Col1] have determined the enthalpies of formation of some intermediate phases. The results are given in Table 2.

Table 2. Fe–Gd. Enthalpy of formation of intermediate phases at 298 K (Collinet et al. [87 Col1]).

Phase	ΔH^S [kJ g-atom^{-1}]
$Fe_{17}Gd_2$	− 2.3
Fe_3Gd	− 9.3
Fe_2Gd	− 11.6

Fe–Ge (Iron–Germanium)

Phase diagram

First experimental work to disclose the phase equilibria in this system has been done by Ruttevit et al. [40 Rut1] using thermal analysis and metallographic observations. Later on, investigations were done by Übelacker et al. [67 Übe1] (thermal analysis, magnetic investigations) and some others (Lecoqc [63 Lec1], Chessin [63 Che1], Predel et al. [72 Pre1] (metallography), Richardson [67 Ric1], Kanematu et al. [65 Kan2], Maier et al. [72 Mai1] (thermal and magnetic analysis), Shtolts et al. [64 Sht1] (thermal analysis), Nunoue et al. [89 Nun1] (mass spectrometry) and others. Reviews of this system were given by Kubaschewski [82 Kub1] and Kato et al. [93 Kat1]. The phase diagrams of the Fe–Ge system given by these reviewers do not agree with each other in detail. The assessed diagram published by Kato et al. [93 Kat1] was preferred for it includes more recent information. It was taken as a basis for the phase diagram in Fig. 1.

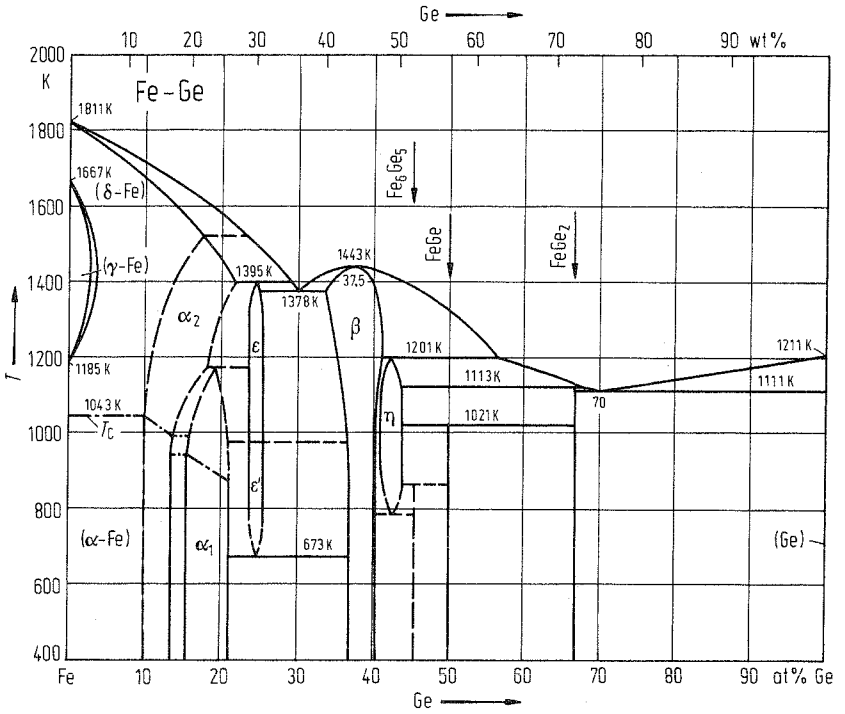

Fig. 1. Fe–Ge. Phase diagram.

Crystal structure

Lattice parameters of the (α-Fe) solid solutions are plotted in Fig. 2 (taken from Turbil et al. [73 Tur1]). Lattice parameters of the α_2-phase are given in Fig. 3 (taken from Buschow et al. [83 Bus2]). The transition (α-Fe) $\rightarrow \alpha_2$, $\alpha_2 \rightarrow \alpha_1$ is not a first-order reaction.

Crystallographic data of intermediate phases are listed in Table 1.

Amorphous alloys have been prepared by vacuum deposition on NaCl in the concentration range between 50 at% Ge and 95 at% Ge (Bilyak et al. [75 Bil1]). By electron diffraction these authors found that a mixture exists of short-range ordered regions and really amorphous ones.

Table 1. Fe–Ge. Crystal structure and lattice parameters of intermediate phases.

Phase	Structure	Type	a [nm]	b [nm]	c [nm]	Ref.
α_1	cub	BiF_3	0.575			87 Eno1, 75 Sob1
ε	hex	Ni_3Sn	0.5169		0.4222	61 Sht1, 67 Kan1, 69 Tur1, 65 Kan2
ε'	cub	Cu_3Au	0.3665			65 Kan2, 63 Kan3
Fe_2Ge	hex	$InNi_2$	0.4056		0.5030	80 Mal1, 89 Kim1
β (Fe_3Ge_2)	hex	$Pd_{13}Tl_9$	0.796		0.499	68 Sch1, 69 Pan1, 65 Kan3
β (Fe_5Ge_3)	hex	$InNi_2$	0.4020		0.5024	81 Bar1, 53 Cas1, 63 Kan2
η	hex	NiAs	0.3998		0.5010	80 Mal1, 41 Lav1
Fe_6Ge_5	mon	Fe_6Ge_5	0.9965	0.7826 $\beta = 109.67°$	0.7801	74 Mal1
FeGe	mon	CoGe	1.1815	0.39283 $\beta = 103.91°$	0.49224	67 Ric2, 83 Fel1
FeGe (903...1013K)	hex	CoSn	0.50027		0.40548	67 Ric1, 65 Ade1, 65 Kan2
FeGe (<903 K)	cub	FeSi	0.4698			67 Ric1, 89 Leb1, 83 Sat1
$FeGe_2$	tetr	Al_2Cu	0.5908		0.4957	72 Hav1, 64 Kre1

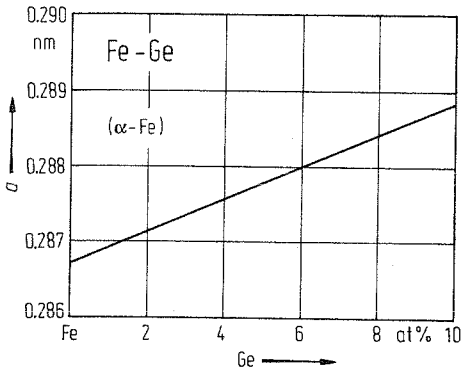

Fig. 2. Fe–Ge. Lattice parameter for bcc (α-Fe) solid solutions.

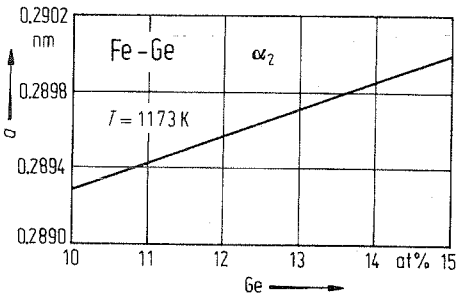

Fig. 3. Fe–Ge. Lattice parameter for cubic (CsCl-type) phase α_2 at 1173 K.

Thermodynamics

By high-temperature calorimetry Shalpak et al. [80 Sha1] have determined the enthalpies of mixing of liquid Fe–Ge alloys. The results are given in Fig. 4.

Excess free enthalpies of mixing of liquid Fe–Ge alloys were calculated by Frohberg et al. [85 Fro1] from hydrogen solubilities in Fe–Ge melts. The $\Delta G^{L,ex}$ values as a function of concentration are given in Fig. 5.

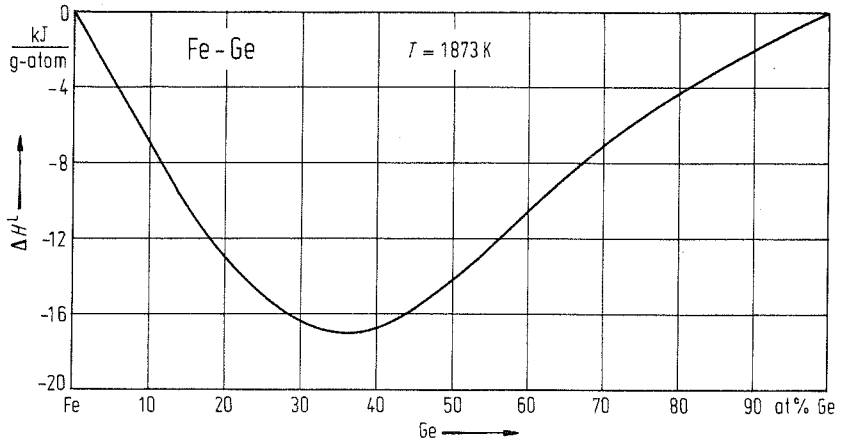

Fig. 4. Fe–Ge. Enthalpy of mixing for liquid alloys at 1873 K.

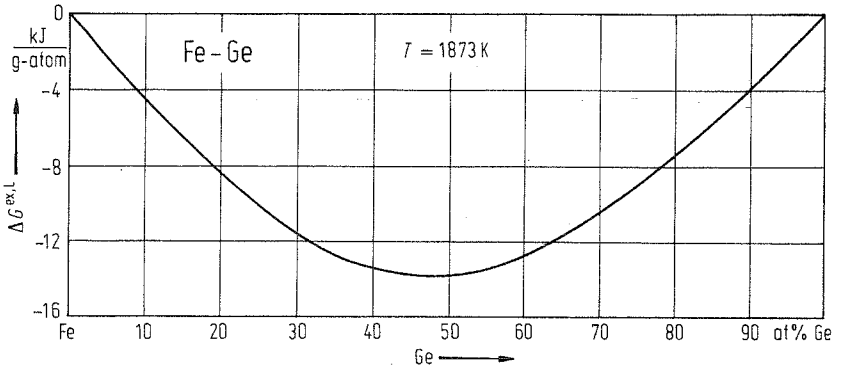

Fig. 5. Fe–Ge. Excess Gibbs free energy of mixing for liquid alloys at 1873 K.

Fe–H (Iron–Hydrogen)

Solubility of hydrogen in iron at normal pressure

Hydrogen, deuterium and tritium are forming interstitial solid solutions with solid Fe. The solubility of H in Fe has been determined at fist by Sieverts [11 Sie1], Martin [29 Mar1] and Luckemeyer-Hasse et al. [32 Luc1]. Later on, solubility measurements have been performed several times (see reviews given by Kubaschewski [82 Kub1] and San-Martin et al. [93 San1]). Up to ≈ 10 MPa the solubility Σ obeys Sieverts' law

$$\Sigma = k\sqrt{p_{H_2}}$$

Assessed results of solubility of H in solid iron at ≈ 0.1 MPa are plotted in Fig. 1 and those for the solubility of H in liquid Fe are given in Fig. 2 (see Kubaschewski [82 Kub1]).

Sieverts et al. [38 Sie1] as well as Heumann et al. [66 Heu1] have determined the solubility of deuterium in α-Fe and γ-Fe. Both series of results are in good agreement, whereas the solubilities of D

in γ-Fe calculated by Demin et al. [72 Dem1] are lower than the experimentally determined ones. The assessed solubilities of D in solid Fe are plotted in Fig. 3 (see Kubaschewski [82 Kub1]).

Solubility of tritium in solid Fe has been calculated by theoretical considerations (Demin et al. [72 Dem1]). This method applied also to the iron–deuterium system by the same authors has yielded lower values for the solubility of D in Fe than experimental methods (see above). The difference between experimental and calculated values for the Fe–D system has been taken by Kubaschewski [82 Kub1] to adjust the calculated solubilities of T in Fe to real ones, and these corrected data are plotted in Fig. 3, too.

The influence of H on the temperature of phase transition of Fe at $p = 0.1$ MPa is very small. Geller et al. [50 Gel1] and Bunin et al. [77 Bun1] found a depression of the melting point of Fe by solution of H of the order of magnitude of 1.8 K.

An assessed Fe–H phase diagram for $p = 1$ atm (≈ 0.1 MPa) has been calculated from available solubility data by San-Martin et al. [93 San1] (see Fig. 4). The dashed lines represent assessed maximum solubilities at a pressure of 0.1 MPa. The hydrogen solved influences the temperature of the phase equilibria only little.

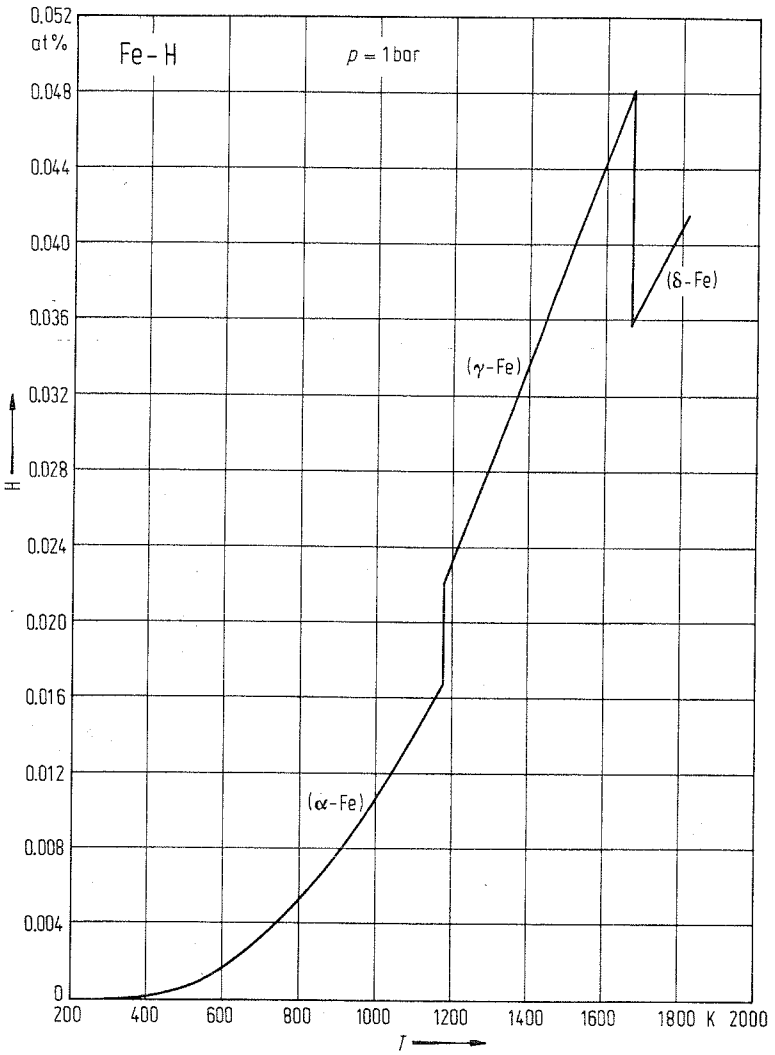

Fig. 1. Fe–H. Solubility of hydrogen in solid iron at 1 bar.

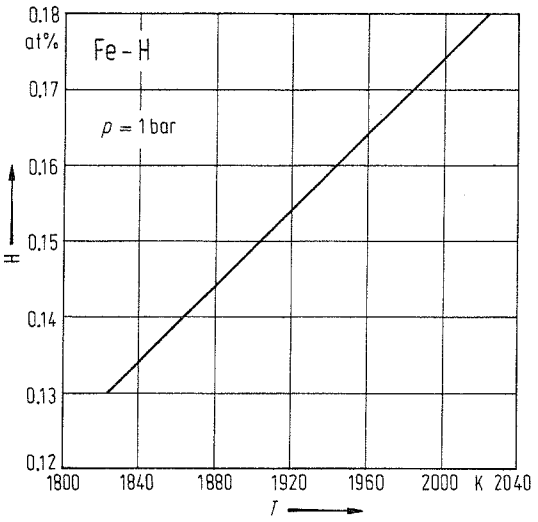

Fig. 2. Fe–H. Solubility of hydrogen in liquid iron at 1 bar.

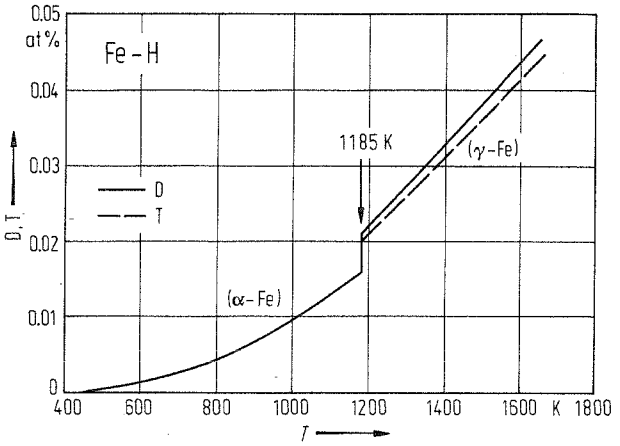

Fig. 3. Fe–H. Solubility of deuterium and tritium in solid iron.

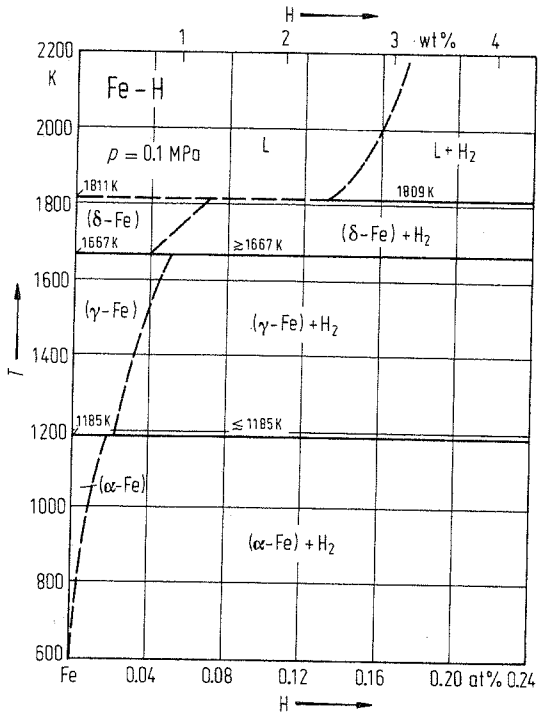

Fig. 4. Fe–H. Phase diagram at 0.1 MPa.

Phase diagram at high pressures

The dependence of the solubility of H in Fe on H_2-pressure is shown in Fig. 5 (taken from [93 San1]. (See also [78 Sha1] who has constructed the curves from data found in the literature.) It should be pointed out that at higher pressures the solubility of H is smaller at higher temperatures than at lower temperatures.

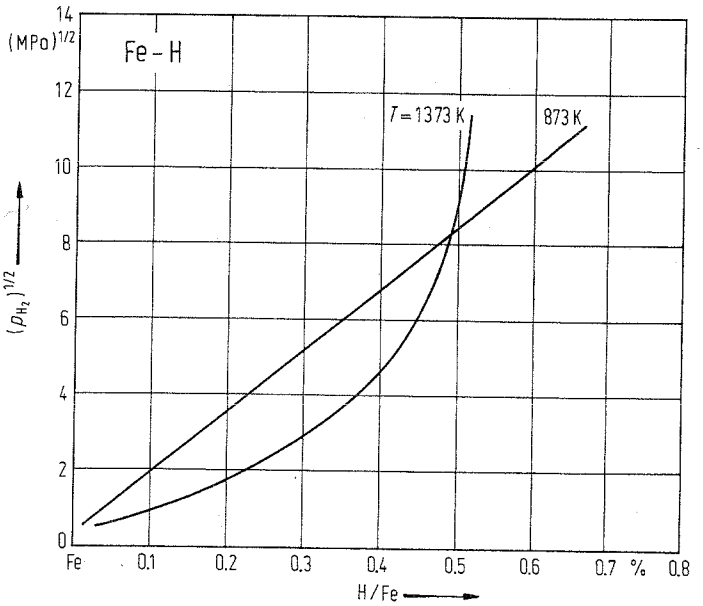

Fig. 5. Fe–H. Pressure dependence of the solubility of hydrogen in solid iron at 873 K and 1373 K.

At high pressures the influence of hydrogen on transition temperatures of Fe is much higher than at 0.1 MPa. Shapovalov et al. [78 Sha1] have published a phase diagram at p = 40 MPa, which has been redrawn by San-Martin et al. [93 San1] and which also has been taken to construct Fig. 6. It should be mentioned that a lot of experimental values for the solubility of H in Fe at high pressures are available in the literature. They have been analysed and discussed thoroughly by Kiuchi et al. [83 Kiu1].

At a pressure of 6.7 GPa and at 523 K, Antonov et al. [80 Ant1] were able to prepare a new phase (ε), which is ferromagnetic with Curie temperature at ≈ 80 K (Antonov et al. [81 Ant1]).

The pressure-temperature diagram of Fe–H given by Antonov et al. [82 Ant1] and Ponyatovskii et al. [82 Pon1] and also presented by San-Martin [93 San1] was taken as a basis to draw Fig. 7. The hatched field indicates the hysteresis of the α-Fe → ε transition. Two-phase boundaries are drawn as single lines, as Antonov et al. [82 Ant1] did.

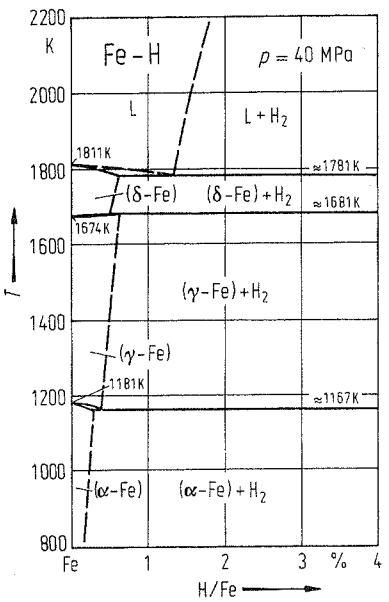

Fig. 6. Fe–H. Phase diagram at 40 MPa.

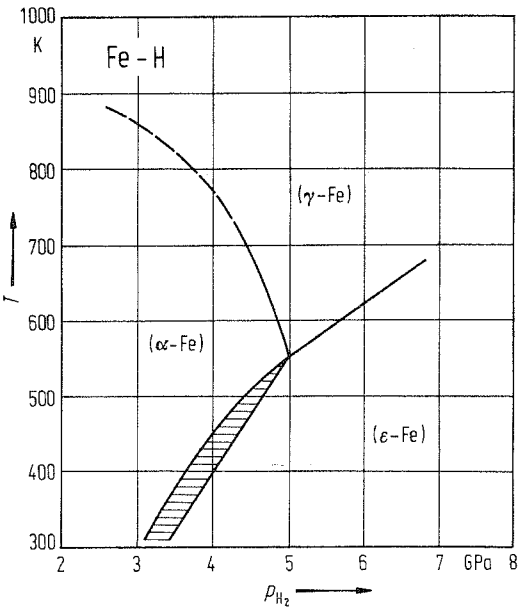

Fig. 7. Fe–H. Pressure-temperature phase diagram.

Crystal structure

As Plusquelle et al. [57 Plu1] found first, the protons are not always located at interstitial sites, but partially are accumulated in other lattice defects (see also [76 Sil2, 76 Sil1]).

Antonov et al. [80 Ant1] determined the structure of the high pressure ε phase. In the concentration range between 39 and 44.5 at% H they found that the ε phase has a cph structure with lattice parameters a = 0.2686 nm and c = 0.4380 nm (determined at 83 K). Schneider et al. [91 Sch1] have found a deuteride in analogy to ε. Further on, the latter authors have found three other hydrides (deuterides), one of them is nonmagnetic at 4.2 K.

Thermodynamics
Enthalpies of solution of H in Fe have been determined several times. The results, taken from a compilation by San-Martin et al. [93 San1], are given in Table 1.

Table 1. Fe–H. Enthalpy of solution of hydrogen in iron.

Phase	Enthalpy of solution [kJ / 0.5 mol H_2]	Ref.
α-Fe	27.2	50 Gel1
	24.1	70 Sal1
	28.6	78 Qui1
	28.0	79 Sha1
	26.0	85 Fuj1
γ-Fe	22.6	50 Gel1
	26.6	61 Hil1
	27.0	79 Sha1
	26.7	85 Fuj1
δ-Fe	73.0	79 Sha1
	26.0	85 Fuj1
Liquid Fe	31.4	50 Gel1
	30.6	74 Boo1
	34.9	74 Boo1
	34.4	85 Fuj1

Fe–Hf (Iron–Hafnium)

Phase diagram
Using differential thermal analysis, dilatometry and X-ray diffractography, Svechnikov et al. [61 Sve1] have determined the phase equilibria in this system. The results obtained are not in good agreement with those found by Hayes et al. [56 Hay1]. Later on, Kripyakevich et al. [64 Kri4] have examined some alloys by metallography and X-ray diffraction analysis. These investigations were followed by several others. The appreciable disagreement of results is obviously due to using of Hf of not sufficient purity. On the basis of results obtained by Svechnikov et al. [61 Sve1] and Kocherzinskiy et al. [73 Koc1], Okamoto [93 Oka2] has constructed an assessed phase diagram, which has been taken to draw Fig. 1.

All three types of the Laves phases exist in the neighbourhood of Fe_2Hf (λ, α-Fe_2Hf, β-Fe_2Hf). As Okamoto [93 Oka2] pointed out, the phase equilibria between them are not clear. On the other hand λ possibly exists only as a high-temperature phase, and the existence of β-Fe_2Hf is doubtful. Also in doubt are phases Fe_3Hf and FeHf mentioned by Hayes et al. [56 Hay1]. See the thorough discussion by Okamoto [93 Oka2].

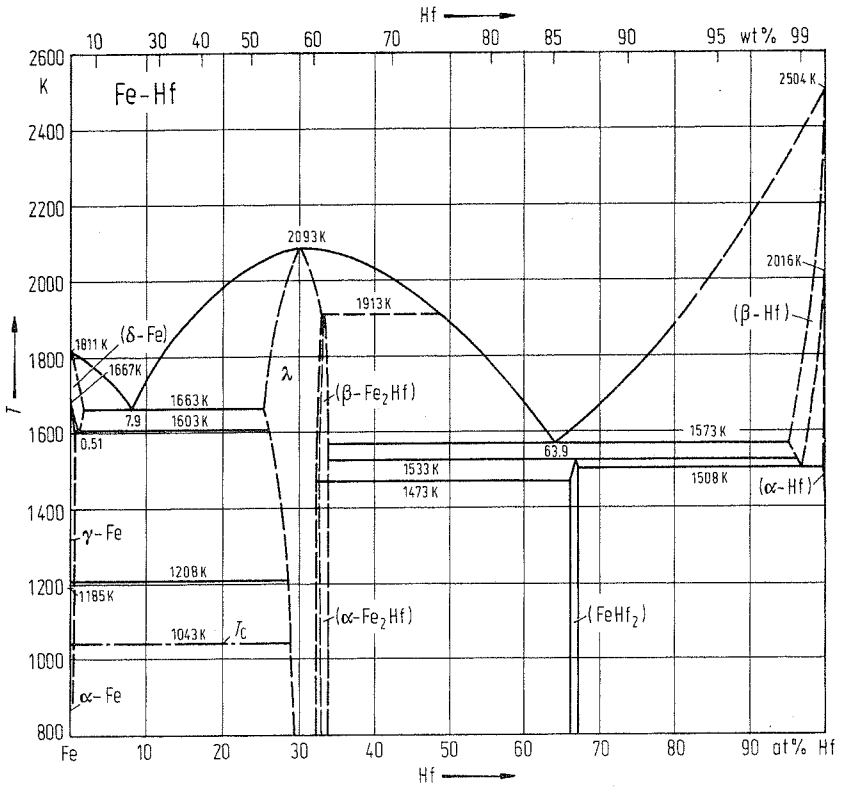

Fig. 1. Fe–Hf. Phase diagram.

Crystal structure

Crystallographic data of intermediate phases are summarized in Table 1.

Buschow et al. [80 Bus1] have prepared amorphous Fe–Hf alloys by melt-spinning in the concentration range between 82 and 60 at% Hf. The crystallization temperatures increase from 1013 K (at 82 at% Hf) to 1138 K (at 60 at% Hf).

Table 1. Fe–Hf. Crystal structure and lattice parameters of intermediate phases.

Phase	Structure	Type	*a* [nm]	*c* [nm]	Ref.
λ (33.3 at% Hf)	hex	$MgZn_2$	0.4980	0.8129	58 Ell1, 77 Ike1
α-Fe_2Hf	cub	$MgCu_2$	0.7025		54 Ell1, 77 Ike1
β-Fe_2Hf	hex	$MgNi_2$	0.4968	1.6167	61 Ell1, 64 Kri4
$FeHf_2$	cub	$NiTi_2$	1.20246		60 Nev1, 79 Ess1, 91 Cek1

Fe–Hg (Iron–Mercury)

Phase diagram

The solubility of Fe in Hg has been determined by many authors, the results obtained are in wide discrepancy. According to discussions by Jangg et al. [63 Jan1] this disagreement is caused by the experimental methods used. Jangg et al. [65 Jan1] stated that no intermediate phase is existing in this system.

Mostly on the basis of results published by Marshall et al. [50 Mar1], Kubaschewski [82 Kub1] has constructed an assessed solubility curve, which has been used to draw Fig. 1.

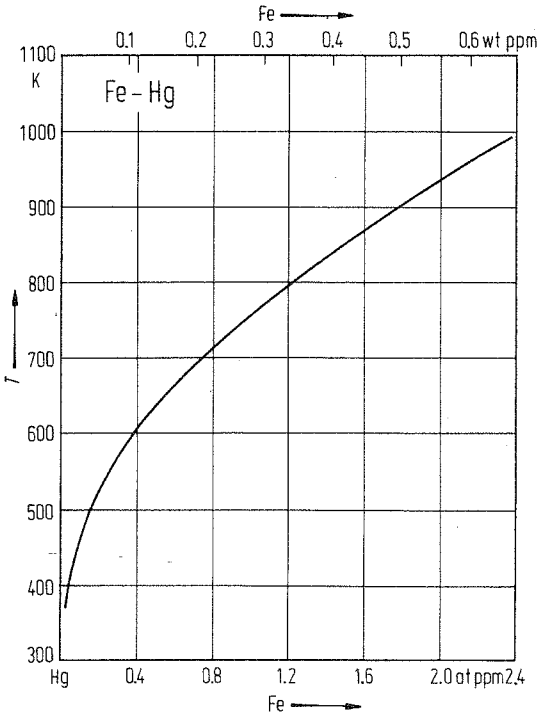

Fig. 1. Fe–Hg. Solubility of iron in liquid mercury.

Metastable phases

By different methods (electrical resistivity [78 Hoo1], X-ray diffractography [58 Jan1], viscosity [78 Hoo1], electron microscopy [75 Win1], magnetic measurements [88 Lin1]) suspensions of Fe particles in liquid Hg could be proven. From such amalgams no α-Fe crystals could be precipitated. Additions of a third component like Sn, Ga or Sb, stabilize such suspensions (Falk et al. [65 Fal1]).

A thorough discussion of the Fe–Hg system is given by Guminski [93 Gum1].

Fe–Ho (Iron–Holmium)

Phase diagram

Roe et al. [70 Roe1] have established the phase diagram using thermal analysis, metallography and X-ray diffraction analysis. The results were taken by Okamoto [93 Oka2] to construct an assessed phase diagram, which was the basis of Fig. 1.

Applying thermodynamic considerations, Okamoto [93 Oka2] stated that the liquidus is not in all parts of the system correctly determined. A redetermination seems to be necessary.

An intermediate phase Fe_5Ho has been found by Nassau et al. [60 Nas1] which, however, has not been confirmed by other authors.

By quenching (10^2...10^3 K/s) a liquid alloy of ≈ 50 at% Ho at a pressure of 7.7 GPa, Tsvyshchenko et al. [85 Tsv1] obtained a crystalline solid containing a hexagonal phase of $MgNi_2$-type.

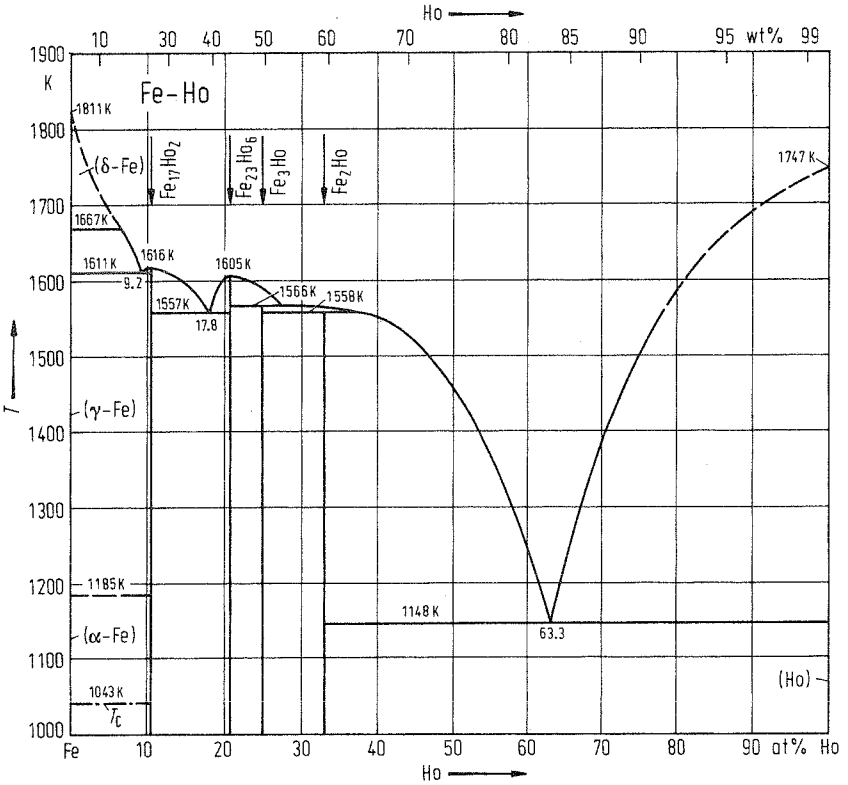

Fig. 1. Fe–Ho. Phase diagram.

Crystal structure

Crystallographic data of intermediate phases are listed in Table 1.

Table 1. Fe–Ho. Crystal structure and lattice parameters of intermediate phases.

Phase	Structure	Type	*a* [nm]	*c* [nm]	Ref.
$Fe_{17}Ho_2$	hex	$Ni_{17}Th_2$	0.8434	0.8284	65 Kri3, 66 Bus2
$Fe_{23}Ho_6$	cub	$Mn_{23}Th_6$	1.2032		65 Kri3, 70 Roe1
Fe_3Ho	hex	Ni_3Pu	0.51097	2.4526	68 Dwi1, 70 Roe1
Fe_2Ho	cub	Cu_2Mg	0.73014		60 Nas1, 68 Man2

Fe–In (Iron–Indium)

Phase diagram

Using thermal analysis as well as magnetic and microscopic investigations, Stadelmaier et al. [67 Sta1], Dasarathy [67 Das1, 69 Das1, 72 Das1, 74 Das1] and Malingih et al. [70 Mal1] have experimentally investigated phase equilibria from which Kubaschewski [82 Kub1] and Okamoto [93 Oka2] have drawn an assessed phase diagram. From the latter author information has been taken to construct Fig. 1.

On the basis of the regular solution model the critical temperature of the miscibility gap has been estimated to be ≈ 3130 K (Predel et al. [79 Pre1]).

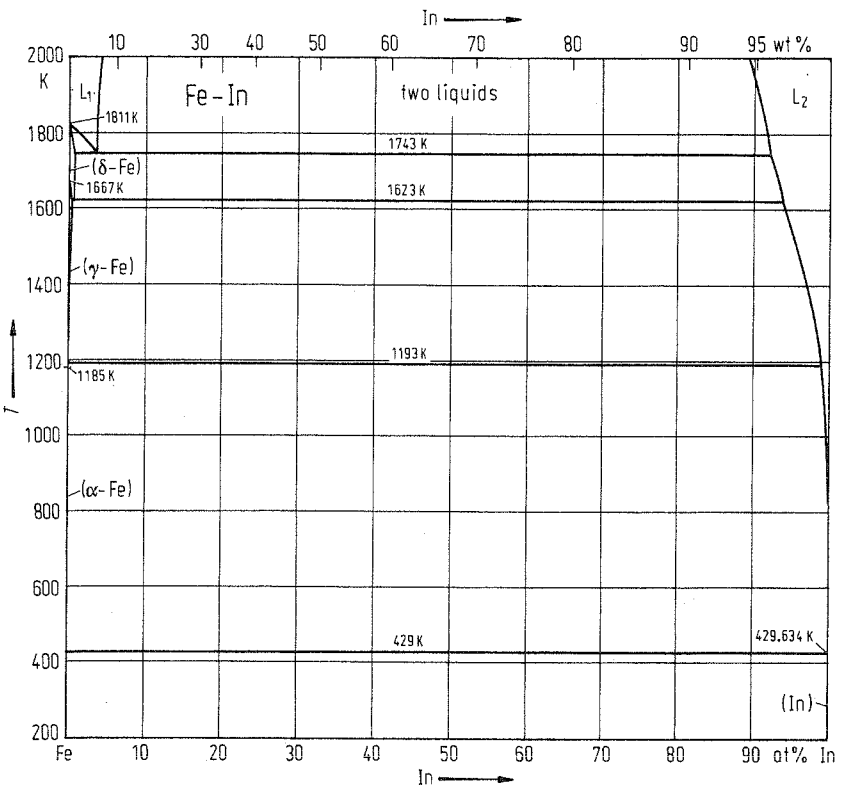

Fig. 1. Fe–In. Phase diagram.

Fe–Ir (Iron–Iridium)

Phase diagram

Experimental investigations of phase equilibria have been performed by Buckley et al. [63 Buc1], Raub et al. [64 Rau2], and Fallot [37 Fal2]. On the basis of the results obtained by these authors Kubaschewski [82 Kub1] and Swartzendruber [93 Swa2] have drawn an assessed phase diagram, from which information was taken to construct Fig. 1.

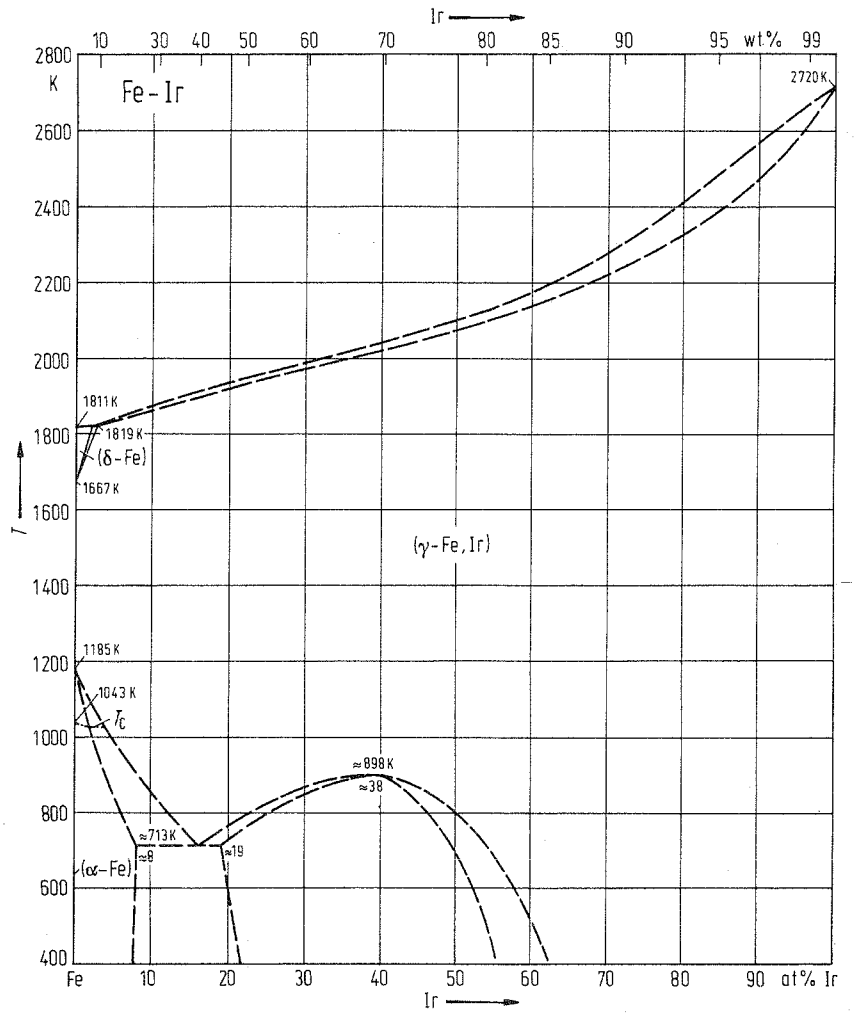

Fig. 1. Fe–Ir. Phase diagram.

Crystal structure

Raub et al. [64 Rau2] have determined the lattice parameters at concentrations up to 80 at% Ir. Results for fcc (γ-Fe) are plotted in Fig. 2. For the ε phase (close packed hexagonal structure) these authors found, more or less independent of concentration, the lattice paramter a = 0.260 nm and an almost constant value of $c/a \approx 1.61$. All lattice constants have been determined at room temperature.

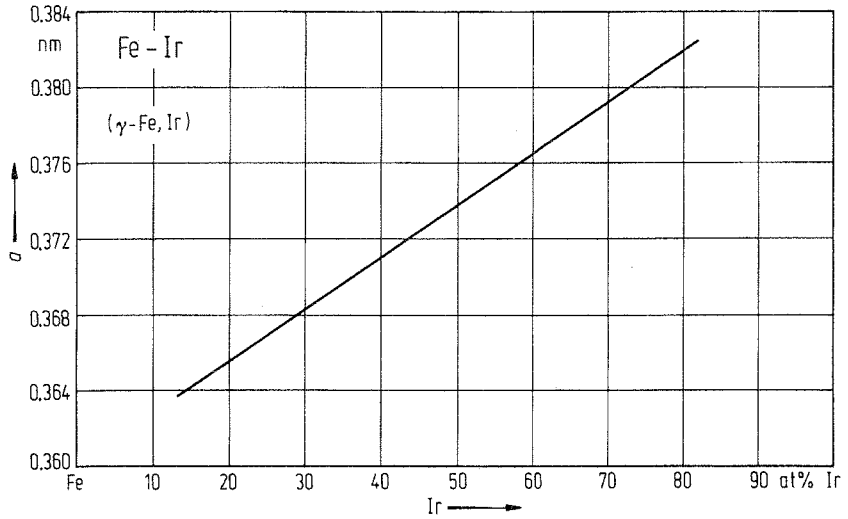

Fig. 2. Fe–Ir. Lattice parameter for fcc (γ-Fe, Ir) solid solution.

Thermodynamics

Thermodynamic activities of iron have been determined in the fcc (γ-Fe) solid solution at 1473 K by equilibrating the alloys with iron oxide (wüstite or magnetite) with a CO_2–CO gas mixture (Schwerdtfeger et al. [68 Sch2]). Results obtained are plotted in Fig. 3.

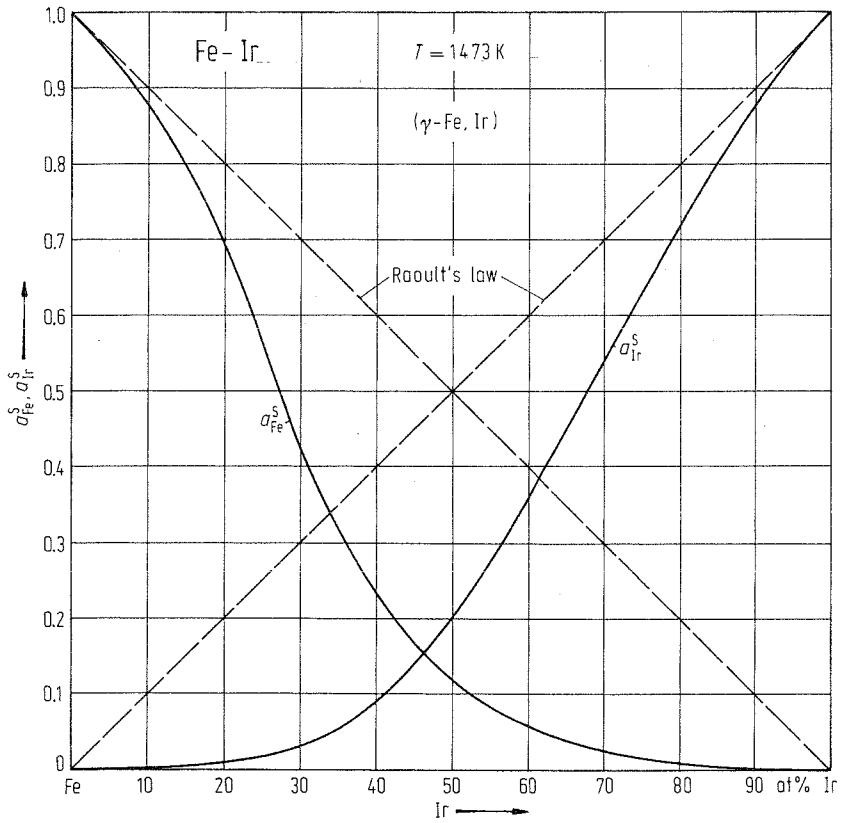

Fig. 3. Fe–Ir. Thermodynamic activity for fcc (γ-Fe, Ir) solid solution at 1473 K.

Fe–K (Iron–Potassium)

Phase diagram

"No" solubility of K in (Fe) has been assumed by Wever [29 Wev1, 28 Wev1] on the basis of systematic considerations of the influence of elements on the polymorphism of iron. This has been "confirmed" by diffusion experiments (Jones [34 Jon2]). Reliable solubility measurements of (γ-Fe) in liquid K have been done by Swisher et al. [65 Swi1] in the temperature range between 943 K and 1328 K. Due to the influence of oxygen on the solubility of Fe in liquid K the results are approximations only. Similar experiments equilibrating iron with liquid K have been performed by Ginell et al. [65 Gin1, 66 Gin1], Teitel [65 Tei1] and McKisson et al. [66 McK1]. Results obtained by Swisher [65 Swi1] and Ginell et al. [66 Gin1] are given in Table 1 (see the review by Sangster et al. [93 San2]).

On the basis of information taken from the literature (see above), Sangster et al. [93 San2] have proposed a phase diagram, which has been taken to draw Fig. 1.

Table 1. Fe–K. Solubility of Fe in liquid K (see Sangster et al. [93 San2]).

T [K]	Solubility [at% Fe]	Ref.	*T* [K]	Solubility [at% Fe]	Ref.
943	0.0030	65 Swi1	1198	0.0320	66 Gin1
1003	0.0175	65 Swi1	1198	0.0313	66 Gin1
1143	0.0455	65 Swi1	1273	0.0389	66 Gin1
1203	0.0910	65 Swi1	1273	0.0311	66 Gin1
1273	0.0700	65 Swi1			
1333	0.0700	65 Swi1			

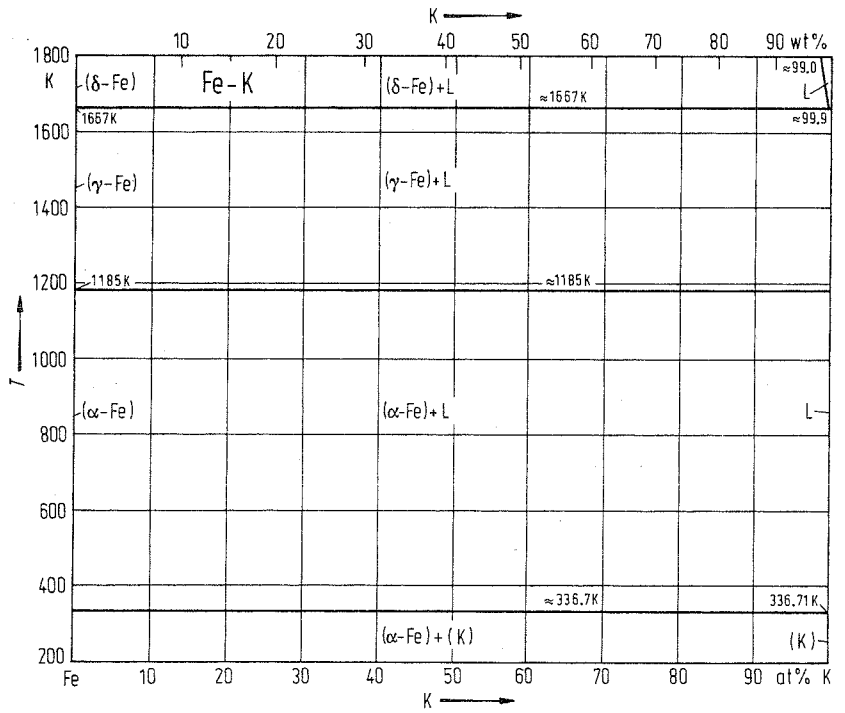

Fig. 1. Fe–K. Phase diagram.

Thermodynamics
On the basis of a thermodynamic model Niessen et al. [83 Nie1] have estimated enthalpies of formation of Fe–K alloys. The values are positive and thus consistent with the demixing tendency of the phase diagram.

Fe–Kr (Iron–Krypton)

Sieverts et al. [12 Sie1] have found that Kr is not absorbed by iron in the temperature range from 1473 K to 1773 K.

Fe–La (Iron–Lanthanum)

Phase diagram
Richard [62 Ric1] has investigated the phase equilibria by thermal analysis, X-ray diffractography and metallographic observations using materials with a purity better than 99 %. Nassau et al. [60 Nas1] and Kepka et al. [72 Kep1] confirmed the results obtained by Richard [62 Ric1], whereas the results obtained by Savitskii [59 Sav1] are deviating from these findings. The latter author found two intermediate phases: Fe_5La and Fe_2La, which obviously are metastable ones or are stabilized due to impurities. Nassau et al. [60 Nas1] stated that no stable intermediate phases are existing in this system.

Gschneidner et al. [61 Gsc1], after thorough discussion of the experimental results mentioned above, has proposed an assessed phase diagram, which was redrawn by Kubaschewski [82 Kub1] and also by Okamoto [93 Oka2]. From there information has been taken to construct Fig. 1.

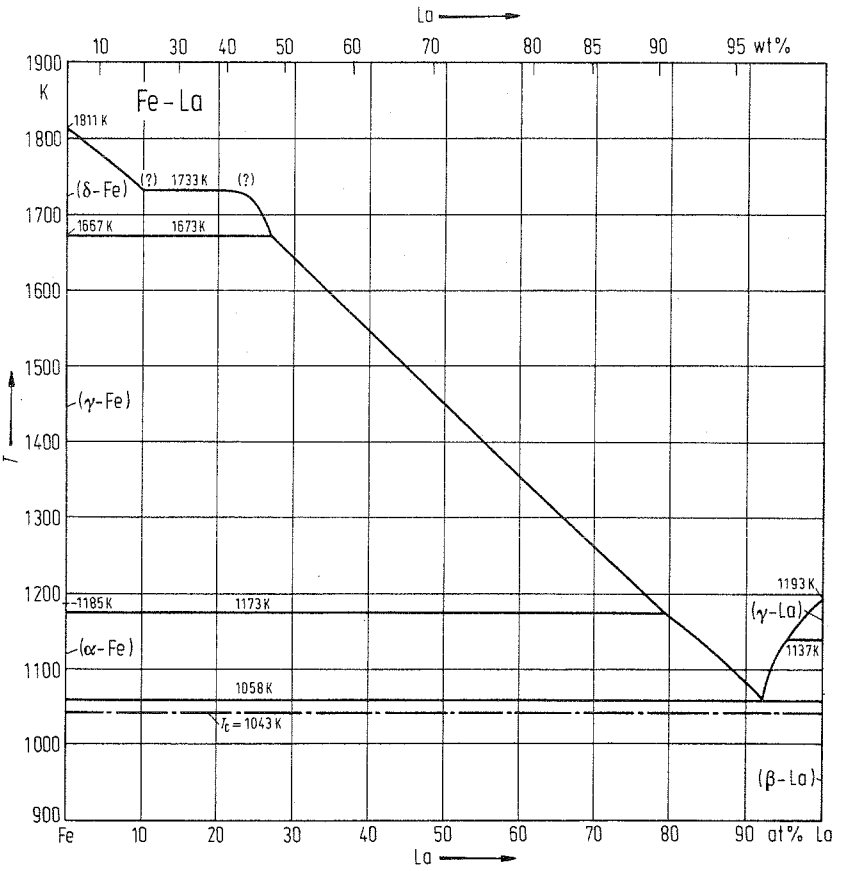

Fig. 1. Fe–La. Phase diagram.

As a reason for the anomaly in the liquidus (between ≈ 8 and ≈ 19 at% La) the existence of two miscibility gaps has been discussed (see Kubaschewski [82 Kub1]). But Okamoto [93 Oka2] stated that this is improbable. More experimental investigations are needed.

Fe–Li (Iron–Lithium)

Phase diagram

Lithium, obviously, is not soluble in solid Fe (Wever [29 Wev1, 28 Wev1], Ageev et al. [28 Age1]). The solubility of Fe in liquid Li has been investigated using different analytical methods by Jesseman et al. [50 Jes1], Sand [58 San1], Bychkov et al. [59 Byc1], Beskorovainyi et al. [60 Bes1], Bychkov et al. [60 Byc1], Kelly [61 Kel1], Leavenworth et al. [61 Lea2, 61 Lea1], Minushkin [61 Min1], Weeks [63 Wee1], and Beskorovainyi et al. [80 Bes1]. Reviews of the solubility data published in the literature have been given by McKinson et al. [66 McK2], Anthrop [67 Ant1], Kubaschewski [82 Kub1], and Sangster et al. [93 San2].

After thorough discussion of the individual experimental values, Sangster et al. [93 San2] have proposed mean solubilities, which have been used to draw Fig. 1. An assessed phase diagram published by the same authors [93 San2] was taken to construct Fig. 2.

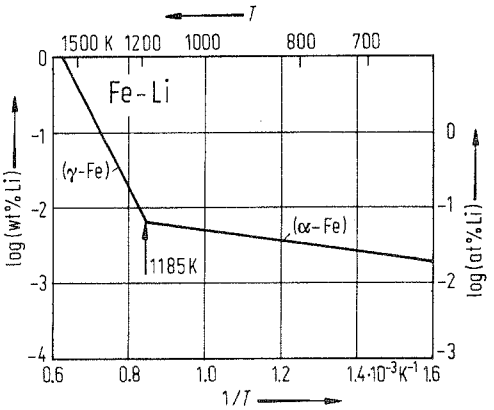

Fig. 1. Fe–Li. Solubility of lithium in solid iron.

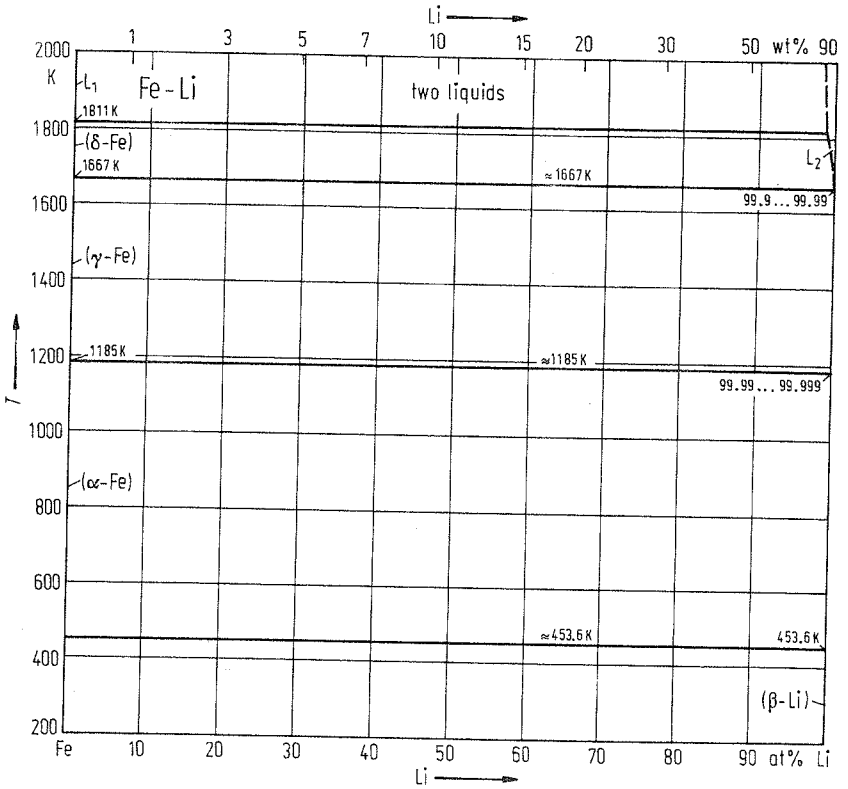

Fig. 2. Fe–Li. Phase diagram.

Thermodynamics

Niessen et al. [83 Nie1] have estimated enthalpies of formation of Fe–Li alloys on the basis of an atomistic thermodynamic model. Though the ΔH^L-values obtained may be not accurate, the sign of them, which is positive, obviously is correct and therefore is in agreement with the demixing character of the phase diagram.

Fe–Lu (Iron–Lutetium)

Phase diagram

Using thermal analysis and X-ray diffractography, Kolesnichenko et al. [72 Kol1] have investigated the phase equilibria. The phase diagram thus obtained has been redrawn by Kubaschewski [82 Kub1] and Okamoto [93 Oka2]. From the latter author information has been taken to draw Fig. 1.

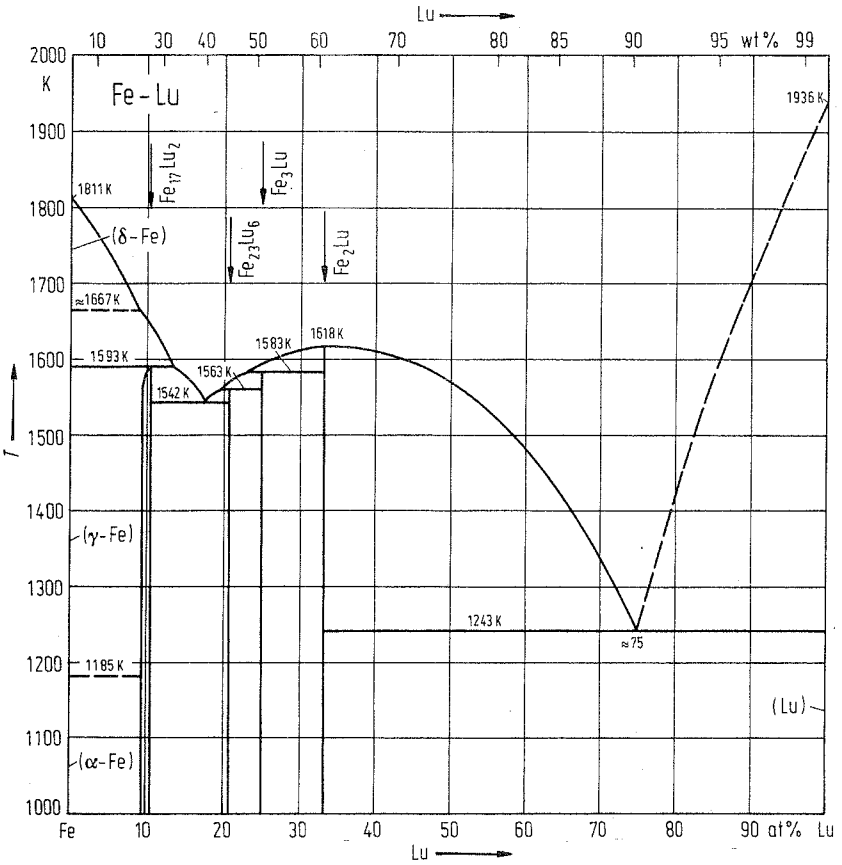

Fig. 1. Fe–Lu. Phase diagram.

Crystal structure

Crystallographic data of intermediate phases are listed in Table 1.

Table 1. Fe–Lu. Crystal structure and lattice parameters of intermediate phases.

Phase	Structure	Type	*a* [nm]	*c* [nm]	Ref.
$Fe_{17}Lu_2$ (9.5 at% Lu)	hex	$Ni_{17}Th_2$	0.8401	0.8272	72 Kol1, 68 Ray1, 72 Giv1
$Fe_{23}Lu_6$	cub	$Mn_{23}Th_6$	1.195		65 Kri3, 68 Ray1
Fe_3Lu	hex	Ni_3Pu	0.5052	2.433	72 Kol1, 68 Ray1
Fe_2Lu	cub	Cu_2Mg	0.7222		61 Dwi2, 65 Ell1, 65 Kri6, 68 Ray1, 72 Can1, 74 Atz1, 87 Bro1

Fe–Mg (Iron–Magnesium)

Phase diagram

Using several different methods the solubility of Mg in Fe and of Fe in Mg has been determined rather often, however, the results obtained are not in agreement with each other. The solubility data have been

compiled and discussed by Hansen et al. [58 Han1], Elliott [65 Ell1], Shunk [69 Shu1], Kubaschewski [82 Kub1] and Nayeb-Hashemi et al. [93 Nay1]. There is, however, not enough information to construct the whole phase diagram. An assessed partial phase diagram for high Mg concentrations, as published by Nayeb-Hashemi et al. [93 Nay1], is given in Fig. 1. A phase diagram calculated by [93 Nay1] up to concentrations of 2 at% Fe (under constrained gas pressure) is given in Fig. 2 (see [93 Nay1] and Burylev [66 Bur1]).

The miscibility gap in the liquid state in the middle part of the phase diagram is confirmed by experimental investigations (Burylev [65 Bur1], Tavadze et al. [61 Tav1], Trojan et al. [61 Tro1]). Tavadze et al. [61 Tav1] and Levchenko et al. [63 Lev1] expect a mutual solubility of Mg and Fe at high pressures and high temperatures in the liquid state.

The liquidus on the Fe-rich side of the system has been investigated by Yensen et al. [31 Yen1], Fahrenhorst et al. [41 Fah1], Bulian et al. [42 Bul1], Beerwald [41 Bee1], Mitchell [48 Mit1] and Siebel [48 Sie1]. An assessed partial diagram for high Fe concentrations has been published by Nayeb-Hashemi et al. [93 Nay1] which is included in Fig. 2.

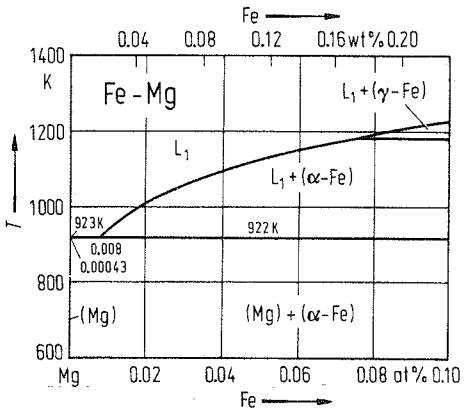

Fig. 1. Fe–Mg. Partial phase diagram (0...0.1 at% Fe).

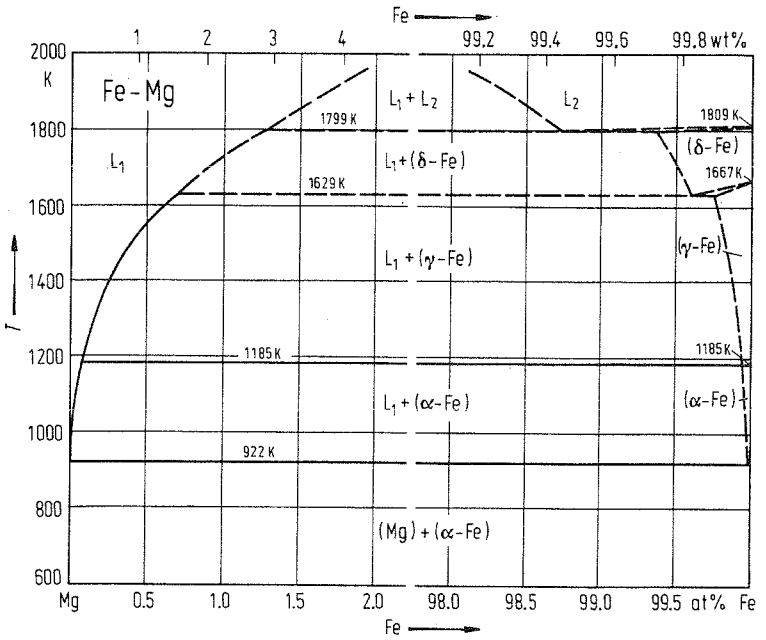

Fig. 2. Fe–Mg. Phase diagram showing the Mg-rich (0...2 at% Fe) and Fe-rich (98...100 at% Fe) parts.

Fe–Mn (Iron–Manganese)

Phase diagram

Experimental work to determine the phase equilibria has been done, besides others, by Hellawell et al. [57 Hel1], and Hume-Rothery et al. [64 Hum1]. The phase diagram has been calculated by Steiler [81 Ste1], Rao et al. [74 Rao2], Kirchner et al. [73 Kir2], and Kaufman [78 Kau3]. Reviews of this system have been published by Kurnakow et al. [53 Kur1], Hellawell [56 Hel1], Hansen et al. [58 Han1], Elliott [65 Ell1], Shunk [69 Shu1], Kubaschewski [82 Kub1], Bannykh et al. [86 Ban1], Brandes et al. [80 Bra1], Rivlin [84 Riv1], Huang et al. [87 Hua1] and Okamoto [93 Oka2]. The assessed phase diagram published by Okamoto [93 Oka2], which was taken to construct Fig. 1, has been based on thermodynamic modelling done by Huang [87 Hua1].

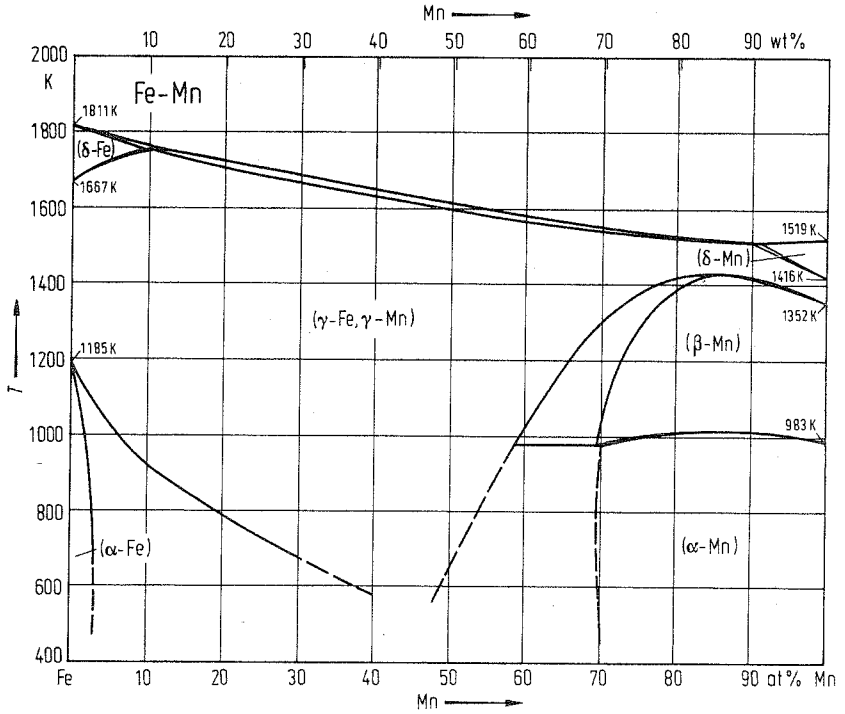

Fig. 1. Fe–Mn. Phase diagram.

Martensitic transformations

By cooling (γ-Fe, γ-Mn) solid solutions, two different martensitic transformations occur depending on concentration. Product of the transition in the concentration range between 3 and 18 at% Mn is a tetragonal phase α' (Bogachev et al. [76 Bog1]), and between 12 and 30 at% Mn a hexagonal phase ε (Parr [52 Par1]). Fig. 2 gives the temperatures for the start (M_s) and finish (M_f) of the martensitic transitions, as well as the temperatures for the reverse transition (A_s and A_f) as a function of concentration. The transition temperatures have been measured rather often (see [93 Oka2]). Information to draw this figure was taken from Gulyaev et al. [78 Gul1] (see also Okamoto [93 Oka2]). Both martensitic phases, α' and ε, are metastable, of course.

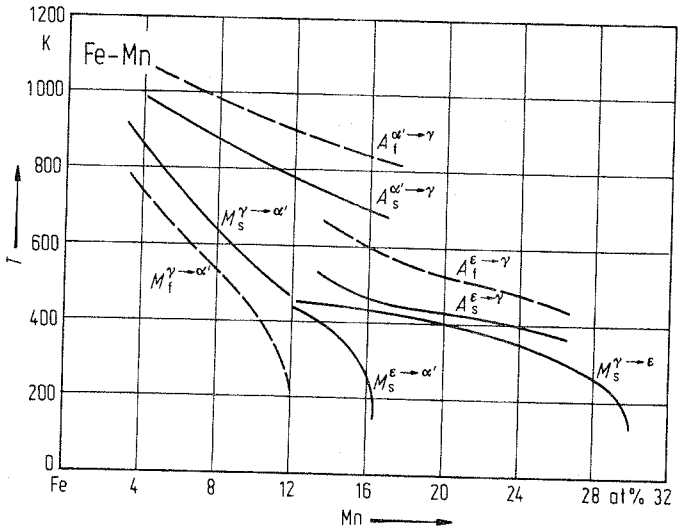

Fig. 2. Fe–Mn. Martensitic transformation temperatures for metastable phases α' and ε: starting (M_s) and finishing (M_f) temperatures on cooling, and starting (A_s) and finishing (A_f) temperatures on heating.

Phase equilibria at high pressures

At 12.6 GPa and 300 K pure bcc α-Fe transforms to cph ε-Fe (see Okamoto [93 Oka2]). Adding Mn, this transition pressure decreases to 5.5 GPa at 11 at% Mn (Loree et al. [66 Lor1], Giles [71 Gil1]). As Clausen [63 Cla1] has found, the (α-Fe)⇌(γ-Fe, γ-Mn) equilibria are shifted to lower temperatures with increasing pressure. Up to 5 GPa the boundaries of these equilibria have been estimated by Ershowa et al. [67 Ers1]. The ε-Fe high-pressure phase corresponds to the ε phase obtained by martensitic transformation from (γ-Fe, γ-Mn) solid solutions (Genshaft [64 Gen1]).

Crystal structure

Lattice parameters of fcc (γ-Fe, γ-Mn) solid solutions have been measured first by Schmidt [29 Sch1] and were redetermined rather often (see Okamoto [93 Oka2]). In Fig. 3 the mean of the lattice constants obtained are plotted as a function of concentration (after [93 Oka2]).

Lattice parameters of cubic (β-Mn) solid solutions (β-Mn-type) are plotted in Fig. 4 (taken from [93 Oka2] based on several experimental works).

(α-Mn) of cubic α-Mn-type structure has a lattice parameter which is drawn in Fig. 5 as a function of concentration. Information to construct this figure has been taken from [93 Oka2] based on experimental results obtained by several authors.

First measurements of the lattice parameters of the metastable (tetragonal) phase α' have been performed by Nishiyama [29 Nis1]. Later on, more investigations were done. The results obtained scatter appreciably (see [93 Oka2]). *c/a*-values determined by Charnushnikova et al. [79 Cha2] are: $c/a = 1.008$ at 8 at% Mn and $c/a = 0.990$ at 14 at% Mn. *c/a* increases linearly with Mn concentration. The *a*-value, as a rough mean of the results present in the literature is plotted in Fig. 6.

Lattice parameters of ε, as published by Gensamer et al. [32 Gen1], are plotted in Fig. 7.

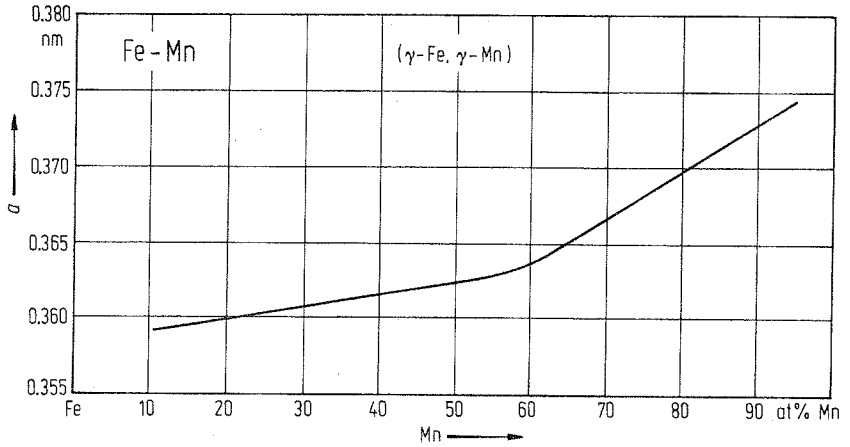

Fig. 3. Fe–Mn. Lattice parameter for fcc (γ-Fe, γ-Mn) solid solution.

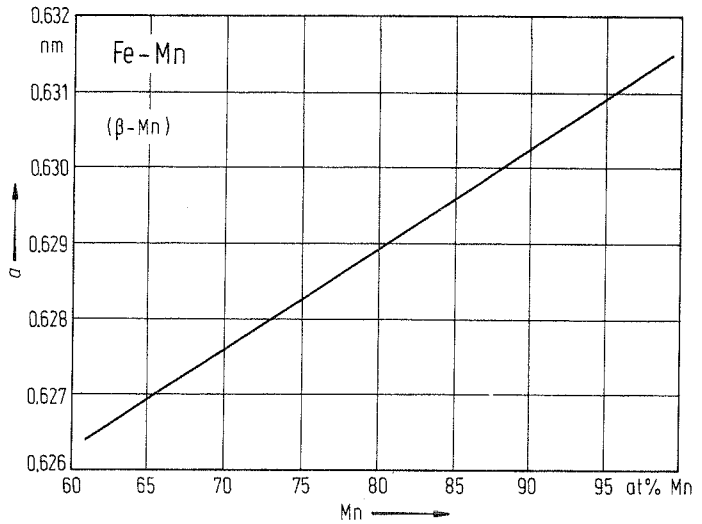

Fig. 4. Fe–Mn. Lattice parameter for cubic (β-Mn-type) solid solution (β-Mn).

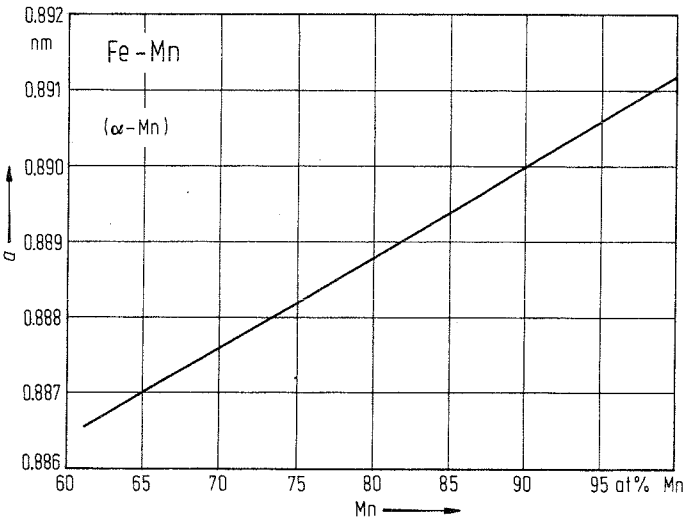

Fig. 5. Fe–Mn. Lattice parameter for cubic (α-Mn-type) solid solution (α-Mn).

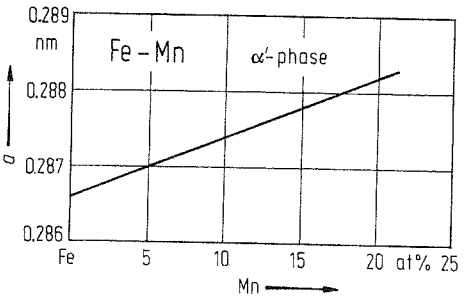

Fig. 6. Fe–Mn. Lattice parameter a for the metastable tetragonal phase α'.

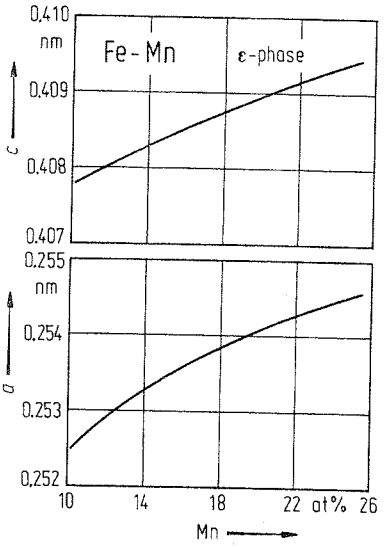

Fig. 7. Fe–Mn. Lattice parameters for the metastable cph phase ε.

Thermodynamics

Batalin et al. [74 Bat1] have determined experimentally enthalpies of mixing of liquid Fe–Mn alloys. By modelling Huang [89 Hua1] has obtained assessed ΔH^L values, which are taken to draw Fig. 8.

Rather often thermodynamic activities of Mn in liquid Fe–Mn alloys have been measured. Steiler et al. [73 Ste1] and Mukai et al. [82 Muk1] found a positive deviation from Raoult's law. No deviation has been stated by Sanboungi et al. [55 San1] and Schultz et al. [66 Sch1], whereas Jacob et al. [84 Jac1] found a weak negative deviation from ideality. The activity isotherms for liquid Fe–Mn alloys at 1823 K, as obtained by [84 Jac1] (EMF method) are given in Fig. 9. Activities presented in this figure are in good agreement with calculations done by [89 Hua1] (see also the compilation by Hultgren et al. [73 Hul1]).

The integral enthalpies of formation of (γ-Fe, γ-Mn) solid solutions have been determined by Kendall et al. [61 Ken1] and, later on, by Kubitz et al. [87 Kub1]. Optimizing the thermodynamic data of the Fe–Mn system, Huang [89 Hua1] has obtained assessed ΔH^S values for (γ-Fe, γ-Mn) solid solutions at 1443 K, which have been taken to construct Fig. 10.

Within the limits of experimental error the assessed ΔH^S data are in agreement with those obtained experimentally by Kubitz et al. [87 Kub1].

Similar to the situation in liquid Fe–Mn alloys, there is only little deviation of the experimentally determined thermodynamic activities from Raoult's law in the (γ-Fe, γ-Mn) region.

Roy et al. [65 Roy1] found for (γ-Fe, γ-Mn) solid solutions positive deviations, whereas negative deviations from Raoult's law have been determined by Jacob et al. [84 Jac1], Benz [74 Ben1] and Buttler et al. [61 But1]. Results published by Jacob et al. [84 Jac1] seem to be the most reliable ones (agreeing with results of calculations by Huan [89 Hua1]), and therefore have been taken to construct the activity isotherms in Fig. 11.

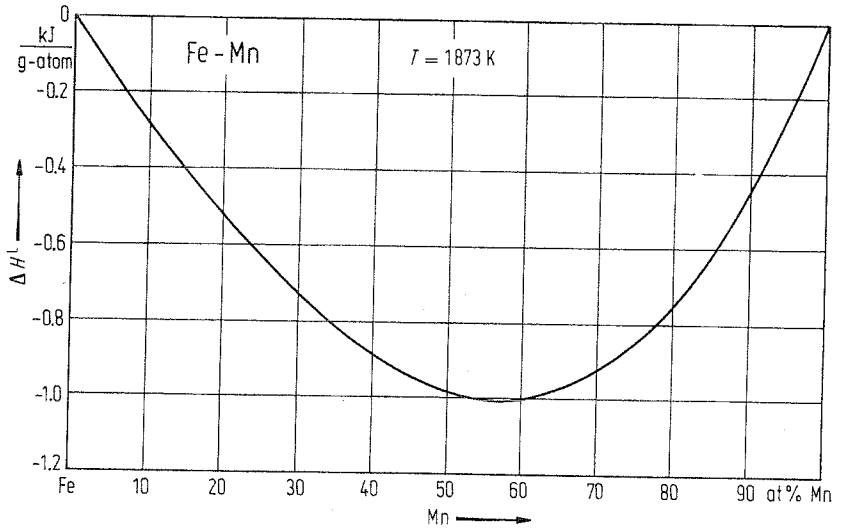

Fig. 8. Fe–Mn. Enthalpy of mixing for liquid alloys at 1873 K.

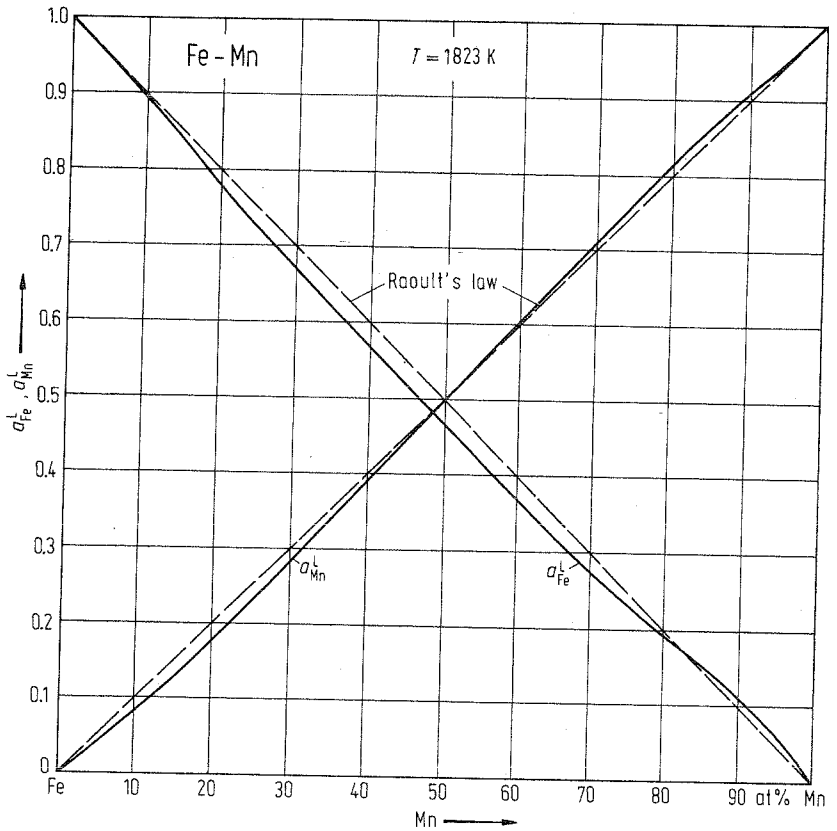

Fig. 9. Fe–Mn. Thermodynamic activities for liquid alloys at 1823 K.

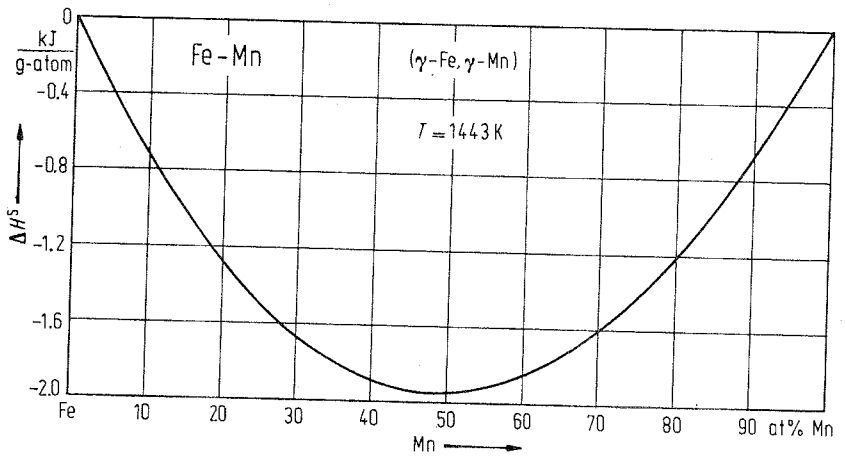

Fig. 10. Fe–Mn. Enthalpy of formation for (γ-Fe, γ-Mn) solid solution at 1443 K.

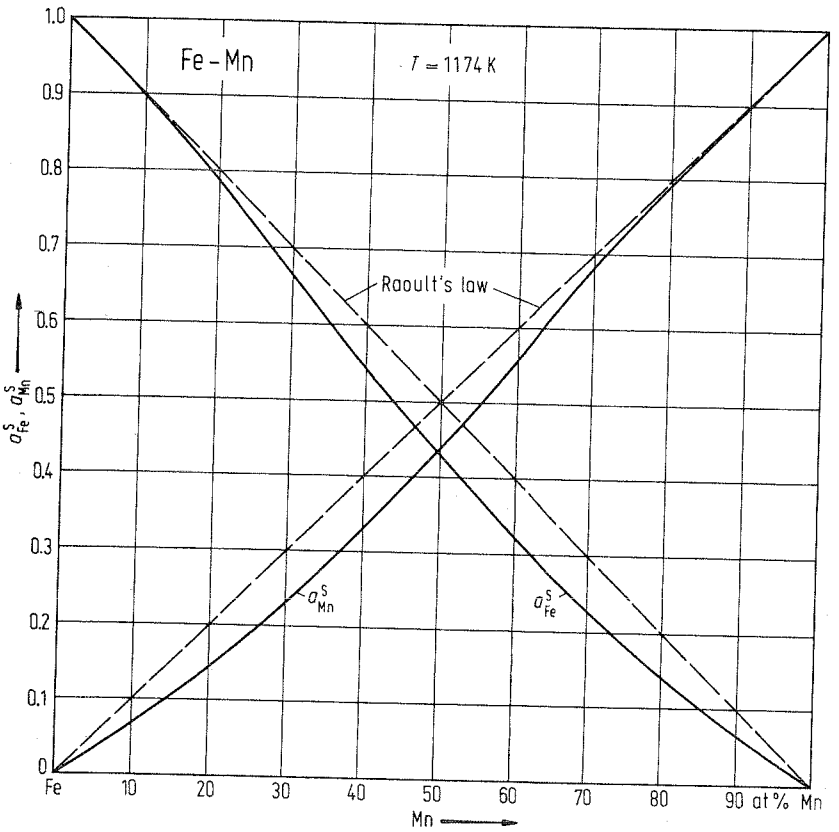

Fig. 11. Fe–Mn. Thermodynamic activities for solid solutions at 1174 K. Standard state for Mn: β-Mn.

Fe–Mo (Iron–Molybdenum)

Phase diagram

Since the first work of Sykes [26 Syk1] phase equilibria in the Fe–Mo system have been investigated very often. Several reviews have been published where the original papers are listed. Such compilations are given by Hansen et al. [58 Han1], Elliott [65 Ell1], Shunk [69 Shu1], Brewer et al. [80 Bre3], Kubaschewski [82 Kub1] and Guillermet [93 Gui1]. The latter author has discussed comprehensively the reliability of individual results, and also has calculated an assessed phase diagram by thermodynamic modelling, which is in excellent agreement with the best experimental results. This phase diagram has been taken to construct Fig. 1. The γ-Fe loop is given in Fig. 2 on enlarged scale.

Assessed phase diagrams obtained on the basis of thermodynamic calculation have been published by Kaufman [78 Kau1] and Nüssler et al. [80 Nüs1], too.

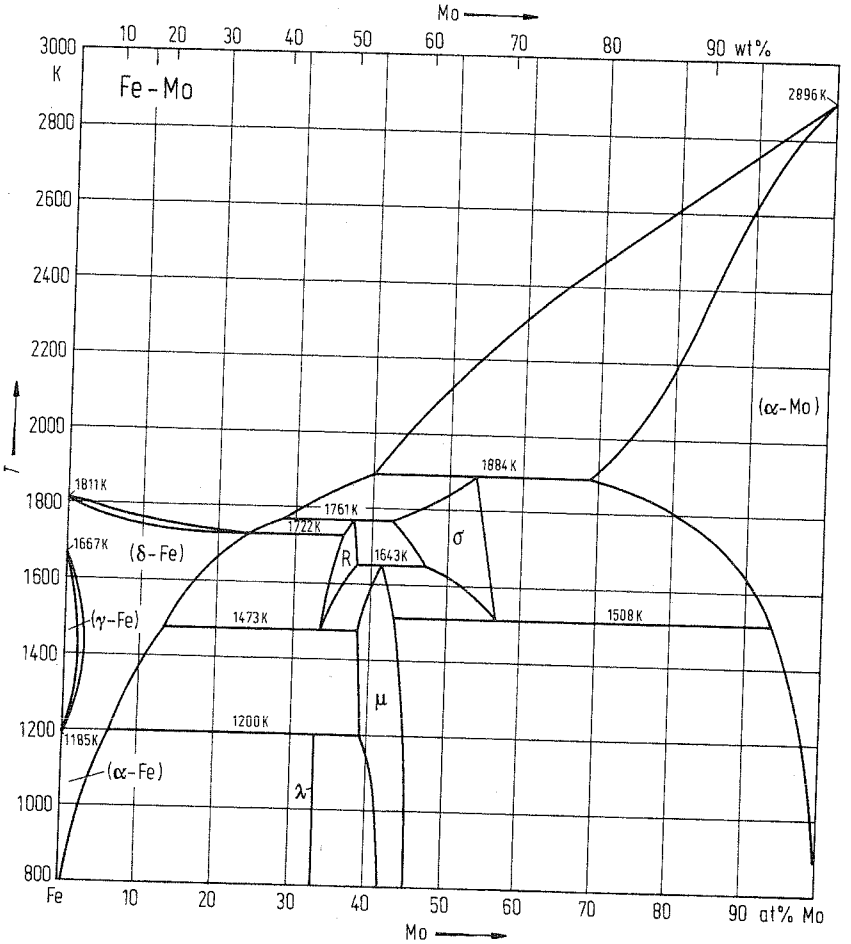

Fig. 1. Fe–Mo. Phase diagram.

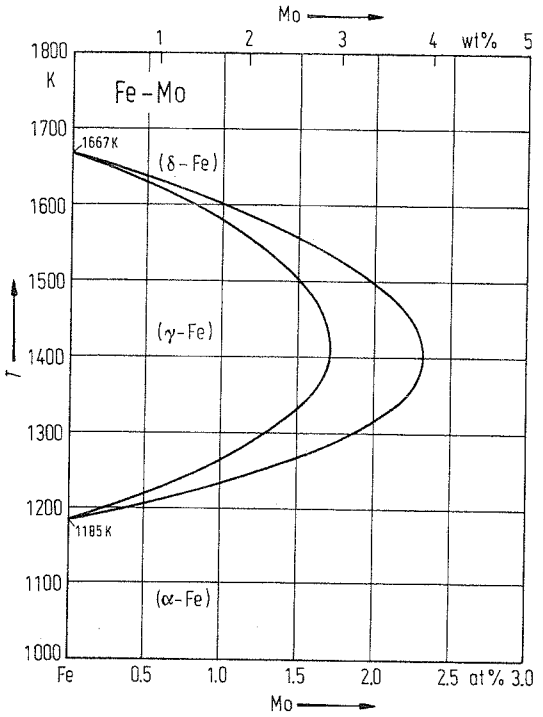

Fig. 2. Fe–Mo. Phase equilibria (γ-Fe) - (α-Fe).

Crystal structure

Crystallographic data of intermediate phases are listed in Table 1.

By vapor quenching, Sumiyama et al. [87 Sum1] have prepared amorphous alloys in the concentration range between 30 at% Mo and 60 at% Mo. There it has been shown by Mössbauer spectroscopy that the local atomic configuration of the amorphous alloys correspond to that in the stable intermediate phase at the same concentration.

Using a sputtering method, Hsu et al. [88 Hsu1] succeeded in preparing amorphous alloys in the concentration range between 40 and 80 at% Mo. At other concentrations a single phase with bcc structure was obtained. The authors found extremely high crystallization temperatures of the amorphous alloys of ≈ 1100 K.

Table 1. Fe–Mo. Crystal structure and lattice parameters of intermediate phases.

Phase	at% Mo	Structure	Type	a [nm]	c [nm]	Ref.
λ	33.3	hex	$MgZn_2$	0.4744	0.7725	74 Ito1, 67 Sin1, 80 Sem1
μ	39.0...44.0	hex	Fe_7W_6	0.4751	2.568	67 Sin1
σ	42.9...56.7	tetr	CrFe	0.9190	0.4814	85 Sam1

Thermodynamics

By Knudsen method using a mass spectrometer to analyze the vapor Ichise et al. [80 Ich1] have determined thermodynamic activities of Fe across the system. The a_{Fe}-values obtained have been assessed by Guillermet [93 Gui1] and from there were taken to draw the activity isotherm in Fig. 3. This isotherm agrees well with the experimentally obtained data ([80 Ich1]).

Spencer et al. [75 Spe1] and Nüssler et al. [80 Nüs1] have determined the enthalpy of formation of the μ phase. The value reported by Spencer [75 Spe1] amounts to $\Delta H_{\mu}^{S} = -2.53$ kJ g-atom^{-1}. Within the limits of experimental error this value agrees with that obtained by the assessment performed by Guillermet [93 Gui1] ($\Delta H_{\mu}^{S} = -2.92$ kJ g-atom^{-1}). This value seems to be independent on concentration and temperature considering the experimental scatter. The value reported by Nüssler et al. [80 Nüs1] is somewhat lower ($\Delta H_{\mu}^{S} = -2.20$ kJ g-atom^{-1}) (see also Kleykamp et al. [81 Kle1].

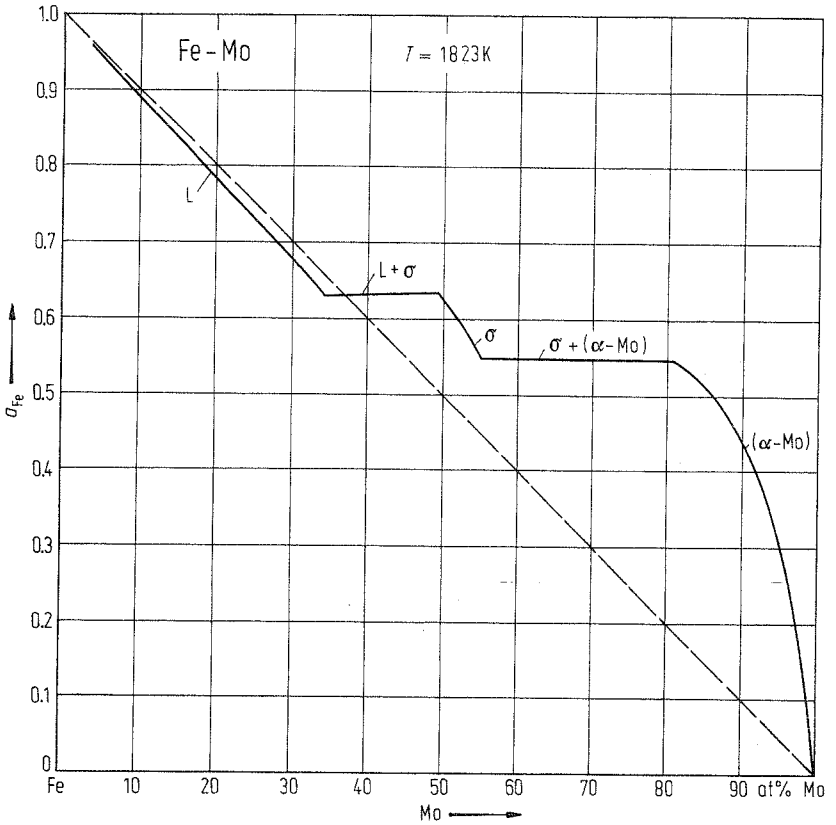

Fig. 3. Fe–Mo. Thermodynamic activity of Fe in liquid and solid alloys at 1823 K.

Fe–N (Iron–Nitrogen)

Phase diagram

Fry [23 Fry1] and Sawyer [23 Saw1], obviously, have been the first who investigated phase equilibria of this system. Later on, many authors have been engaged in establishing the Fe–N phase diagram. Reviews were given by Hansen et al. [58 Han1], Elliott [65 Ell1], Shunk [69 Shu1], Kubaschewski [82 Kub1] and Wriedt et al. [93 Wri1]. For original works the reader is referred to the listings of literature in these reviews.

As Kubaschewski [82 Kub1] pointed out, the phase diagram usually presented for a pressure of 0.1 MPa includes metastable phases like Fe_4N and Fe_2N. The assessed phase diagram in Fig. 1, which has been based on information from Wriedt et al. [93 Wri1], thus shows metastable solid-solid phase equilibria.

The amount of solubility of N in liquid iron has been determined by Gomersall et al. [68 Gom1] and Ishii et al. [82 Ish1]. The results have been confirmed by thermodynamic modelling by Frisk [89 Fri1]. From the latter author information was taken to draw Fig. 2.

The solubility of N in solid iron has been measured rather often (see for instance McLellan [64 McL1], McLellan et al. [80 McL1]). The results are in good agreement with calculated ones on the basis of thermodynamic considerations by Guillermet et al. [94 Gui1] and Du [93 Du1]. The solubility data presented by Du [93 Du1] (for N_2 gas pressure of 1 atm) are plotted in Fig. 3.

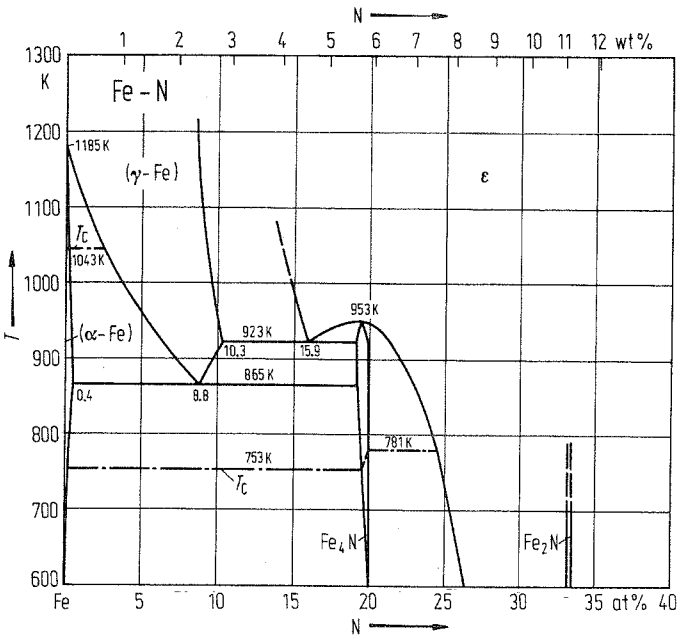

Fig. 1. Fe–N. Phase diagram including metastable solid-solid equilibria.

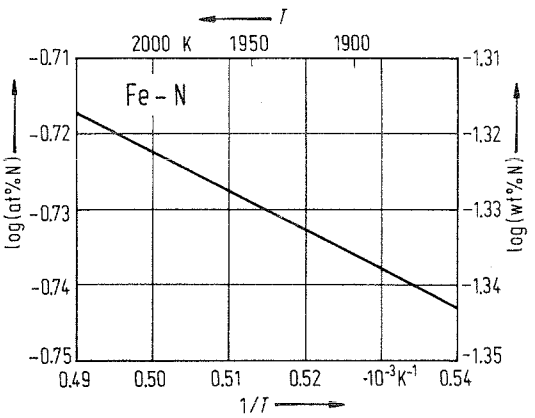

Fig. 2. Fe–N. Solubility of nitrogen in liquid iron.

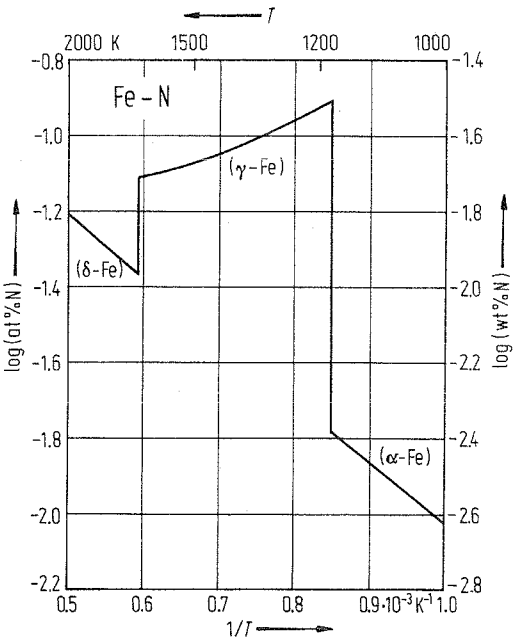

Fig. 3. Fe–N. Solubility of nitrogen in solid iron.

Crystal structure

Crystallographic data of some intermediate phases are listed in Table 1. For other phases lattice parameters are plotted in Figs. 4 to 6.

Lattice constants of the fcc (γ-Fe) solid solutions have been determind rather often (see discussion by Wriedt et al. [93 Wri1]). Measurements were performed using samples quenched to room temperature. Means of the results as published by Wriedt et al. [93 Wri1] are plotted in Fig. 4.

For cubic (Fe_4N) lattice parameters have been determined by Jack [48 Jac1], Paranjpe et al. [50 Par1], Burdese [55 Bur1], Bridelle [55 Bri1] and Somers et al. [89 Som1]. After discussion of all available data, Somers et al. [89 Som1] have proposed lattice parameters which are given in Fig. 5.

Lattice parameters of the ε phase have been determined several times, too (see discussion by Wriedt et al. [93 Wri1]). Comprehensive data published by Paranjpe et al. [50 Par1] are given in Fig. 6.

Table 1. Fe–N. Crystal structure and lattice parameters of intermediate phases.

Phase	Structure	Type	*a* [nm]	*c* [nm]	Ref.
Fe_8N	tetr	Fe_8N	0.5720	0.6292	51 Jac1
Fe_4N	cub	CaO_3Ti	0.3795		55 Wie1, 87 Jac1
Fe_3N	hex	NiAs	0.2705	0.4376	75 Ino1
Fe_5N_2	hex	NiAs	0.27442	0.44025	74 Bou1
Fe_2N	hex	V_2N	0.4787	0.4418	57 Bur1

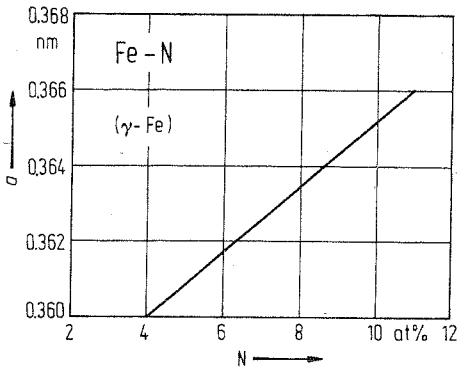

Fig. 4. Fe–N. Lattice parameter for fcc (γ-Fe) solid solution.

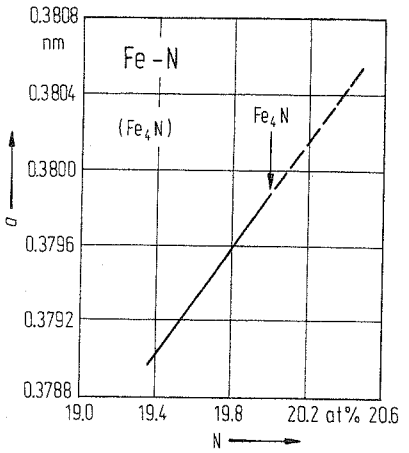

Fig. 5. Fe–N. Lattice parameter for cubic (Fe_4N) solid solution.

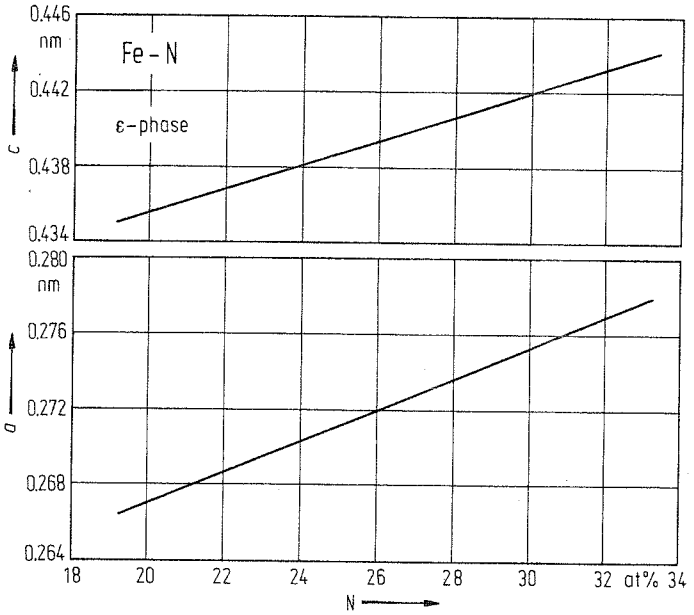

Fig. 6. Fe–N. Lattice parameter for cph phase ε.

Thermodynamics

By thermodynamic modelling Guillermet et al. [94 Gui1] have calculated enthalpies of formation of (metastable) nitrides of Fe. Results are listed in Table 2. In the order of magnitude, these data are in agreement with some ΔH^S values from other sources.

Table 2. Fe–N. Enthalpy of formation of nitrides of iron calculated by Guillermet et al. [94 Gui1].

Phase	ΔH^S [kJ g-atom^{-1}]
Fe_4N	– 0.43
Fe_2N	– 1.88
FeN	3.21
FeN_3	75.31

Fe–Na (Iron–Sodium)

Phase diagram

No solubility of Na in Fe could be found (Wever [29 Wev1, 28 Wev1]).

The solubility of Fe in liquid Na has been investigated several times. The most comprehensive research work was done by Awasthi et al. [83 Awa1]. Data from the literature were discussed thoroughly by Sangster et al. [93 San2], who published a comprehensive review of this system. A decisive influence on the solubility of Fe in Na has the content of oxygen in liquid sodium. Obviously therefore solubility results are scattering widely. At ≈ 800 K the solubility of Fe in liquid Na amounts to ≈ 1 wt ppm with an experimental scatter between 0.1 and 0.001 wt ppm [93 San2].

On the basis of the above mentioned information, Sangster et al. [93 San2] have proposed an assessed phase diagram, which was taken to construct Fig. 1

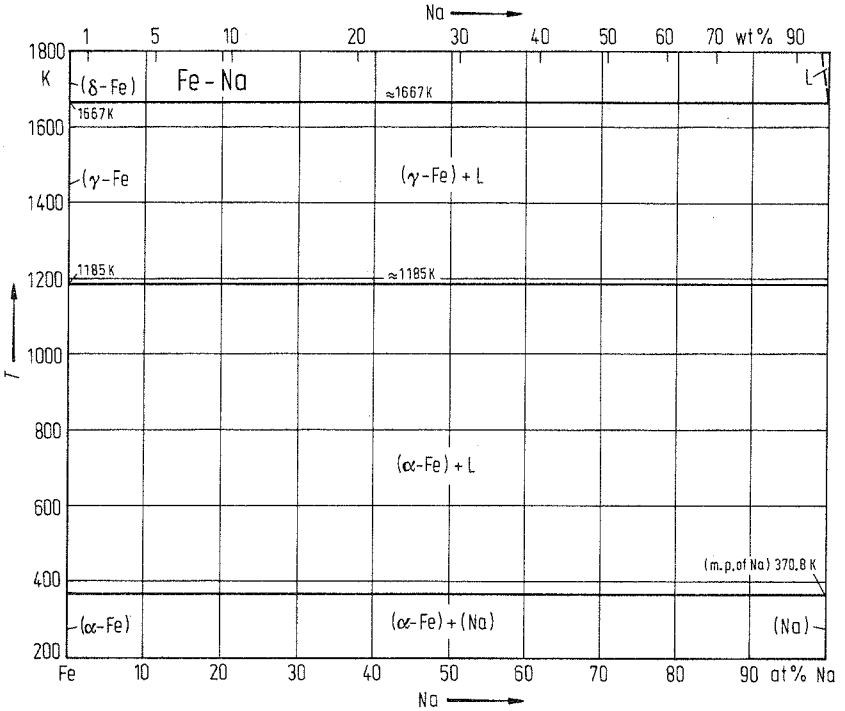

Fig. 1. Fe–Na. Phase diagram.

Fe–Nb (Iron–Niobium)

Phase diagram

Phase equilibria have been determined first by Eggers et al. [38 Egg1] (liquidus; thermal analysis), as well as Vogel et al. [38 Vog1] and Voronov [37 Vor1]. Later on, several more authors have investigated experimentally the phase diagram, especially Gibson et al. [61 Gib1] (solid-liquid equilibria; thermal analysis), Fischer et al. [70 Fis1], Ferrier et al. [64 Fer1] and Goldschmidt [57 Gol1, 60 Gol1]. By thermodynamic modelling Kaufman et al. [78 Kau2] have optimized the phase equilibria. Kubaschewski [82 Kub1] published a review of the phase diagram. Paul et al. [93 Pau1] have discussed phase equilibria and properties of this system and reported an assessed phase diagram, which has been taken as a basis for Fig. 1.

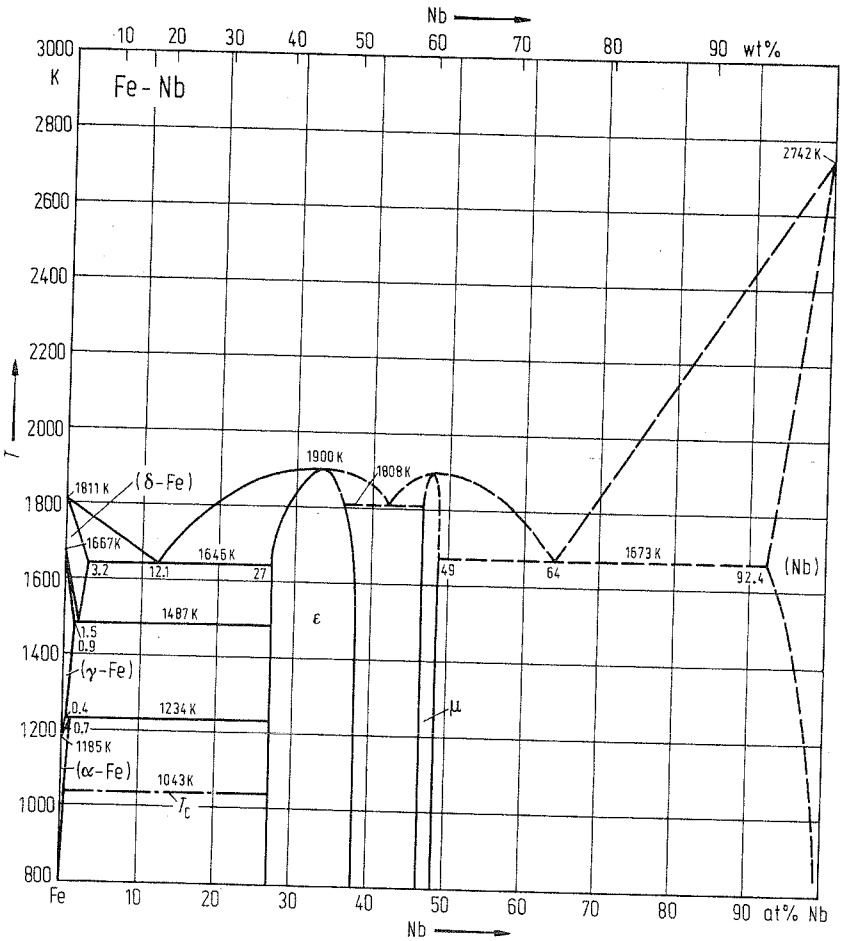

Fig. 1. Fe–Nb. Phase diagram.

Crystal structure

Intermediate phases of the Fe–Nb system have been investigated very often (see Paul et al. [93 Pau1]). Lattice parameters of bcc (α-Fe) solid solutions are plotted in Fig. 2 (taken from Abrahamson et al. [66 Abr1]).

The lattice parameters of the hexagonal ε phase ($MgZn_2$ Laves-type) have been reported by Denham [67 Den1] to be $a = 0.48414$ nm and $c = 0.78933$ nm (at 32.7 at% Nb; $T = 298$ K).

Kripyakevich et al. [68 Kri1] found for the lattice parameters of the hexagonal μ phase (Fe_7W_6-type): $a = 0.4928$ nm; $c = 2.683$ nm (at 50 at% Nb; $T = 298$ K).

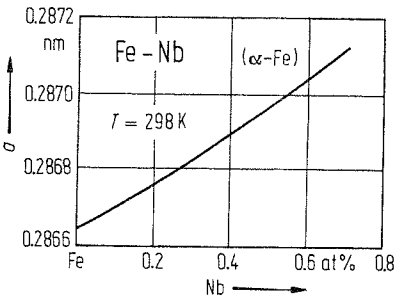

Fig. 2. Fe–Nb. Lattice parameter for bcc (α-Fe) solid solution at 298 K.

Thermodynamics

The enthalpies of mixing of liquid Fe–Nb alloys have been measured calorimetrically by Iguchi et al. [82 Igu1]. The results are plotted in Fig. 3.

Using the EMF method the enthalpies and entropies of formation of Fe_2Nb (ε phase) have been determined. The results are given in Table 1.

Table 1. Fe–Nb. Enthalpy of formation and entropy of formation of Fe_2Nb.

ΔH^S [kJ g-atom^{-1}]	ΔS^S [J g-atom^{-1} K^{-1}]	Ref.
− 20.5	− 4.6	66 Dro1
− 23.7	− 4.6	69 Bar1

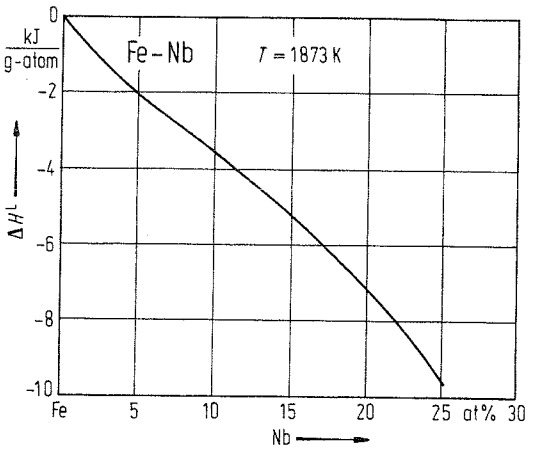

Fig. 3. Fe–Nb. Enthalpy of mixing for liquid alloys at 1873 K.

Fe–Nd (Iron–Neodymium)

Phase diagram

Phase equilibria at concentrations up to 80 at% Nd have been investigated by Terekhova et al. [65 Ter1] (thermal analysis, X-ray diffractography, metallographic observations, microhardness measurements, measurements of electrical resistivity). A review of this system has been published by Kubaschewski [82 Kub1].

Later on, Schneider et al. [87 Sch1] have cleared up the phase equilibria applying differential thermal analysis and X-ray diffraction analysis. Other work was done, too (see the review of the system by Zhang et al. [93 Zha1]). Especially should by mentioned the optimization of the phase diagram by thermodynamic calculation (Schneider et al. [87 Sch1]). Discussing all available works, Zhang et al. [93 Zha1] has proposed an assessed phase diagram, which was the basis for Fig. 1.

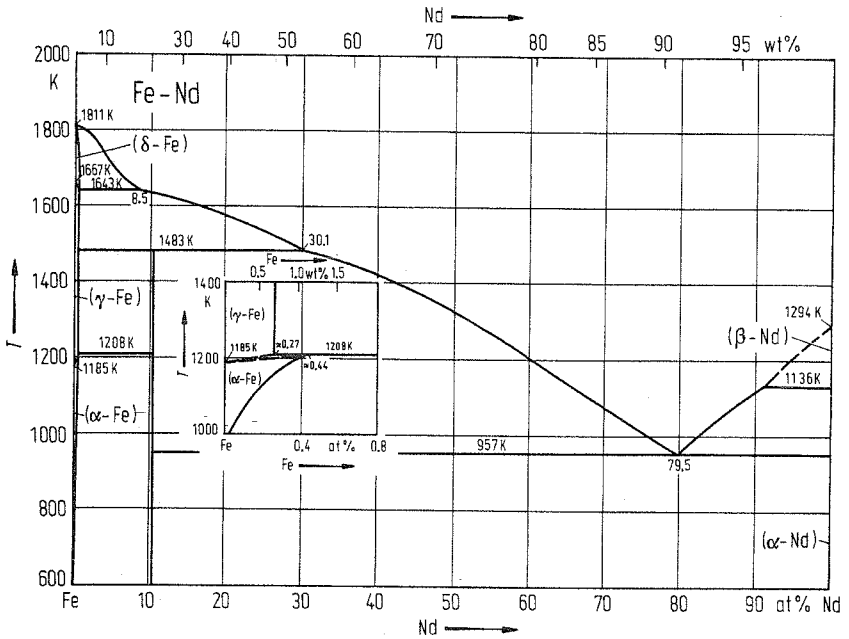

Fig. 1. Fe–Nd. Phase diagram.

Crystal structure

The only stable intermediate phase found in this system is $Fe_{17}Nd_2$ (Schneider et al. [87 Sch1]). Its crystallographic data are: hexagonal, isotypic with Th_2Zn_{17}; $a = 0.8571$ nm, $c = 1.245$ nm (Stadelmaier et al. [86 Sta1], Terekhova et al. [65 Ter1], Ray [66 Ray1]).

Gschneidner jr. [61 Gsc1] and Terekhova et al. [65 Ter1] have found the phase Fe_2Nd, but this could not be confirmed by later investigations.

By splat cooling, $Fe_{5+x}Nd$ could be prepared by Stadelmaier et al. [86 Sta1], where $x < 3.5$. Its structure is hexagonal ($CaCu_5$-type); $a = 0.4946$ nm, $c = 0.4170$ nm (see [86 Sta1]).

Fe_7Nd could be obtained also as a metastable phase by rapid cooling of the melt (Schneider et al. [86 Sch1]). This phase has a hexagonal structure (Co_4Fe_4 Th-type) with $a = 0.8578$ nm and $c = 1.2462$ nm (Ray [66 Ray1], Ray et al. [64 Ray1]).

Fe–Ni (Iron–Nickel)

Phase diagram

The first attempts to establish the phase diagram in this system were done by Osmond [1899 Osm1], Guertler et al. [05 Gue1] and Ruer et al. [10 Rue1], followed by a lot of other authors. Of the reviews should be mentioned those by March [38 Mar1], Hansen et al. [58 Han1], Elliott [65 Ell1], Shunk [69 Shu1], Kubaschewski [82 Kub1] and Swartzendruber et al. [93 Swa1].

The solid-liquid gap is rather small and the scatter of the experimental results relatively high. Most confidence is given by Swartzendruber et al. [93 Swa1] to thermodynamic calculations by Tomiska et al. [85 Tom1] on the basis of vapor pressure measurements using the Knudsen method combined with mass spectrometry. These results were taken to construct Fig. 1.

The kinetics of transformation in the solid state below 1000 K is rather sluggish. Phase equilibria have been determined several times with great effort. On the basis of results present in the literature, Swartzendruber et al. [93 Swa1] have proposed an assessed phase diagram for temperatures < 1200 K, which has been taken to construct Fig. 2.

The order-disorder transformation concerning $FeNi_3$ has been investigated using different methods, for instance X-ray diffractography (difficult due to almost equal X-ray scattering factors of the components) (Leech et al. [39 Lee1]), magnetic measurements, electrical resistivity and hardness measurements (Dahl [36 Dah1]), electron microscope observations (Heumann et al. [63 Heu1]), neutron scattering (Lefebvre et al. [81 Lev1]) (see Swartzendruber et al. [93 Swa1]).

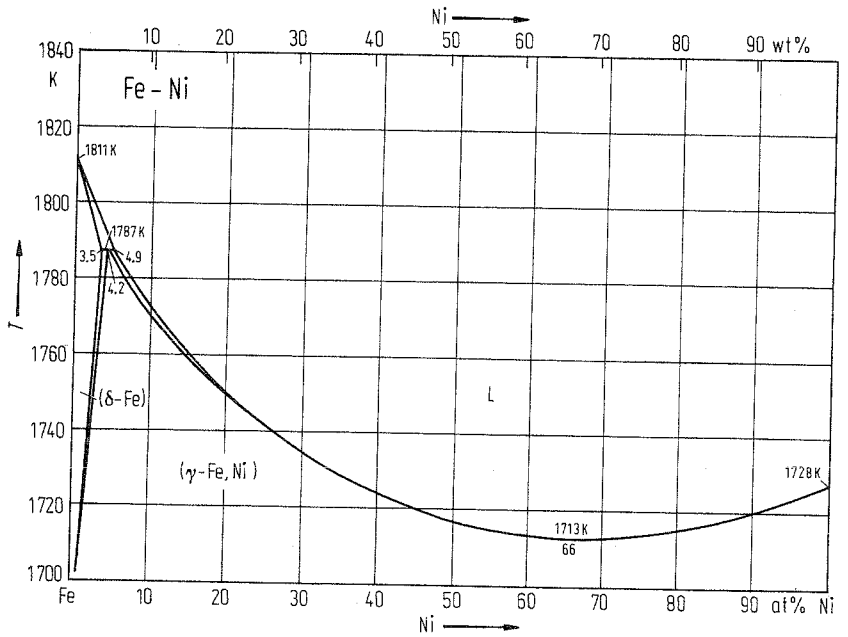

Fig. 1. Fe–Ni. Phase diagram (solid - liquid equilibria).

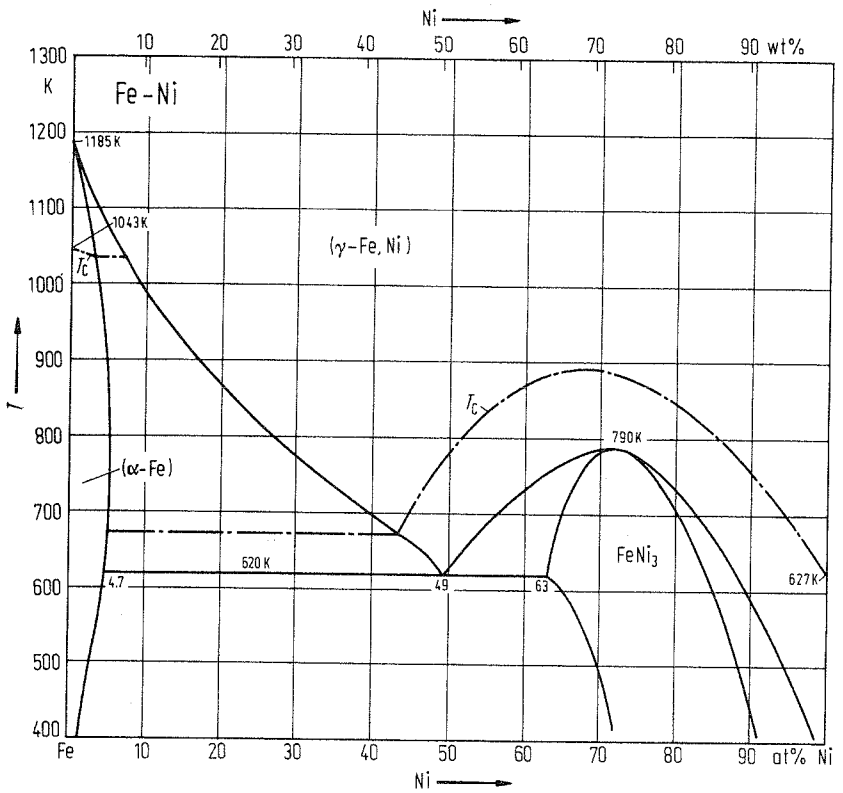

Fig. 2. Fe–Ni. Phase diagram (solid - solid equilibria).

High pressure

Kaufman et al. [61 Kau1] have calculated phase equilibria in the Fe–Ni system at high pressures. The results obtained for 50, 100 and 150 kbar are given in Fig. 3 to 5. The miscibility gap occurring at pressures > 60 kbar may be the reason for the origin of the microstructure of iron–nickel meteorites (plessite), which consist of a mixture of lamellae with low nickel (kamacite, bcc) and high Ni content (taenite, fcc).

The effect of hydrostatic pressure on the martensitic start temperature, M_s, was investigated by Kakeshita et al. [87 Kak1]. M_s is reduced with raising pressure, as can be seen from Fig. 6, where the difference, $\Delta M_s = M_s(p) - M_s(0)$, is plotted as a function of pressure, with $M_s(p)$ and $M_s(0)$ respectively denoting the martensite start temperature with and without application of hydrostatic pressure.

Pope et al. [73 Pop1] have investigated the influence of hydrostatic pressure on the austenite start temperature, A_s, of an Fe–Ni alloy containing 29.3 at% Ni. The results are plotted in Fig. 7. The minimum of A_s at 2.3 kbar and the maximum at 6 kbar can be explained on the basis of the difference in compressibility of martensite and austenite. Cold working before application of hydrostatic pressure shifts A_s (found without cold working) to higher pressures and higher temperatures.

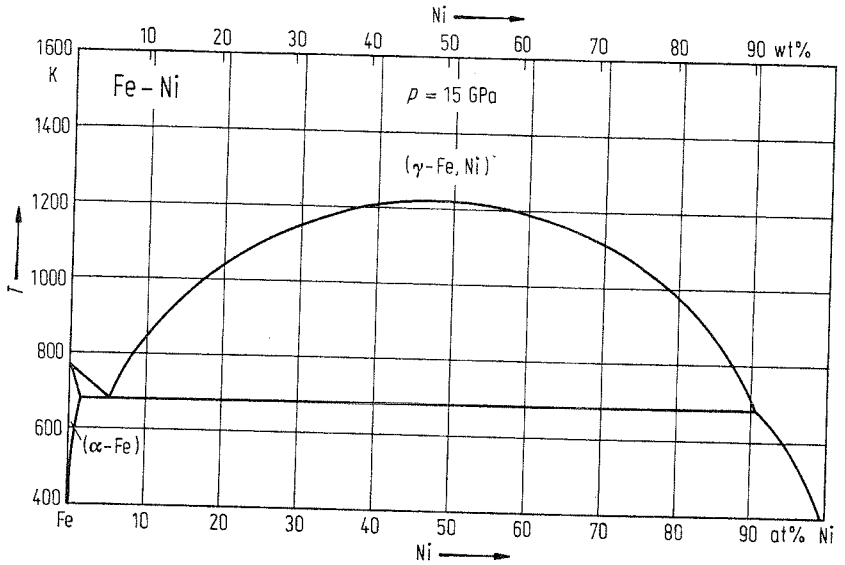

Fig. 5. Fe–Ni. Solid - solid phase equilibria at 15 GPa.

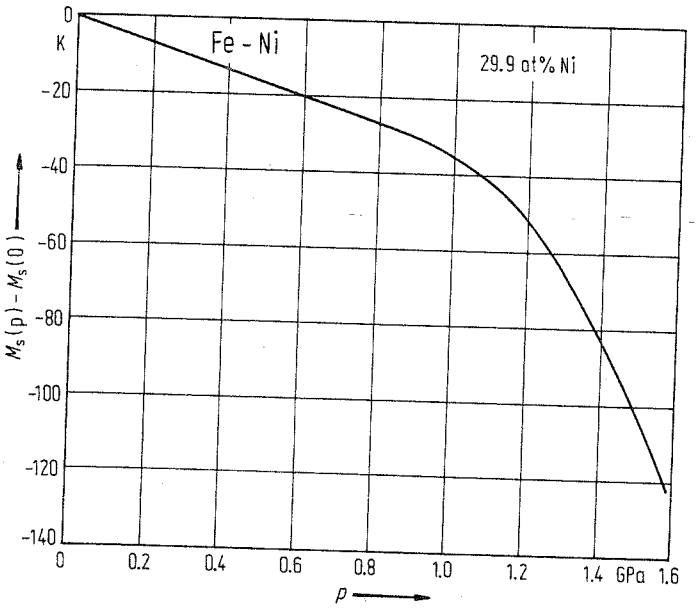

Fig. 6. Fe–Ni. Hydrostatic pressure dependence of the martensitic transformation starting temperature on cooling for an alloy containing 29.9 at% Ni.

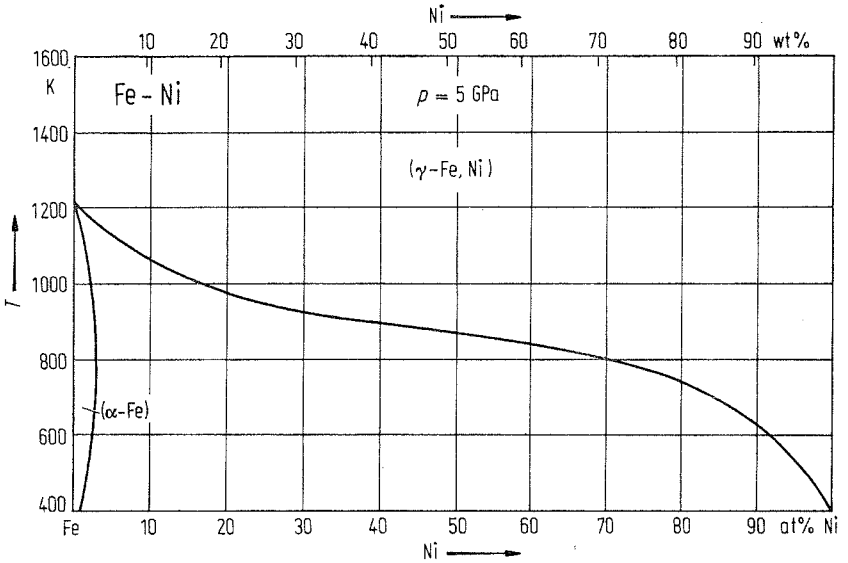

Fig. 3. Fe–Ni. Solid - solid phase equilibria at 5 GPa.

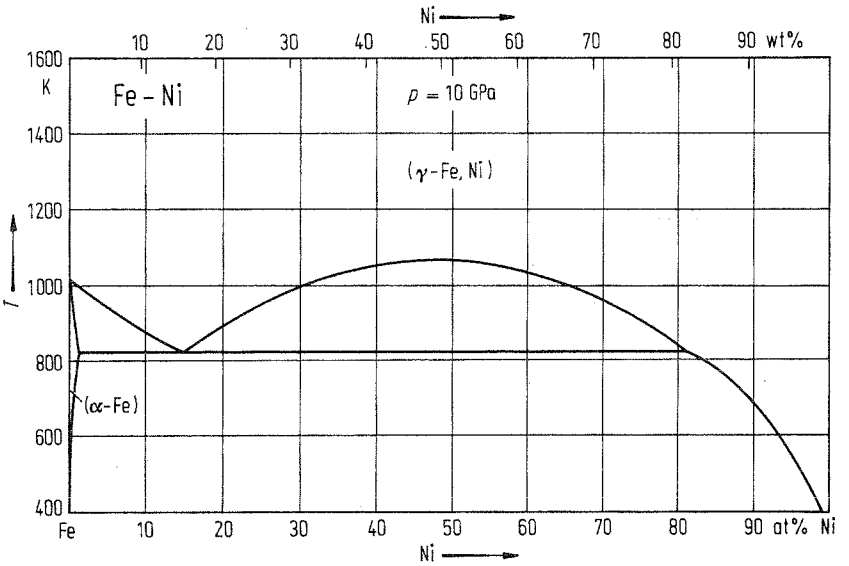

Fig. 4. Fe–Ni. Solid - solid phase equilibria at 10 GPa.

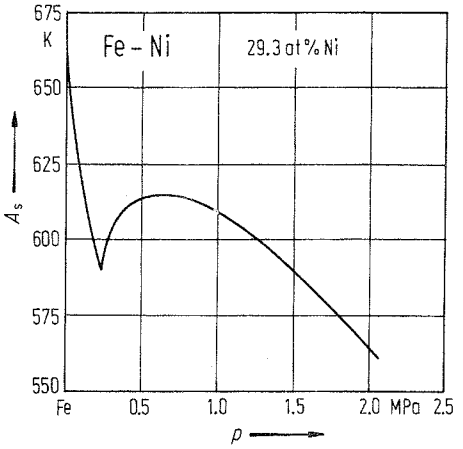

Fig. 7. Fe–Ni. Hydrostatic pressure dependence of the martensitic transformation starting temperature on heating for an alloy containing 29.3 at% Ni.

Metastable phases

Martensitic transformation takes place at concentrations of about ≤ 40 at% Ni if there is not time enough for diffusion to reach equilibrium. Swartzendruber et al. [93 Swa1], on the basis of results present in the literature, have plotted the starting temperature (M_s), the finish temperature (M_f) occurring on cooling, as well as the temperature for the starting of the reverse transformation of the martensite formation on heating (A_s) and the corresponding temperature of the finish of this austenitizing reaction (A_f). This diagram has been taken as a basis to draw Fig. 8.

Just Dehlinger [34 Deh1] stated that the product of the martensitic transformation in the Fe–Ni system has bcc structure.

Metastable superstructures with stoichiometry Fe_3Ni and FeNi have been investigated by Pauleve et al. [62 Pau1] using samples heavily irradiated by neutrons. In meteorites such structures have been found, too (Petersen et al. [77 Pet1]). A metastable phase diagram containing these superstructures has been proposed by Goldstein et al. [82 Gol1]. Phase equilibria calculated by Yamauchi et al. [84 Yam1] ("coherent phase diagram") are taken to draw Fig. 9.

Reuter et al. [89 Reu1] found indications for the presence of FeNi and Fe_3Ni under equilibrium conditions, too. This is not regarded in Fig. 2. More evidence is necessary.

By sputtering technique, Sumiyama et al. [83 Sum1] have prepared metastable bcc solid solutions with Ni content up to 4 at% Ni. From 40 to 50 at% Ni they found a two-phase region, and at more than 50 at% Ni fcc solid solutions. Lattice parameters of (α-Fe) and (γ-Fe) are somewhat higher for samples obtained by sputtering than for bulk alloys.

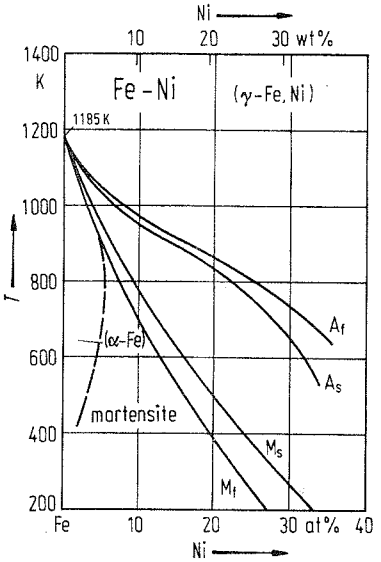

Fig. 8. Fe–Ni. Martensitic transformation temperatures: starting (M_s) and finishing (M_f) temperatures on cooling, and starting (A_s) and finishing (A_f) temperatures on heating.

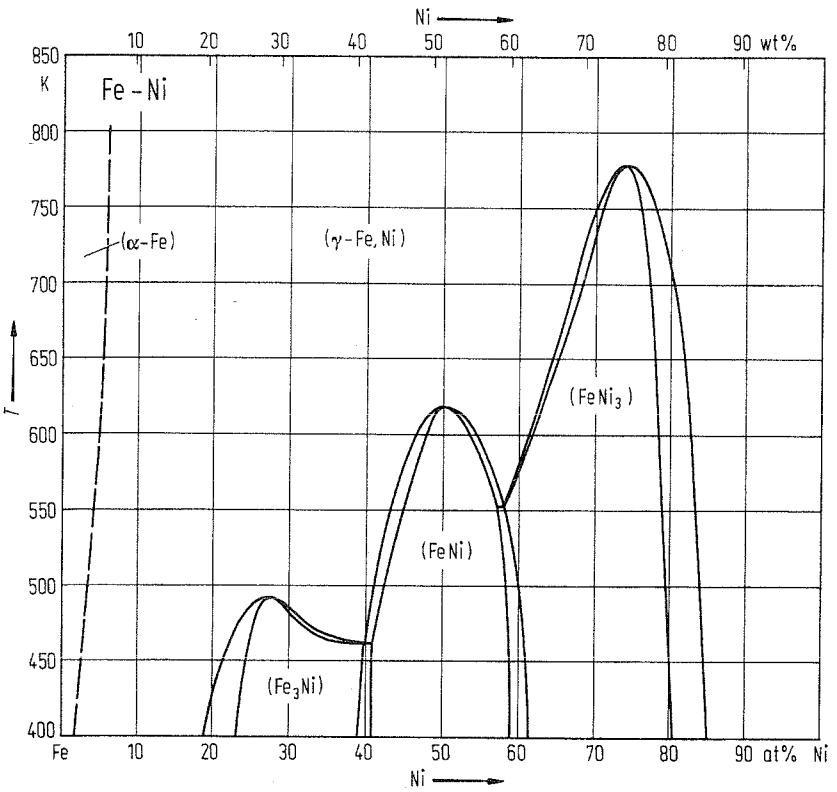

Fig. 9. Fe–Ni. Phase diagram showing metastable phases (Fe_3Ni) and (FeNi).

Crystal structure

Crystallographic data of superstructures in the Fe–Ni system are listed in Table 1.

Lattice parameters of (α-Fe) and of (γ-Fe, Ni) solid solutions are plotted in Fig. 10 and Fig. 11, respectively. The curves given in these figures represent the weighted mean of data found in the literature (Swartzendruber et al. [93 Swa1]).

Table 1. Fe–Ni. Crystal structure and lattice parameters of intermediate phases.

Phase	Structure	Type	*a* [nm]	*c* [nm]	Ref.
$FeNi_3$	cub	Cu_3Au	0.35525		67 Bro1
Metastable phases					
Fe_3Ni	cub	Cu_3Au	0.3575		79 Mio1
FeNi	tetr	AuCu	0.35823	0.35822	80 Cla1

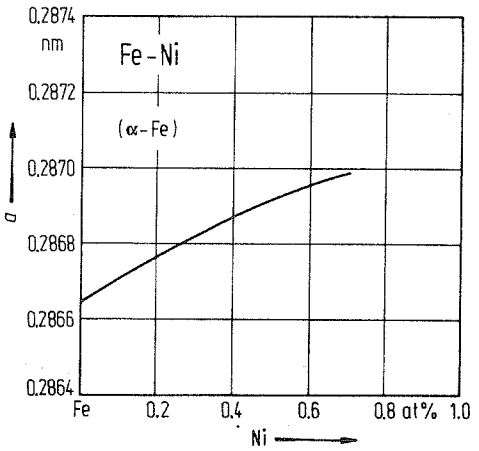

Fig. 10. Fe–Ni. Lattice parameter for bcc (α-Fe) solid solution.

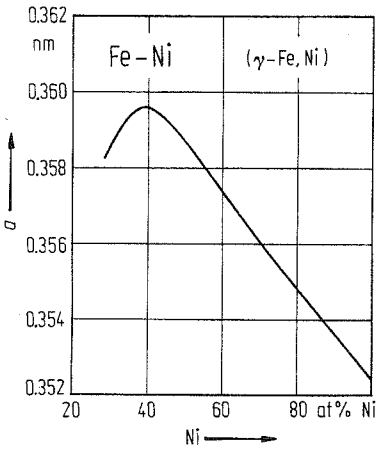

Fig. 11. Fe–Ni. Lattice parameter for fcc (γ-Fe, Ni) solid solution.

Thermodynamics

Reviews of thermodynamic data and of thermodynamic calculations of phase equilibria have been published very often (Hultgren et al. [73 Hul1], Rao et al. [74 Rao1], Kubaschewski et al. [77 Kub1], Chuang et al. [86 Chu2] and others; see [93 Swa1]).

As a result of discussions of available experimentally determined enthalpies of mixing of liquid alloys, Swartzendruber et al. [93 Swa1] have proposed ΔH^L values, which are plotted in Fig. 12.

From the many experimental data for thermodynamic activities in liquid Fe–Ni alloys, Swartzendruber et al. [93 Swa1] using a thermodynamic model constructed figures for the activity coefficient as a function of concentration for 1873 K. These results of careful discussions have been taken to draw Fig. 13 (γ_{Fe}) and Fig. 14 (γ_{Ni}).

Experimentally determined enthalpies of formation of (γ-Fe, Ni) solid solutions have been discussed by Swartzendruber et al. [93 Swa1]. From there information was taken to draw Fig. 15 (ΔH^S as a function of concentration).

As Swartzendruber et al. [93 Swa1] stated in their thorough discussion, the experimental data for ΔH^L and ΔH^S ((γ-Fe, Ni) solid solutions) are more or less equal within the experimental errors.

The thermodynamic activities of the components for solid alloys have been measured several times, too. On the basis of these results, Swartzendruber et al. [93 Swa1] have optimized activity coefficient data by modelling. The results for 1473 K were taken to draw Fig. 16 and Fig. 17. For 1273 K activity coefficients of Fe and Ni are given in Fig. 18 and Fig. 19, respectively [93 Swa1].

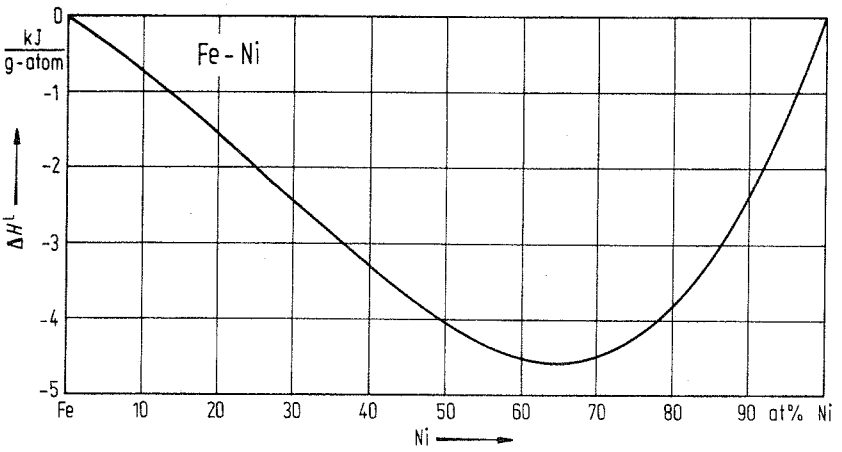

Fig. 12. Fe–Ni. Enthalpy of mixing for liquid alloys.

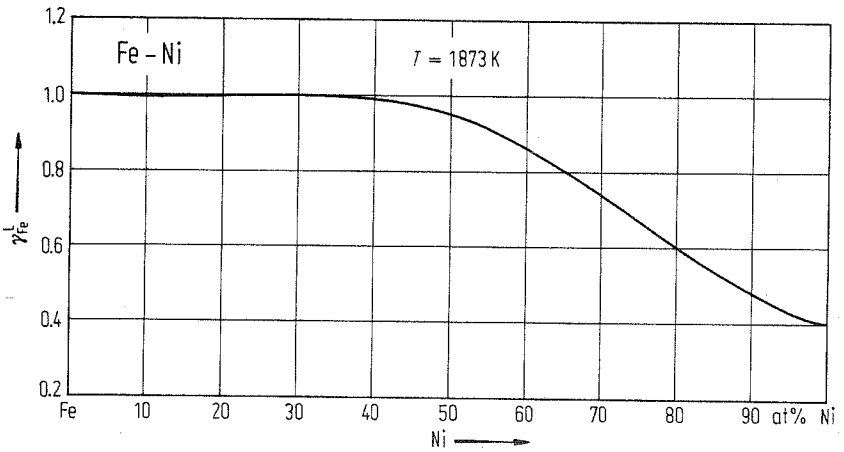

Fig. 13. Fe–Ni. Thermodynamic activity coefficient of Fe in liquid alloys at 1873 K.

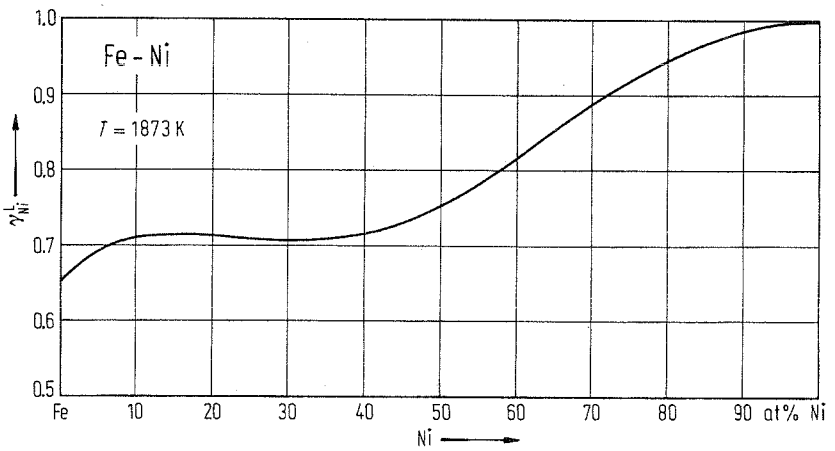

Fig. 14. Fe–Ni. Thermodynamic activity coefficient of Ni in liquid alloys at 1873 K.

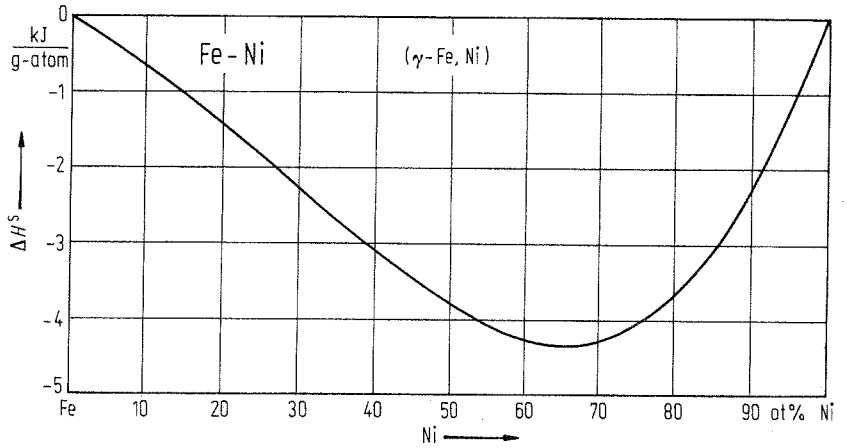

Fig. 15. Fe–Ni. Enthalpy of formation for (γ-Fe, Ni) solid solutions.

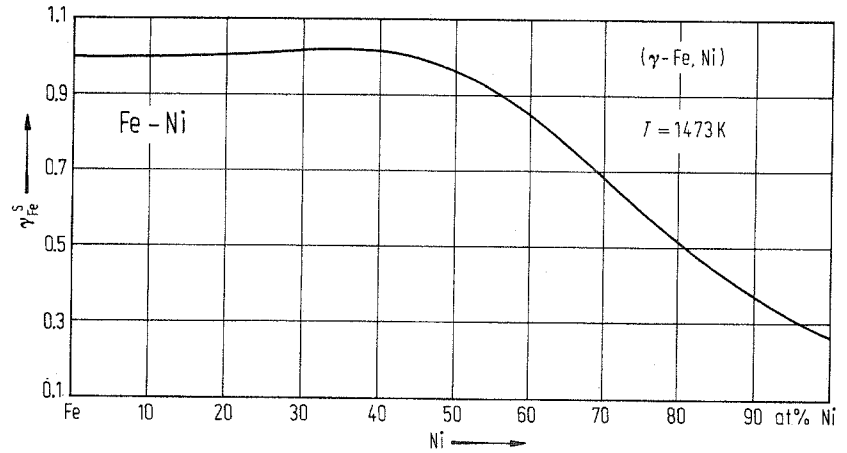

Fig. 16. Fe–Ni. Thermodynamic activity coefficient of Fe in (γ-Fe, Ni) solid solutions at 1473 K.

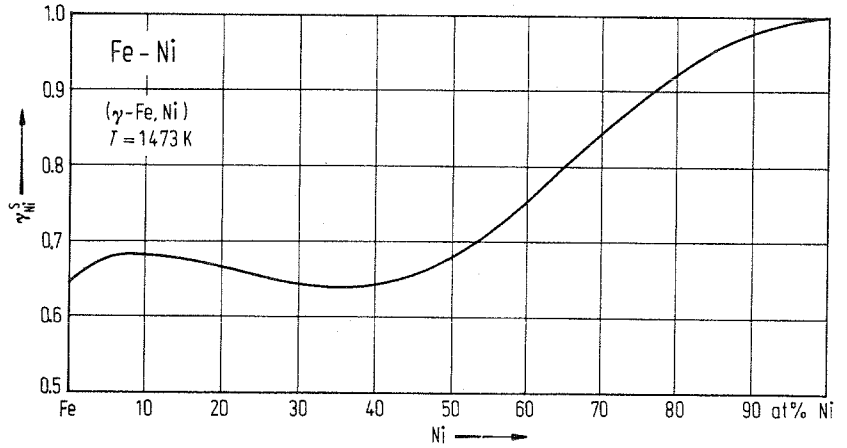

Fig. 17. Fe–Ni. Thermodynamic activity coefficient of Ni in (γ-Fe, Ni) solid solutions at 1473 K.

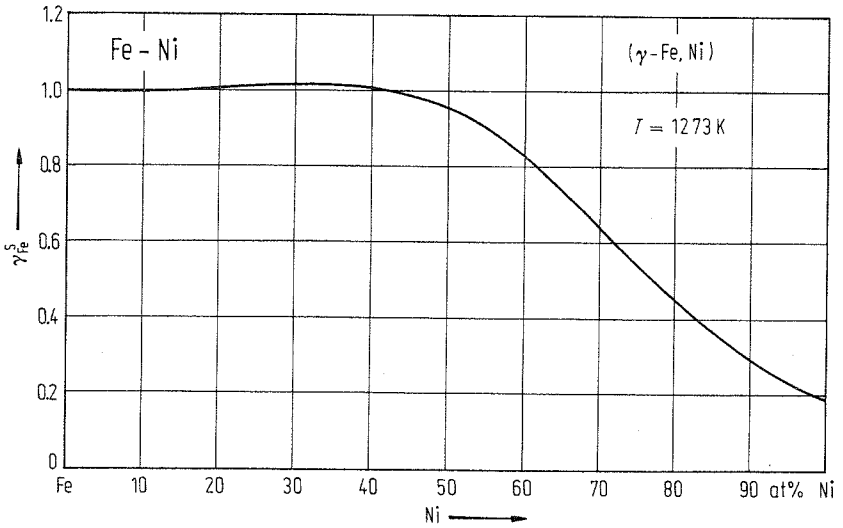

Fig. 18. Fe–Ni. Thermodynamic activity coefficient of Fe in (γ-Fe, Ni) solid solutions at 1273 K.

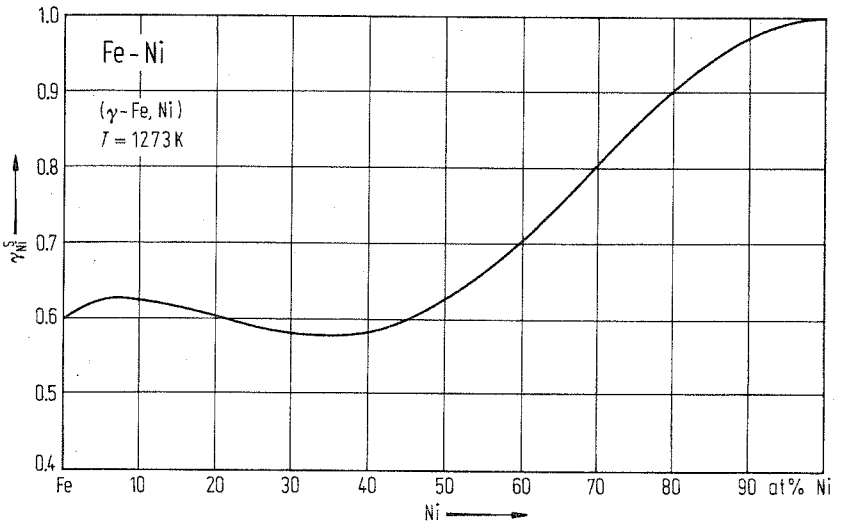

Fig. 19. Fe–Ni. Thermodynamic activity coefficient of Ni in (γ-Fe, Ni) solid solutions at 1273 K.

Fe–Np (Iron–Neptunium)

The phase diagram is not known.

Two intermediate phases have been found and investigated. Their crystallographic data are given in in Table 1.

Table 1. Fe–Np. Crystal structure and lattice parameters of intermediate phases.

Phase	Structure	Type	*a* [nm]	*c* [nm]	Ref.
Fe_2Np	cub	Cu_2Mg	0.71444		72 Lam1, 75 Ald1
$FeNp_6$	tetr	MnU_6	1.0224	0.5238	77 Gie1

Fe–O (Iron–Oxygen)

Phase diagram

Many works have been done to investigate the phase diagram. For reviews see, for instance, Hansen et al. [58 Han1], Kubaschewski [82 Kub1] and Wriedt [93 Wri2]. On the basis of phase equilibria published by Darken et al. [46 Dar1], Wriedt [93 Wri2] has constructed an assessed diagram of phases stable at 0.1 MPa, which has been taken to draw Fig. 1. Fig. 2 shows the phase equilibria in the concentration range between 50 and 61 at% O on enlarged scale.

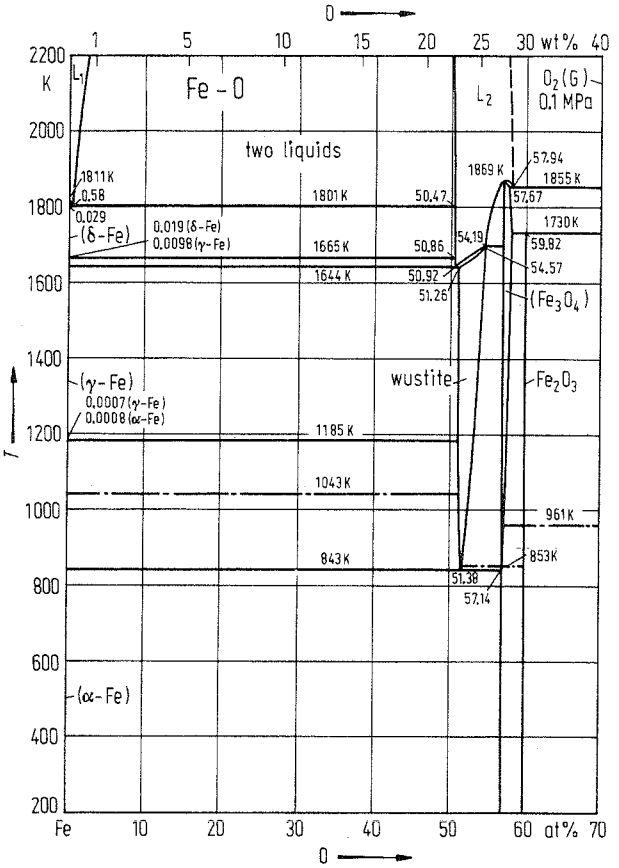

Fig. 1. Fe–O. Phase diagram at 0.1 MPa. Dashed-dotted line: Curie temperature T_C.

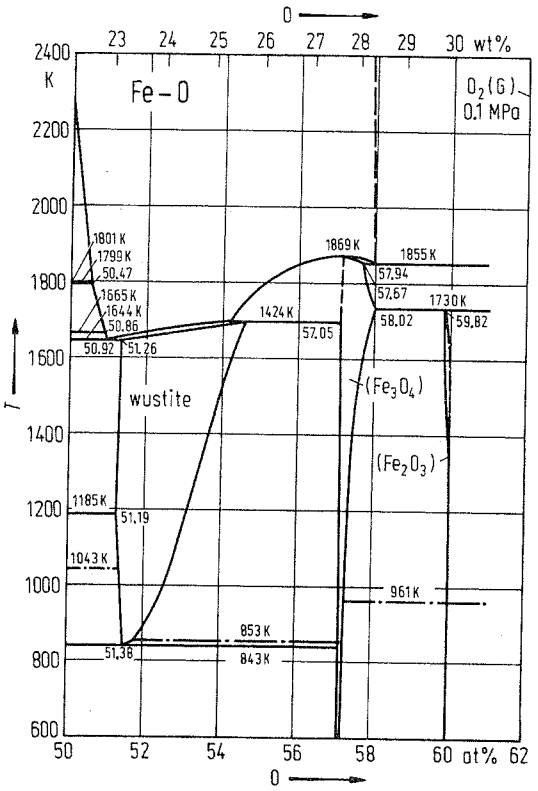

Fig. 2. Fe–O. Partial phase diagram (50...61 at% O).
Dashed-dotted line: Curie temperature T_C.

Metastable phases

If quenched to temperatures < 500 K, wüstite does not decompose into (α-Fe) and Fe_3O_4, but can be retained as a metastable phase. Three types of the metastable wüstite were found. For their atomic arrangement see Manenc [68 Man1] and Wriedt [93 Wri2].

At ≈ 183 K metastable wüstite transforms from the paramagnetic state to an antiferromagnetic state.

Further on, the modifications β-Fe_2O_3, γ-Fe_2O_3 and ε-Fe_2O_3 should be mentioned as metastable ones (see below).

Crystal structure

Crystallographic data of iron oxides are listed in Table 1.

Table 1. Fe–O. Crystal structure and lattice parameters of intermediate phases.

Phase	at% O	T [K]	Structure	Type	a [nm]	b [nm]	c [nm]	Ref.
wüstite	52.1	1273	cub	NaCl	0.43536			74 Toul
Fe_3O_4 (l)	57.1	10	mon	Fe_3O_4 (l)	1.1868	1.1851	1.6752	77 Yos1,
						$\beta = 90.20°$		82 Iiz1
Fe_3O_4	57.23	298	cub	Al_2MgO_4	0.8396			69 Bha1
α-Fe_2O_3	60.0	293	hex	α-Al_2O_3	0.50065		1.36411	68 Kas1,
								80 Fin1
Metastable phases								
β-Fe_2O_3	≈ 60.0	298	cub	Mn_2O_3	0.9393			58 Sve1,
								76 Ben1
γ-Fe_2O_3	≈ 60.0	4	tetr		0.83396		2.4966	83 Gre1
ε-Fe_2O_3	≈ 60.0	298	mon		1.297	1.021	0.844	63 Sch1
						$\beta = 95.33°$		

Thermodynamics

The thermodynamic properties of phases in the Fe–O system have been investigated very often. For individual work the reader is referred to the listing in the comprehensive review published by Spencer et al. [78 Spe2]. From this review assessed data mentioned below have been taken.

For the concentration range between 51 and 53.8 at% O the integral enthalpy of mixing of liquid Fe–O alloys is plotted in Fig. 3. The integral entropy of mixing of liquid alloys in this range is shown in Fig. 4 (see Spencer et al. [78 Spe2]).

Selected values for the integral enthalpy of formation and the integral entropy of formation of wüstite, as proposed on the basis of the assessment done by Spencer et al. [78 Spe2], are plotted in Fig. 5 and Fig. 6, respectively.

As the most probable value for the enthalpy of formation of Fe_3O_4 [78 Spe2] have recommended $\Delta H^S = -159(4)$ kJ / g-atom, and for Fe_2O_3 the same authors have selected $\Delta H^S = -165$ kJ / g-atom.

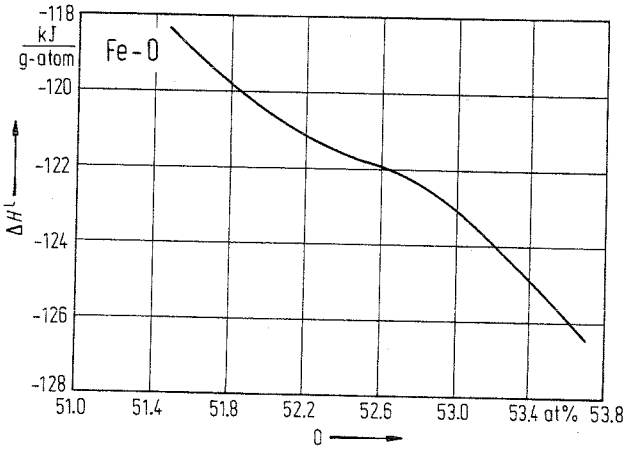

Fig. 3. Fe–O. Enthalpy of mixing for liquid alloys containing 51.5...53.7 at% O.

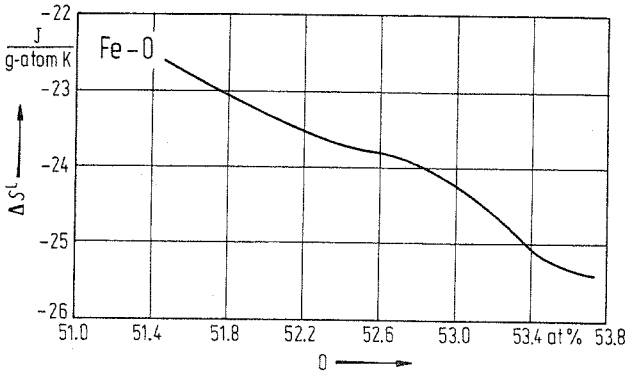

Fig. 4. Fe–O. Entropy of mixing for liquid alloys containing 51.5...53.7 at% O.

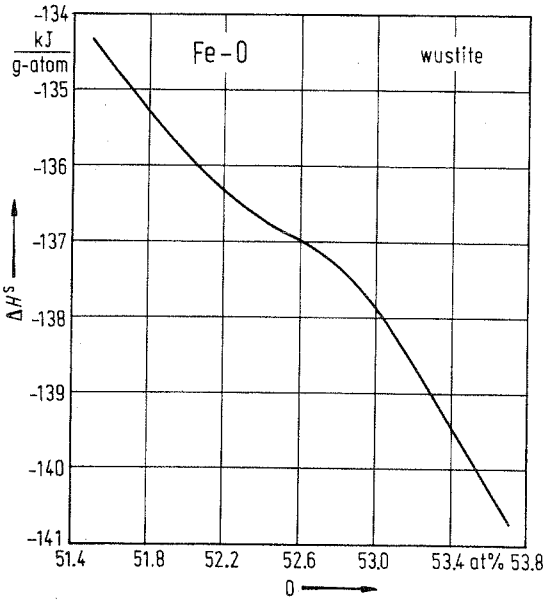

Fig. 5. Fe–O. Enthalpy of formation for wustite.

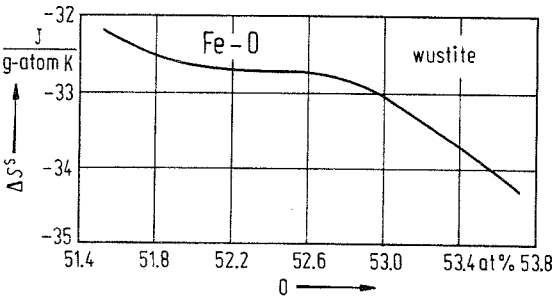

Fig. 6. Fe–O. Entropy of formation for wustite.

Fe–Os (Iron–Osmium)

Phase diagram

Experimental work to establish the phase equilibria has been done by Buckley et al. [63 Buc1] (liquid-solid equilibria up to 7 at% Os) and Fallot [38 Fal1] (thermal analysis concerning the (α-Fe) ⇌ (γ-Fe) transformation). Swartzendruber et al. [93 Swa4], using a regular solution model and applying the above mentioned information, have calculated the phase diagram, which was the basis for Fig. 1.

The Fe-rich part of the phase diagram is given in Fig. 2 on enlarged scale (see Swartzendruber et al. [93 Swa4]).

At concentrations < 15 at% Os a martensitic transformation can take place. The concentration dependence of M_s, M_f, A_s and A_f are plotted in Fig. 3 (see Fallot [38 Fal1] and Swartzendruber et al. [93 Swa4]).

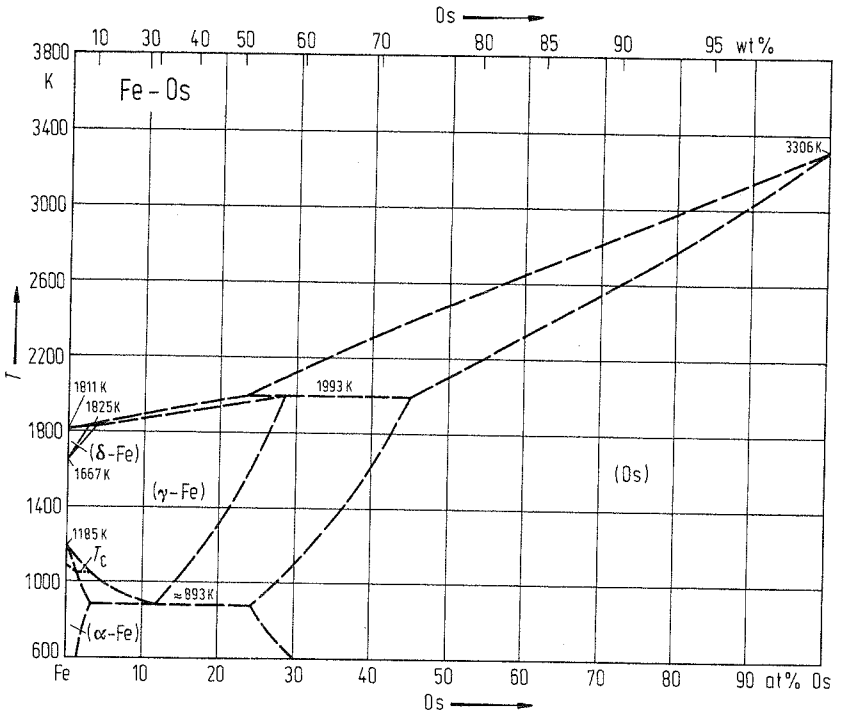

Fig. 1. Fe–Os. Phase diagram.

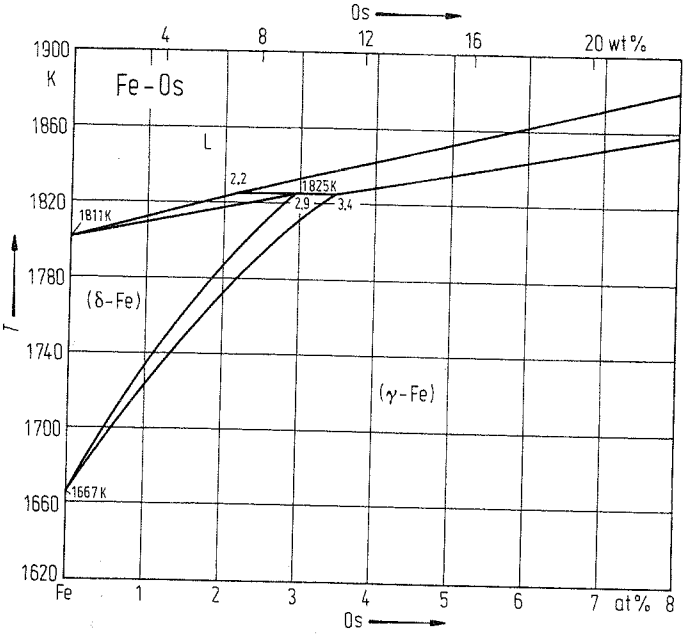

Fig. 2. Fe–Os. Partial phase diagram (Fe-rich part).

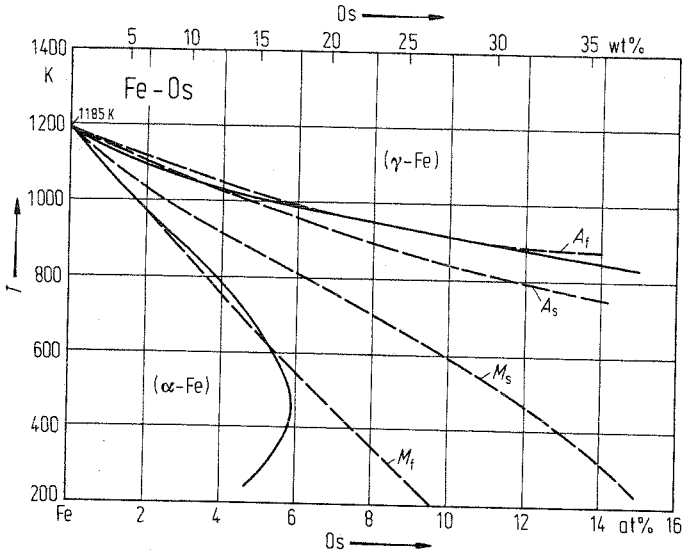

Fig. 3. Fe–Os. Martensitic transformation temperatures for Fe-rich alloys: starting (M_s) and finishing (M_f) temperatures on cooling, and starting (A_s) and finishing (A_f) temperatures on heating. The solid lines indicate the equilibrium phase boundaries.

Fe–P (Iron–Phosphorus)

Phase diagram

Since 1894, where Arnold [1894 Arn1] looked for the (α-Fe) ⇌ (γ-Fe) phase transition in the Fe–P system much work was done to clear up the phase equilibria. Reviews were given by Hansen et al. [58 Han1], Elliott [65 Ell1], Shunk [69 Shu1], Kubaschewski [82 Kub1] and Okamoto [93 Oka2]. The last experimental investigation obtainable is that by Schürmann et al. [81 Sch1]. The results of this work (quantitative thermal analysis) was the basis for the phase diagram assessed by Kubaschewski [82 Kub1]. This latter diagram has been accepted by Okamoto [93 Oka2], and also has been taken to draw Fig. 1.

The (α-Fe) - (γ-Fe) loop is given in Fig. 2 on enlarged scale. Data to draw this figure were taken from Lorenz et al. [62 Lor1] (magnetic measurements) and Okamoto [93 Oka2] (discussion of results from the literature).

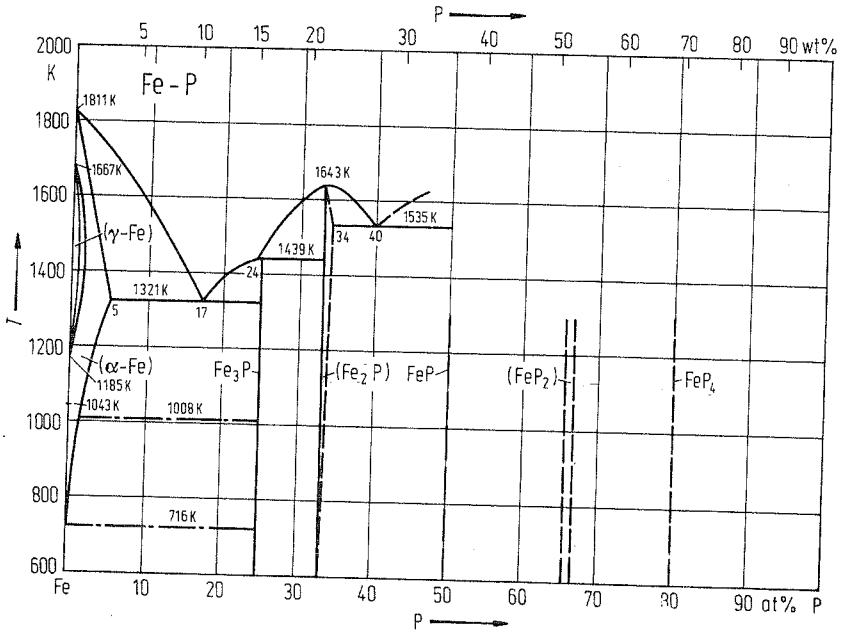

Fig. 1. Fe–P. Phase diagram.

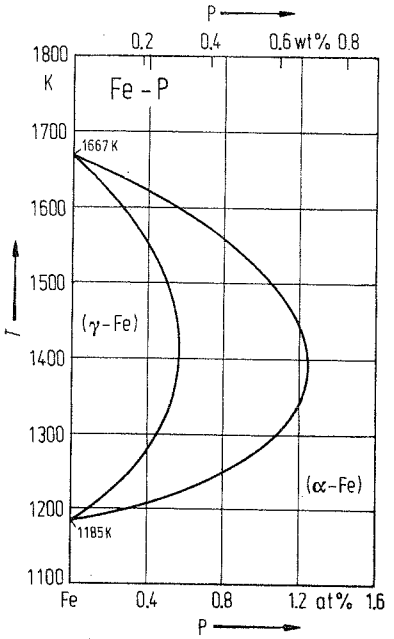

Fig. 2. Fe–P. Partial phase diagram (α-Fe - γ-Fe equilibria).

Metastable phases

(γ-Fe) solid solutions are able to be supersaturated up to 1.9 at% P at 373 K (Kaneko et al. [65 Kan1]).

By precipitation, metastable $Fe_{4+}P$ is obtained in (α-Fe) matrix before Fe_3P occurs, as Hornbogen [61 Hor1] found.

By quenching liquid alloys crystallization of Fe_3P can be omitted. Thus a metastable eutectic L $\rightleftharpoons$ (α-Fe) + Fe_2P occurs at 1203 K (Wachtel et al. [64 Wac1]). The composition of the eutectic point is at 18.7 at% P.

At ≈ 20 at% P amorphous alloys can be prepared by splat-cooling, as Takayama [76 Tak1] reported. The crystallization behavior has been investigated by Hiltunen et al. [83 Hil1, 88 Hil1], and the structural relaxation phenomena were observed calorimetrically by Takayama et al. [81 Tak1].

Crystal structure

Lattice parameters of (α-Fe) solid solutions have been determined by Hattendorf et al. [88 Hat1]. The results obtained on quenched samples are given in Fig. 3.

Crystallographic data of intermediate phases are listed in Table 1.

Table 1. Fe–P. Crystal structure and lattice parameters of intermediate phases.

Phase	Structure	Type	*a* [nm]	*b* [nm]	*c* [nm]	Ref.
Fe_3P	tetr	Ni_3P	0.9108		0.4455	28 Hag1
Fe_2P	hex	Fe_2P	0.5864		0.3460	28 Hag1
FeP	orth		0.51910	0.57909	0.30983	72 Sel1, 68 Bon1
FeP_2	orth	FeS_2 (markasite)	0.49732	0.56570	0.27235	34 Mei1, 68 Hol1
FeP_4	mon		0.4619	1.3670 $\beta = 101.48°$	0.7002	78 Jei1
Metastable phase						
$Fe_{4+}P$	orth		0.359	0.401	0.432	61 Hor1
High-pressure phases						
Fe_2P	orth	Co_2Si	0.5775	0.3571	0.6641	76 Sen1
FeP_4	orth		0.5005	1.0213	0.5530	78 Sug1

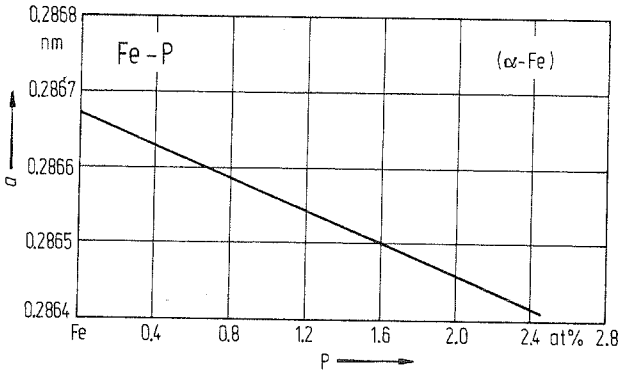

Fig. 3. Fe–P. Lattice parameter for bcc (α-Fe) solid solution.

Thermodynamics

By quantitative thermal analysis, Schürmann et al. [81 Sch1] have determined the enthalpies of mixing in the concentration range up to 33.3 at% P. The results are plotted in Fig. 4.

Spencer et al. [78 Spe1] have assessed the thermodynamic data present in the literature. From there values have been taken for the integral entropies of mixing of liquid alloys at the melting point of iron (1809 K) and the partial Gibbs free enthalpies of mixing of liquid alloys at the same temperature. The data are plotted in Fig. 5 and Fig. 6, respectively. It should be mentioned that in all cases the reference states are liquid iron and liquid "superheated" phosphorus.

By high-temperture calorimetry the enthalpies of formation of Fe_2P and Fe_3P have been determined (Weibke et al. [41 Wei1]). For the formation of Fe_2P (2Fe+P(white)→Fe_2P) and of Fe_3P (3Fe+P(white)→Fe_3P) the enthalpy changes amount to:

Fe_2P: $\Delta H^S = -160.2(84)$ kJ g-atom^{-1},

Fe_3P: $\Delta H^S = -164.0(84)$ kJ g-atom^{-1}.

These data are valid for 298 K.

On the basis of experimental work Spencer et al. [78 Spe1] have selected as reliable enthalpies of formation for other iron phosphides the following data:

FeP: $\Delta H^S = -138.1(125)$ kJ g-atom^{-1},
FeP_2: $\Delta H^S = -220.9(170)$ kJ g-atom^{-1},

each at 298 K.

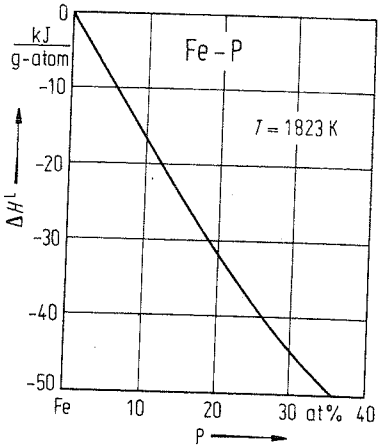

Fig. 4. Fe–P. Enthalpy of mixing for liquid alloys at 1823 K. Reference states: liquid iron and liquid "superheated" phosphorus.

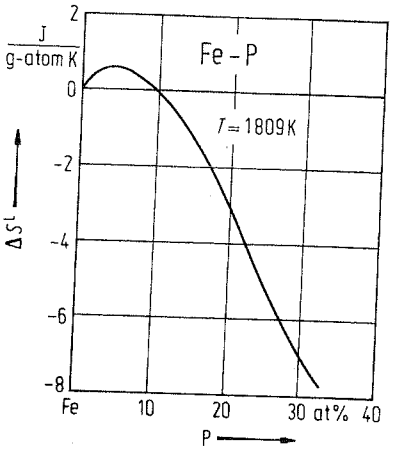

Fig. 5. Fe–P. Entropy of mixing for liquid alloys at 1809 K. Reference states: liquid iron and liquid "superheated" phosphorus.

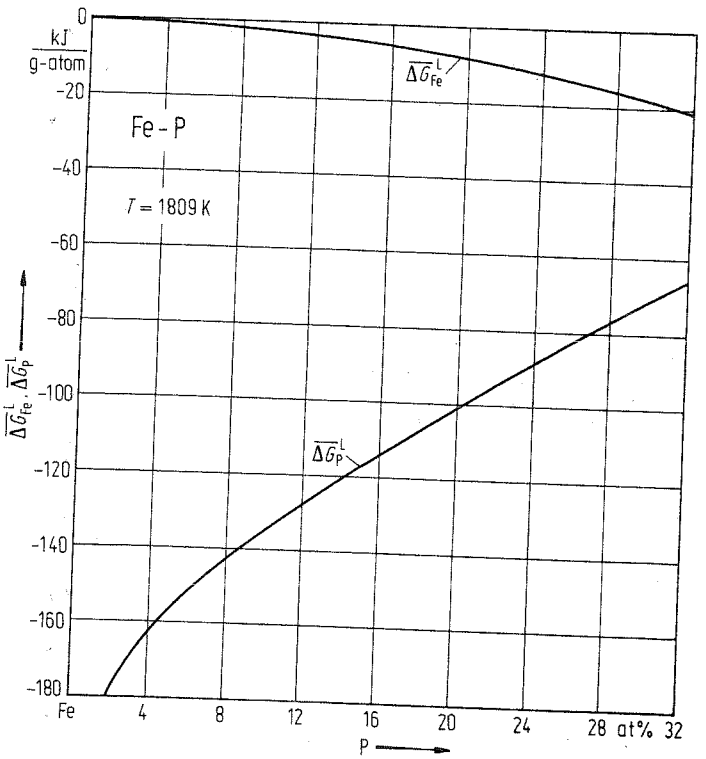

Fig. 6. Fe–P. Partial Gibbs free energies of mixing for Fe and P in liquid alloys at 1809 K. Reference states: liquid iron and liquid "superheated" phosphorus.

Fe–Pb (Iron–Lead)

Phase diagram

The Fe–Pb system is characterized by very low mutual solubility in the solid state as well as in the liquid state. Lord et al. [60 Lor1], Araki [63 Ara1] and Morozov et al. [71 Mor1] have investigated the solubility of Pb in liquid Fe. Later on, more work was done. The most probable solubility data are those reported by [71 Mor1]. They are plotted in Fig. 1 (see Burton [93 Bur1]).

The solubility of Fe in liquid Pb has been determined experimentally by Miller et al. [60 Mil1], Stevenson et al. [61 Ste1] and Ali-Khan [82 Ali1]. The discussion by Burton [93 Bur1] showed that the results obtained by Stevenson et al. [61 Ste1] should be preferred. They were taken to draw Fig. 2.

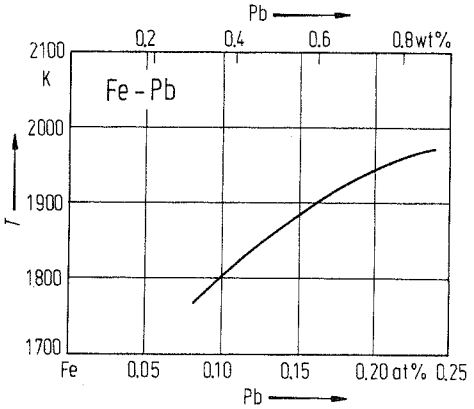

Fig. 1. Fe–Pb. Solubility of Pb in liquid iron.

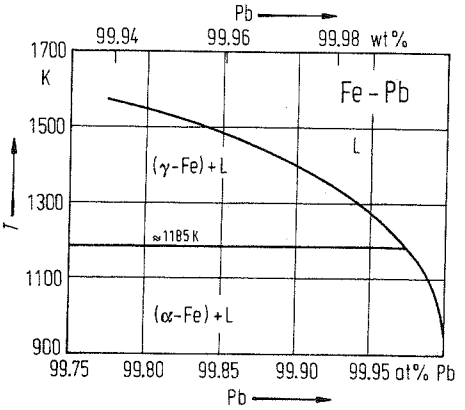

Fig. 2. Fe–Pb. Partial phase diagram (Pb-rich part).

Fe–Pd (Iron–Palladium)

Phase diagram

First experimental work to clear up the phase equilibria has been done by Grigorev [31 Gri1, 32 Gri1], Kuprina et al. [59 Kup1], Raub et al. [63 Rau1] and Kussmann et al. [63 Kus1]. Results of these investigations have been taken by Kubaschewski [82 Kub1] to propose an assessed phase diagram. Further on, an experimental investigation by Gibson et al. [58 Gib1] should be mentioned as well as the thermodynamic calculation of solid-liquid equilibria by Tomiska [89 Tom2]. The results of the latter two authors have been taken by Okamoto [93 Oka2] as a basis to construct an assessed phase diagram, which was taken to draw Fig. 1.

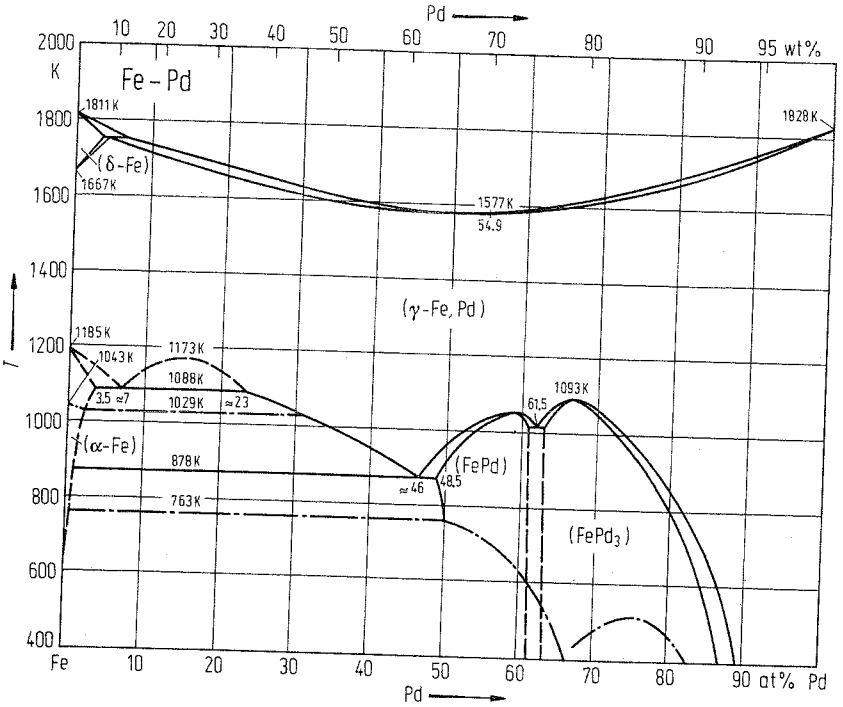

Fig. 1. Fe–Pd. Phase diagram. Dashed-dotted line: Curie temperature T_C.

Metastable phases

Buschow et al. [83 Bus2] prepared and investigated the metastable intermediate phase Fe_3Pd.

In the concentration range between 34.4 and 39.5 at% Pd a martensitic transformation occurs (Sohmura et al. [80 Soh1], Matsui et al. [81 Mat1], Oshima et al. [81 Osh2, 81 Osh1]). The range of the martensitic transformation as estimated by Okamoto [93 Oka2] is shown in Fig. 2. The transformation produces first a face-centered tetragonal structure and on further cooling a body-centered cubic phase ((α-Fe)).

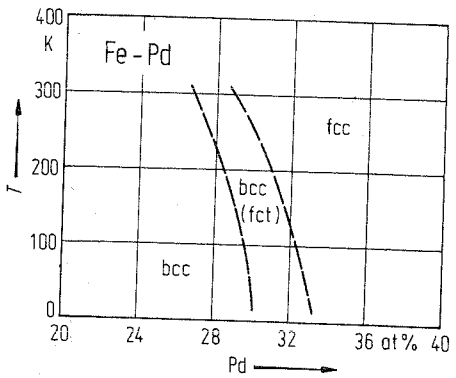

Fig. 2. Fe–Pd. Martensitic transformation producing on cooling a fct, and further on a bcc, structure.

Crystal structure

Lattice parameters of (α-Fe), (γ-Fe, Pd), (FePd) and ($FePd_3$) are plotted in Fig. 3, Fig. 4, Fig. 5 and Fig. 6, respectively. The data for these figures have been taken from Okamoto [93 Oka2], who has discussed the experimentally obtained lattice parameters thoroughly. Fig. 3 to Fig. 6 represent mean values of data present in the literature (see [93 Oka2]).

The metastable phase Fe_3Pd is cubic (W-type) with a lattice parameter: $a = 0.2962$ nm [83 Bus2].

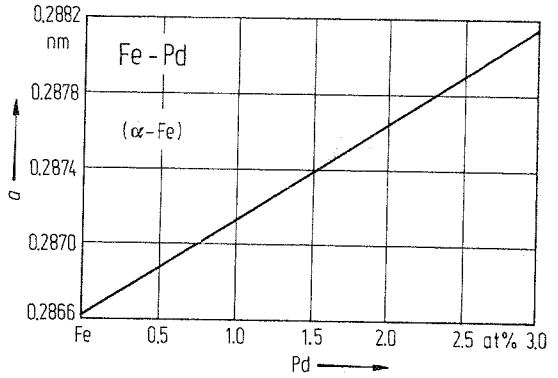

Fig. 3. Fe–Pd. Lattice parameter for bcc (α-Fe) solid solution.

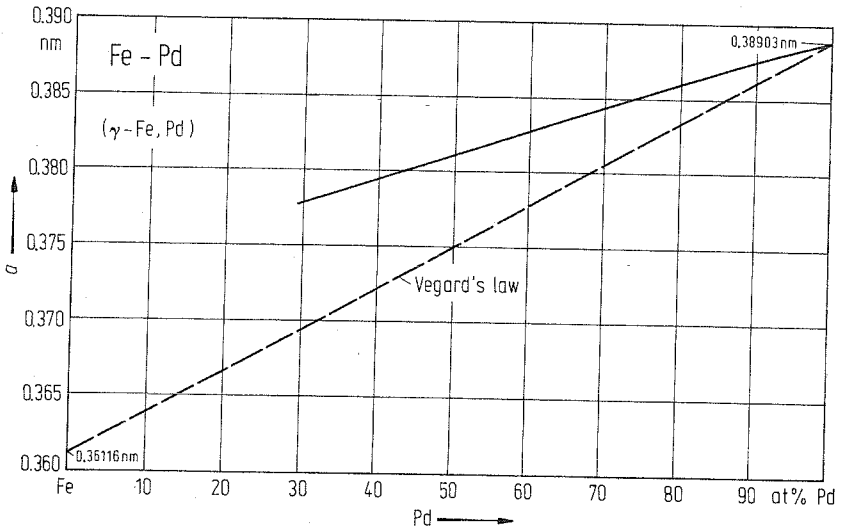

Fig. 4. Fe–Pd. Lattice parameter for fcc (γ-Fe, Pd) solid solution.

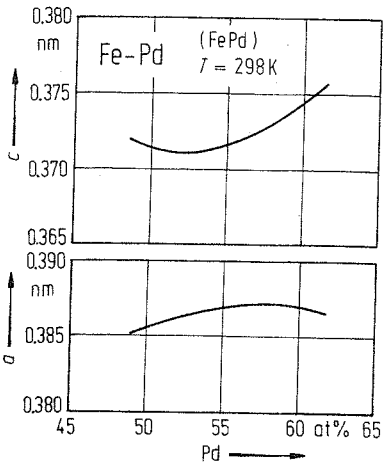

Fig. 5. Fe–Pd. Lattice parameter for tetragonal (AuCu-type) solid solution (FePd) at 298 K.

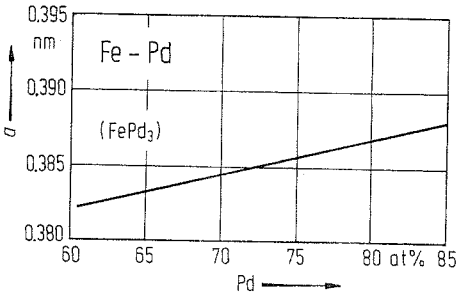

Fig. 6. Fe–Pd. Lattice parameter for cubic (Cu_3Au-type) solid solution ($FePd_3$).

Thermodynamics

Thermodynamic activities of the components in liquid Fe–Pd alloys have been determined several times. However, as Tomiska et al. [89 Tom1] have shown in a thorough discussion, the results of different authors scarcely agree with each other. Using the Knudsen method with a mass spectrometer as the analytical tool, reliable activity data have been obtained recently [89 Tom1]. The results for $T = 1850$ K are plotted in Fig. 7.

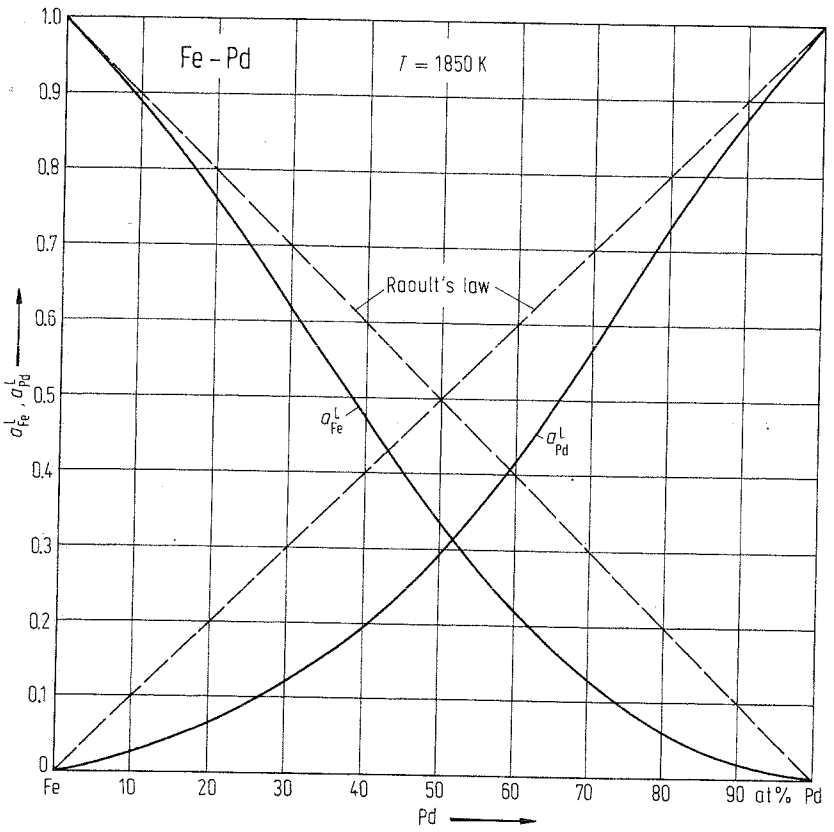

Fig. 7. Fe–Pd. Thermodynamic activities for liquid alloys at 1850 K.

Data for enthalpies of mixing of liquid alloys present in the literature are in disagreement, too. From the temperature dependence of the thermodynamic activities Tomiska et al. [89 Tom1] have calculated ΔH^L values, which have been chosen to draw Fig. 8.

The integral excess entropy of mixing of liquid alloys as published by the same authors [89 Tom1] is plotted in Fig. 9.

Using the same experimental method, Tomiska [89 Tom2] has investigated thermodynamic properties of (γ-Fe, Pd) solid solutions. Again, the thermodynamic data obtained by this author are not in good agreement with older ones, but seem to be reliable. Therefore they were used to draw Fig. 10 (thermodynamic activity isotherms at 1565 K), Fig. 11 (integral enthalpy of formation) and Fig. 12 (integral excess entropy of formation).

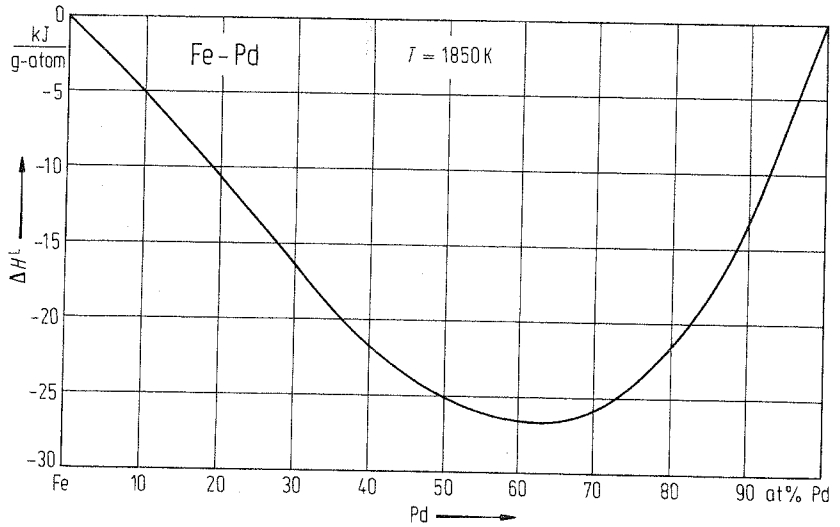

Fig. 8. Fe–Pd. Enthalpy of mixing for liquid alloys at 1850 K.

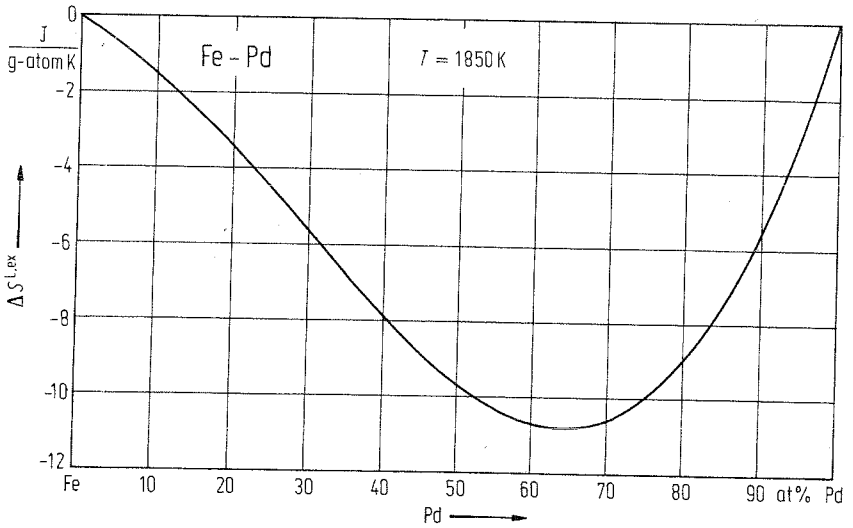

Fig. 9. Fe–Pd. Excess entropy of mixing for liquid alloys at 1850 K.

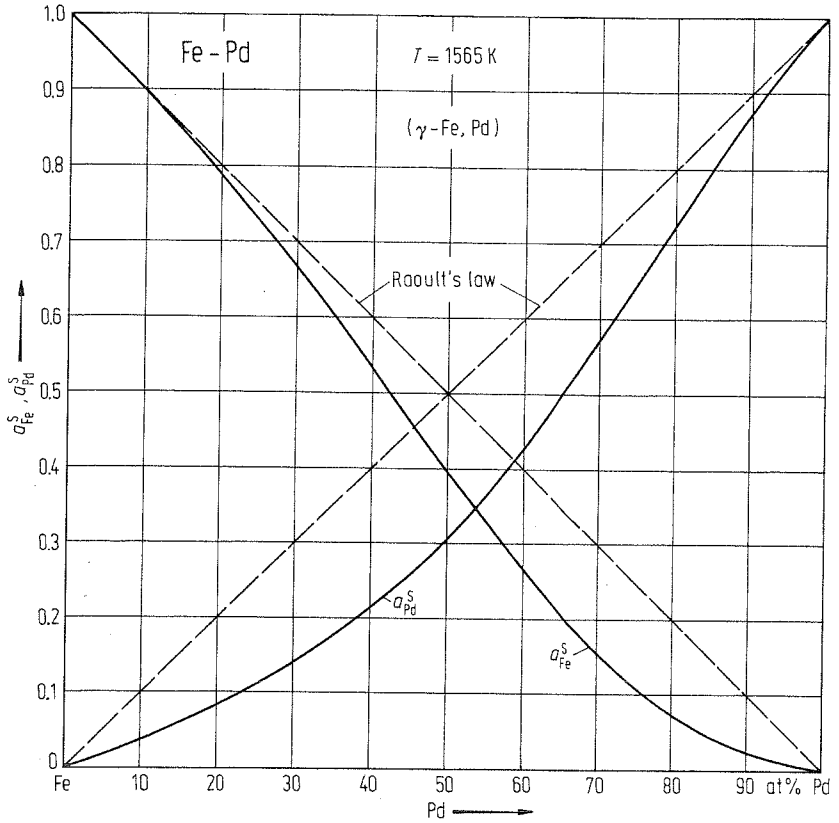

Fig. 10. Fe–Pd. Thermodynamic activities for (γ-Fe, Pd) solid solutions at 1565 K.

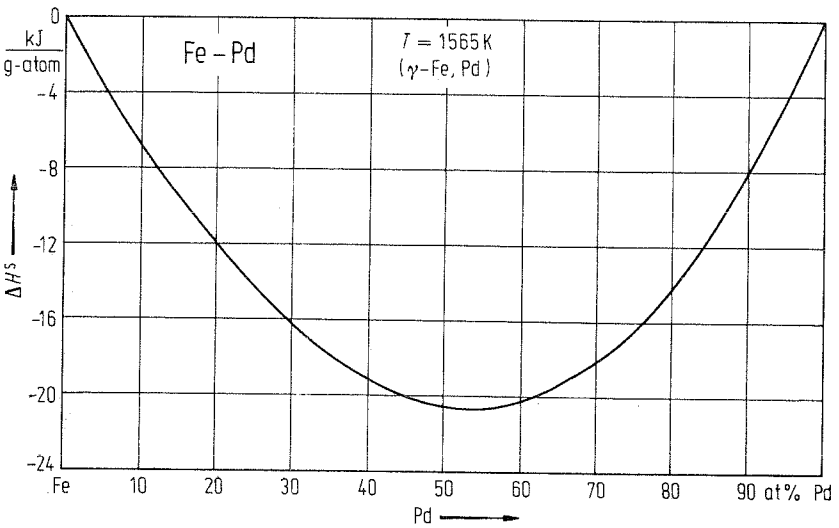

Fig. 11. Fe–Pd. Enthalpy of formation for (γ-Fe, Pd) solid solutions at 1565 K.

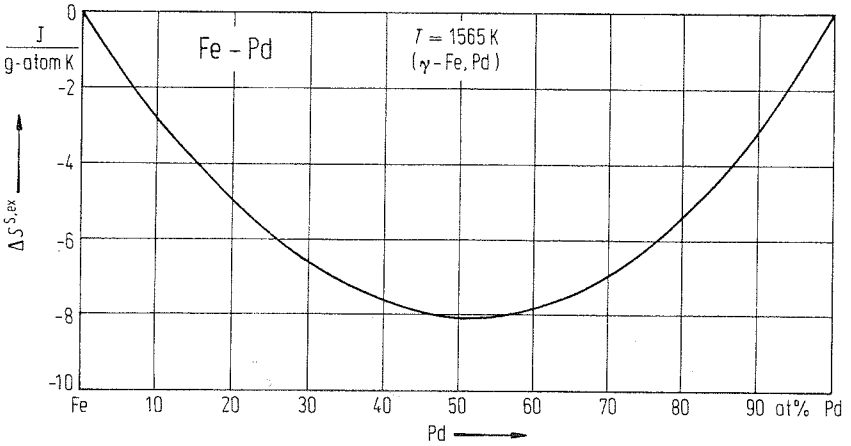

Fig. 12. Fe–Pd. Excess entropy of formation for (γ-Fe, Pd) solid solutions at 1565 K.

Fe–Pm (Iron–Promethium)

Phase diagram

Experimental investigations concerning phase equilibria of this system are not known.

A tentative phase diagram has been reported by Kubaschewski [82 Kub1] and Saccone et al. [90 Sac1]. Landgraf et al. [90 Lan1] found that $Fe_{17}Pm_2$ is the only stable intermediate phase in this system. Discussing the results present in the literature Okamoto [93 Oka2] has accepted the phase diagram proposed by Saccone et al. [90 Sac1]. To draw Fig. 1, the proposal from the latter authors was taken as a basis.

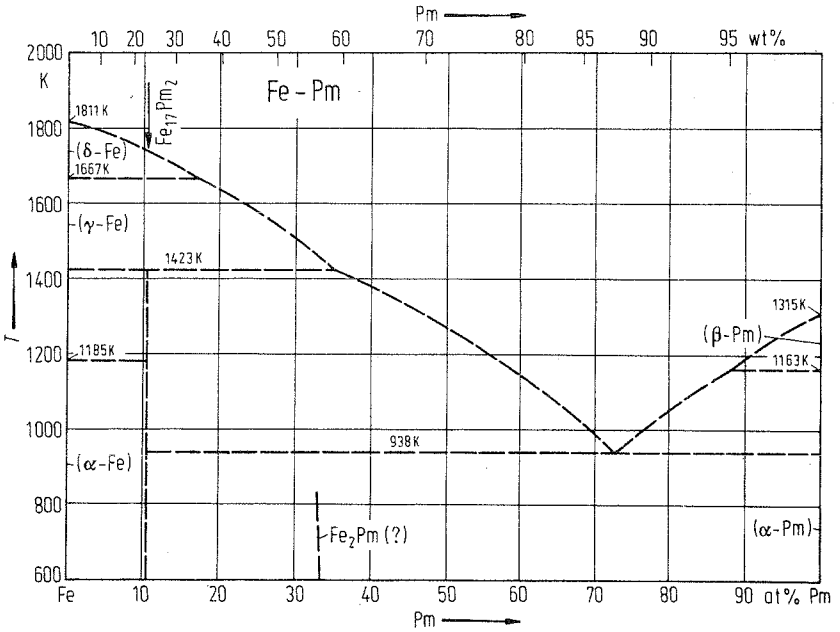

Fig. 1. Fe–Pm. Tentative phase diagram.

Crystal structure

Estimated crystallographic data of intermediate phases are listed in Table 1.

Included is also Fe_2Pm, the stability of which is doubtful (see Saccone et al. [90 Sac1], Schneider et al. [87 Sch1] and Okamoto [93 Oka2]).

Table 1. Fe–Pm. Crystal structure and structure type of intermediate phases.

Phase	Structure	Type	a [nm]	c [nm]
$Fe_{17}Pm_2$	hex	Th_2Zn_{17}	0.856	1.244
Fe_2Pm	cub	Cu_2Mg	0.743	

Fe–Pr (Iron–Praseodymium)

Phase diagram

Experimental work to disclose phase equilibria of this system has been done by Ray [69 Ray1], Tian et al. [87 Tia1] and Zhuang et al. [87 Zhu1]. Mostly accepting results obtained by Tian et al. [87 Tia1], Okamoto [93 Oka2] has constructed an assessed phase diagram, which was used as a basis for Fig. 1.

The intermediate phase Fe_2Pr can be prepared at 1273 K only at high pressure > 3.2 10^6 Pa (Cannon et al. [72 Can1]).

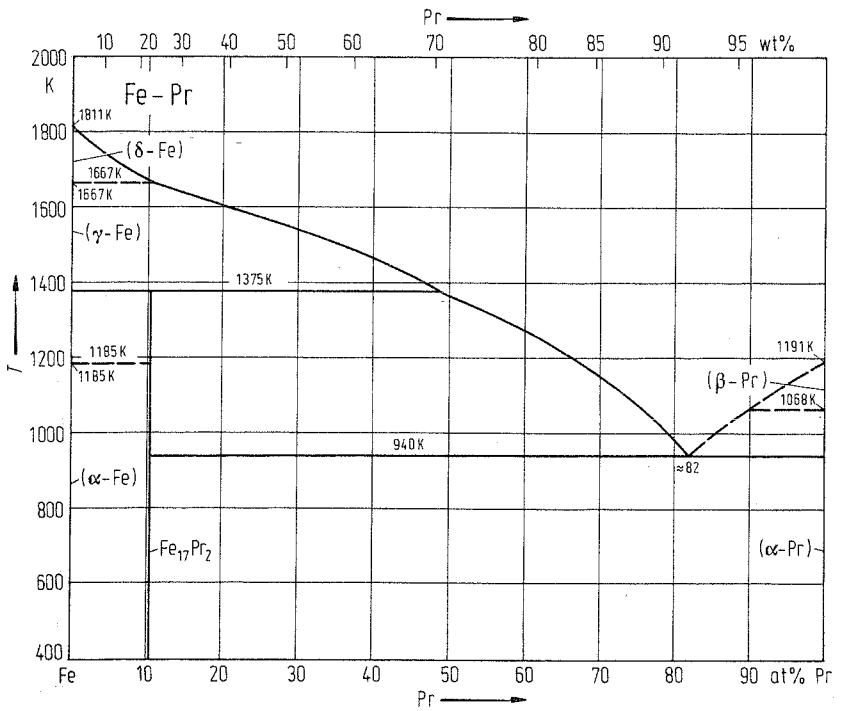

Fig. 1. Fe–Pr. Phase diagram.

Crystal structure
Crystallographic data of intermediate phases are listed in Table 1.

Table 1. Fe–Pr. Crystal structure and lattice parameters of intermediate phases.

Phase	Structure	Type	a [nm]	c [nm]	Ref.
$Fe_{17}Pr_2$	hex	Th_2Zn_{17}	0.8585	1.2464	65 Kri3, 66 Bus2, 68 Joh2
Fe_2Pr	cub	Cu_2Mg	0.7464		72 Can1

Fe–Pt (Iron–Platinum)

Phase diagram
Since the determination of the liquidus-solidus equilibria in 1907 by Isaac et al. [07 Isa3] especially phase equilibria in the solid state have been investigated. A survey is given by Okamoto [93 Oka2], who has constructed an assessed phase diagram, which was used as information to draw Fig. 1.

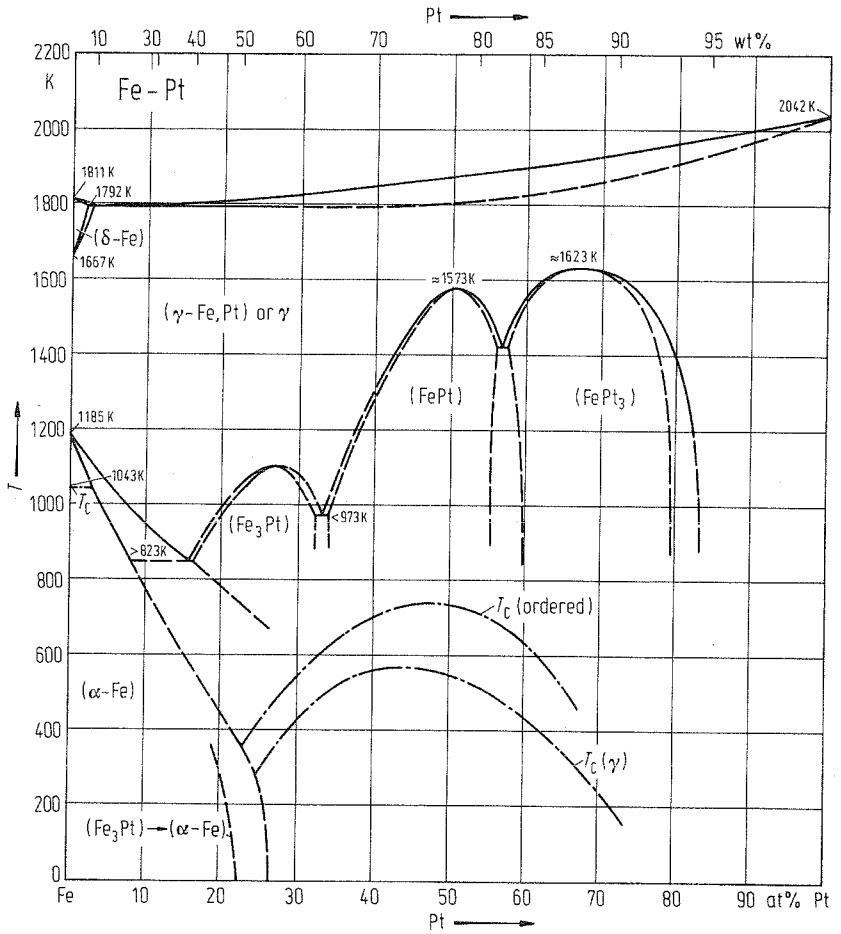

Fig. 1. Fe–Pt. Phase diagram. Dashed-dotted lines: Curie temperature T_C.

Martensitic transformations

Martensitic transitions can occur at different concentrations. The M_s temperature of (Fe_3Pt) depends on the degree of order. It takes place at ≈ 23 at% Pt and ≈ 83 K (Matsui et al. [81 Mat1]) and decreases with increasing order (Chang et al. [80 Cha1]). The product of this reaction is body-centered tetragonal α'.

If the transition starts from the (γ-Fe, Pt) solid solution, (α-Fe) results as an end product (see Matsui et al. [81 Mat1]).

(Fe_3Pt) transforms at 24 to 26 at% Pt martensitically to form face-centered tetragonal γ' at ≈ 120 K. The M_s temperatures are ≈ 123 K at 26at% Pt and ≈ 0 K at 28 at% Pt [81 Mat1].

Crystal structure

Lattice parameters of bcc (α-Fe), fcc (γ-Fe, Pt), fcc Cu_3Au-type (Fe_3Pt), tetragonal AuCu-type (FePt) and fcc Cu_3Au-type ($FePt_3$) are plotted in Fig. 2 to Fig. 6, respectively. The data for these figures were taken from Okamoto [93 Oka2], who has discussed the experimentally obtained values existing in the literature and has, partially, recommended most probable mean data.

Crystallographic data for martensitic phases α' and γ' are listed in Table 1.

Table 1. Fe–Pt. Crystal structure and lattice parameters of intermediate phases [81 Mat1].

Phase	at% Pt	T[K]	Structure	*a* [nm]	*c* [nm]
α'	25	77	tetr	0.2857	0.3176
γ'	25	79	tetr	0.3778	0.3695

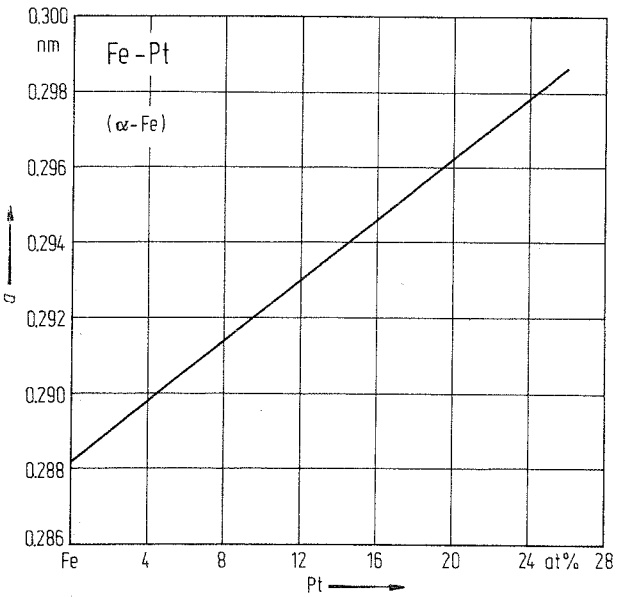

Fig. 2. Fe–Pt. Lattice parameter for bcc (α-Fe) solid solution.

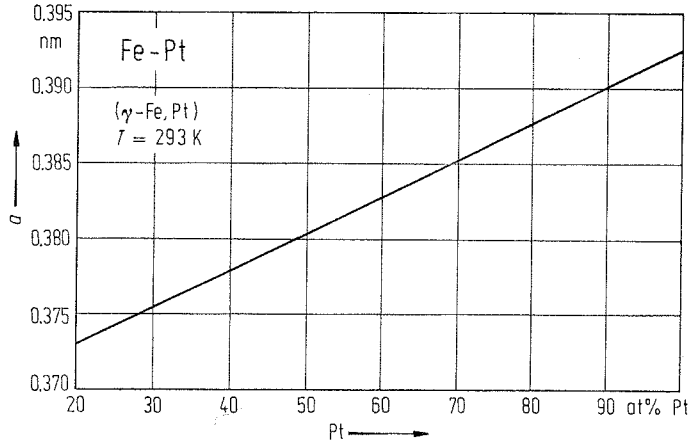

Fig. 3. Fe–Pt. Lattice parameter for fcc (γ-Fe, Pt) solid solution at 293 K.

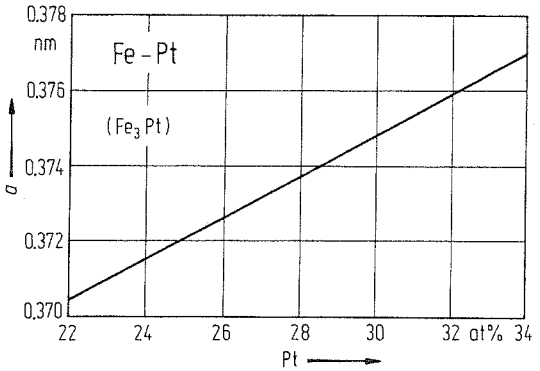

Fig. 4. Fe–Pt. Lattice parameter for cubic (Cu_3Au-type) solid solution (Fe_3Pt).

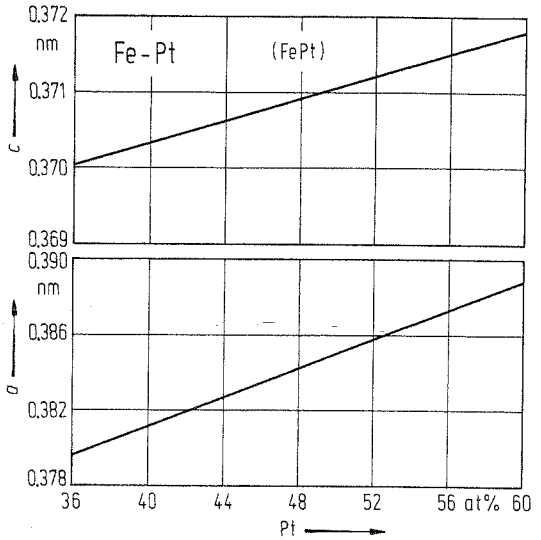

Fig. 5. Fe–Pt. Lattice parameters for tetragonal (AuCu-type) solid solution (FePt).

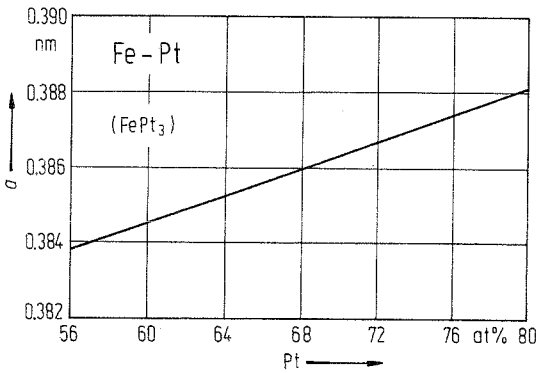

Fig. 6. Fe–Pt. Lattice parameter for cubic (Cu_3Au-type) solid solution ($FePt_3$).

Thermodynamics

Hultgren et al. [73 Hul1] have evaluated thermodynamic investigations present in the literature recommending data which are in rather good agreement with data determined by Sundaresen et al. [63 Sun1], especially at concentrations < 34 at% Pt. At higher Pt concentrations they are markedly more exothermic than those obtained by [63 Sun1]. Nevertheless, the results reported by the latter authors are acceptable and are giving a consistent set of data. Therefore they have been chosen to draw Fig. 7 to Fig. 9, where thermodynamic activity isotherms, integral enthalpies of formation and integral entropies of formation of solid alloys at 1123 K are plotted, respectively.

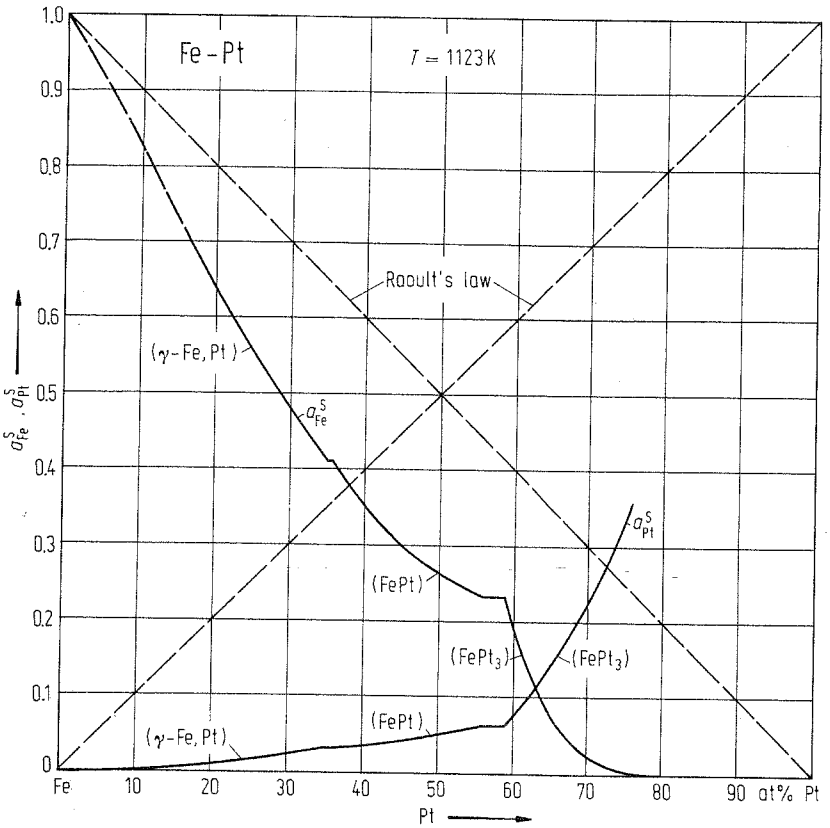

Fig. 7. Fe–Pt. Thermodynamic activities for solid solutions at 1123 K.

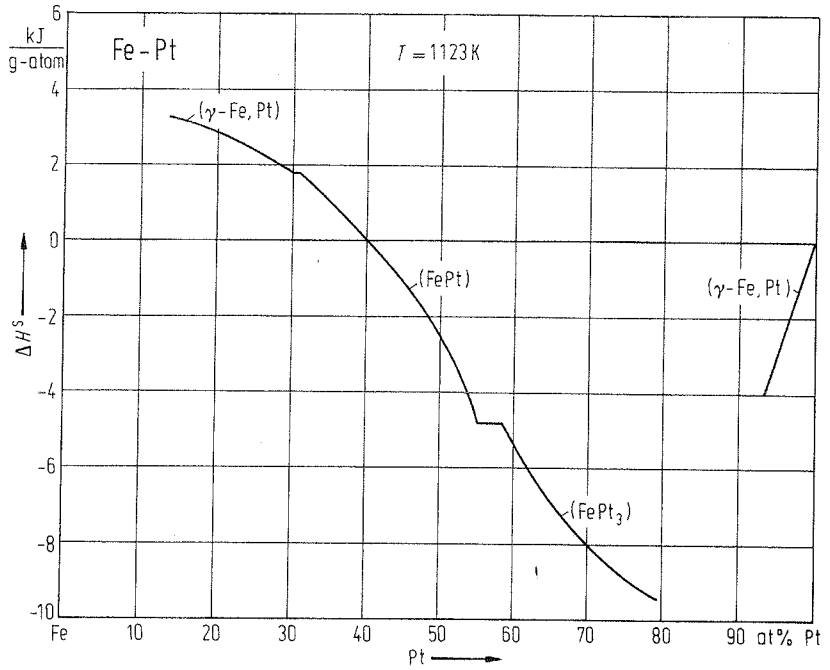

Fig. 8. Fe–Pt. Enthalpy of formation for solid solutions at 1123 K.

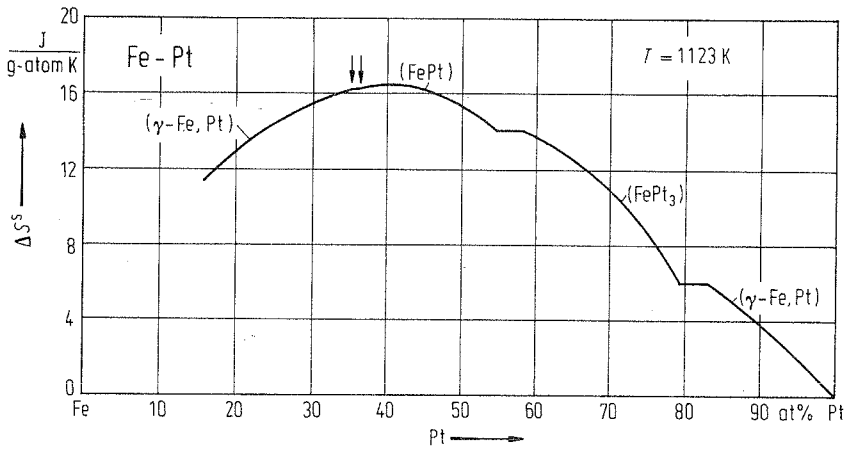

Fig. 9. Fe–Pt. Entropy of formation for solid solutions at 1123 K.

Fe–Pu (Iron–Plutonium)

Phase diagram

The results as basis for the assessment by Okamoto [93 Oka2] have been mainly obtained by Konobeevsky [55 Kon1], Mardon et al. [57 Mar1], Ofte et al. [64 Oft1] and Avivi [64 Avi1] (thermal analysis, metallography, X-ray diffractography and microhardness measurements, all done at samples weighting not more than some hundreds of milligrams). The result of the assessment has been taken to draw Fig. 1.

The areas of transformation of Fe_2Pu (see Kubaschewski [82 Kub1]) and of δ-Pu and δ'-Pu (see Okamoto [93 Oka2]) are shown on enlarged scale in Fig. 2 and Fig. 3, respectively.

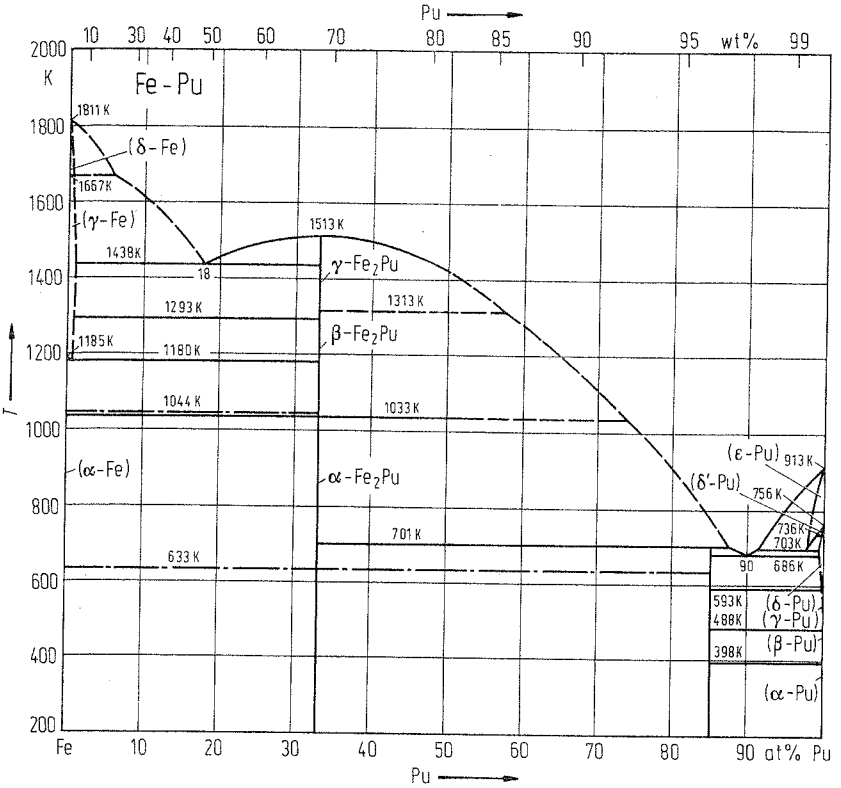

Fig. 1. Fe–Pu. Phase diagram. Dashed-dotted line: Curie temperature T_C.

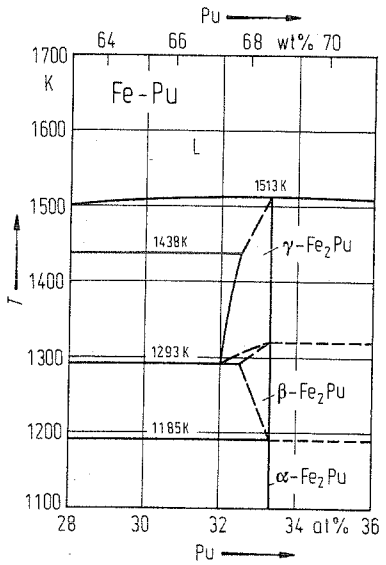

Fig. 2. Fe–Pu. Phase transformations of Fe_2Pu.

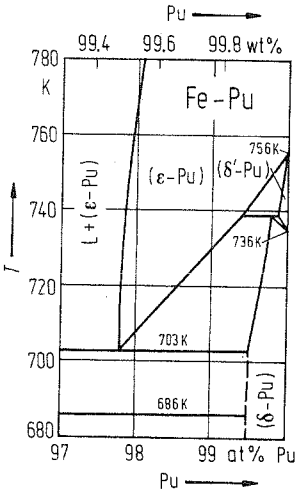

Fig. 3. Fe–Pu. Partial phase diagram (Pu-rich part).

Crystal structure

Crystallographic data of intermediate phases are listed in Table 1.

By triode-sputtering, Rizzo et al. [88 Riz1] have prepared amorphous Fe–Pu alloys in the concentration range from 13 to 75 at% Pu.

Table 1. Fe–Pu. Crystal structure and lattice parameters of intermediate phases.

Phase	Structure	Type	*a* [nm]	*c* [nm]	Ref.
α-Fe_2Pu	cub	Cu_2Mg	0.2189		57 Mar1
β-Fe_2Pu	hex	$MgNi_2$	0.564	1.837	64 Avi1
γ-Fe_2Pu	cub		0.715		64 Avi1
$FePu_6$	tetr	MnU_6	1.0403	0.5359	56 Cof1

Thermodynamics

The enthalpy of formation of Fe_2Pu amounts to ΔH^S = 9.1(10) kJ/g-atom at 298 K (hydrochloric acid solution calorimetry; Akachinskii et al. ([62 Aka1]).

Fe–Rb (Iron–Rubidium)

The components of this system are almost insoluble in each other in the liquid state as well as in the solid state. Indications of immiscibility of Rb in liquid Fe are reported by Wever [29 Wev1, 28 Wev1]. According to Young et al. [62 You1] 18 wt ppm of Fe are soluble in liquid Rb at 813 K, at 1033 K the solubility amounts to 33...115 wt ppm Fe, and at 1203 K about 33...70 wt ppm Fe.

Enthalpies of formation of Fe–Rb alloys possess a positive sign corresponding to the demixing tendency of this system as Niessen et al. [83 Nie1] have calculated on the basis of their atomistic model.

A short recent review of the Fe–Rb system is given by Sangster et al. [93 San2].

Fe–Re (Iron–Rhenium)

Phase diagram

The iron rich part of the phase diagram has been reported by Eggers [38 Egg2] (thermal analysis, metallographic observations, X-ray diffractography). Further results on phase equilibria obtained in the meantime have been discussed by Okamoto [93 Oka2], who at last has proposed an assessed phase diagram based on phase equilibria discussed by Kubaschewski [82 Kub1], the latter author having checked the results given in the literature in respect to thermodynamic consistency at concentrations up to 30 at% Re. The assessed diagram reported by Okamoto [93 Oka2] has been taken as a basis for Fig. 1.

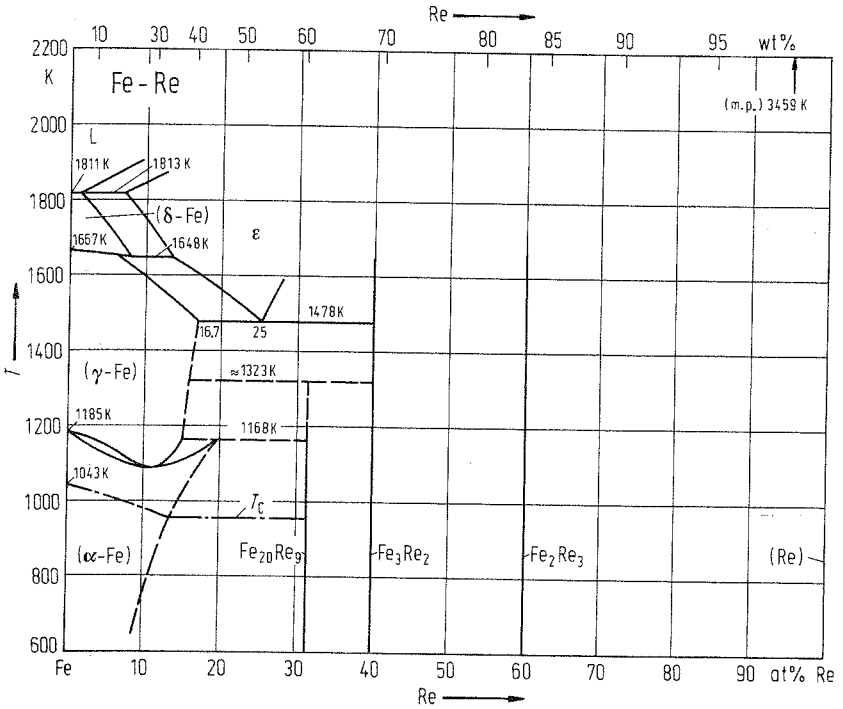

Fig. 1. Fe–Re. Phase diagram. Dashed-dotted line: Curie temperature T_C.

Crystal structure

Crystallographic data of intermediate phases are listed in Table 1.

Table 1. Fe–Re. Crystal structure and lattice parameters of intermediate phases.

Phase	Structure	Type	a [nm]	c [nm]	Ref.
ε	hex	Mg			93 Oka2
$Fe_{20}Re_9$	cub	α-Mn	0.8978		62 Age1
Fe_3Re_2	tetr	α-CrFe	0.908	0.472	56 Nie1
Fe_2Re_3	cub	β-Mn	0.643		64 Gla3

Fe–Rh (Iron–Rhodium)

Phase diagram

From the results of investigation of the (α-Fe) ⇌ (γ-Fe) transition by Fallot [38 Fal1, 37 Fal1] and the determination of solid-liquid equilibria of the Fe-rich side of the system by Gibson et al. [58 Gib1], as well as using data reported by Shirane et al. [63 Shi1], Swartzendruber [93 Swa2] has constructed an assessed phase diagram by thermodynamic modelling, which was taken as a basis to draw Fig. 1.

The α' phase, which is characterized by a superstructure, is ferromagnetic. It transforms in a first-order transition to the antiferromagnetic phase α".

The pressure-temperature diagram of an alloy with 50 at% Rh is given in Fig. 2 (from Swartzendruber [93 Swa2]).

In Fig. 3 phase equilibria concerning the (α-Fe) ⇌ (γ-Fe) transformation and martensitic transition temperatures in this region are given (taken from Swartzendruber [93 Swa2]).

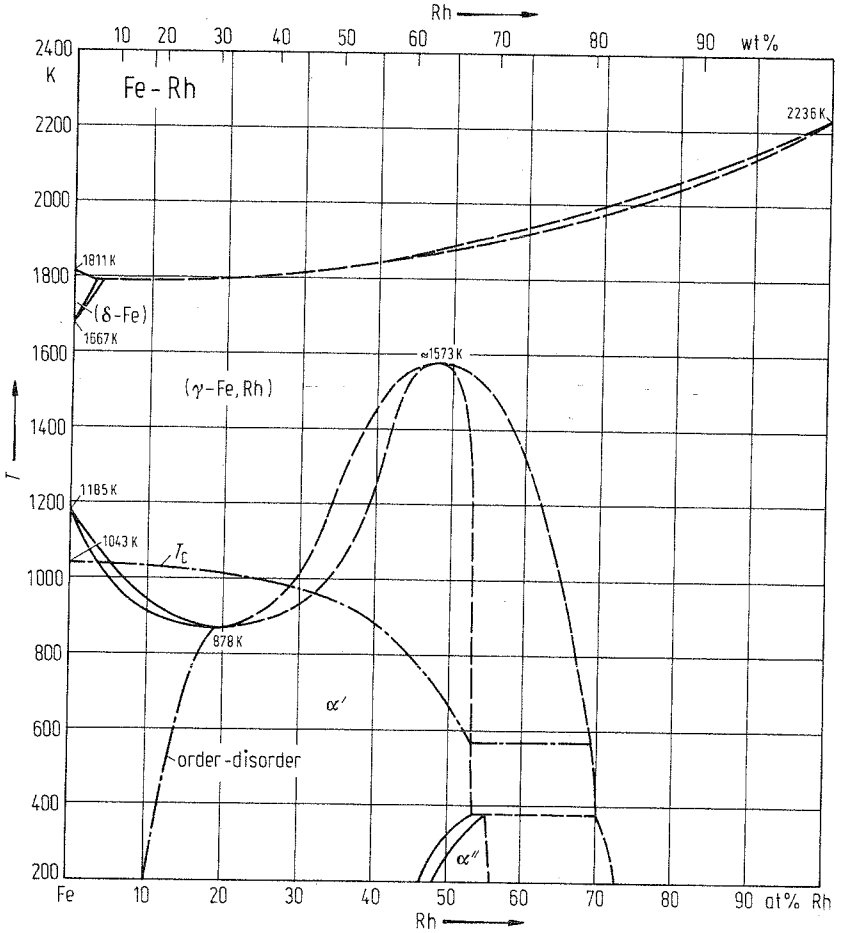

Fig. 1. Fe–Rh. Phase diagram.

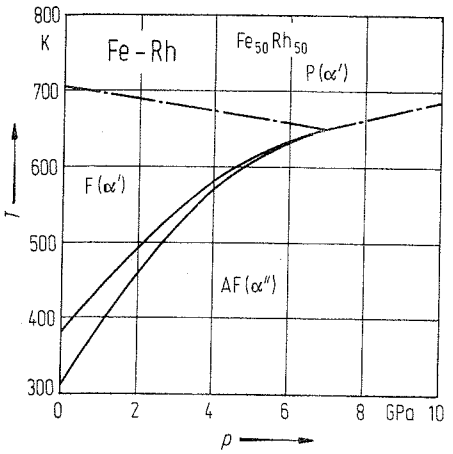

Fig. 2. Fe–Rh. Pressure-temperature phase equilibria for the solid solution containing 50 at% Rh. P: paramagnetic; F: ferromagnetic; AF: antiferromagnetic.

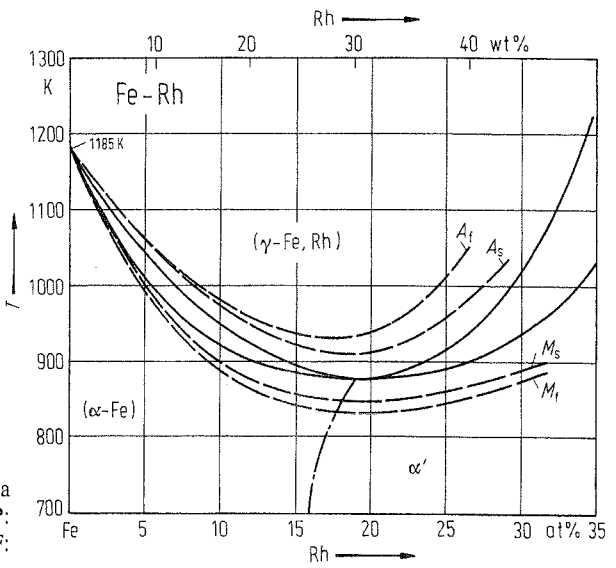

Fig. 3. Fe–Rh. Solid lines: equilibrium phase boundaries for the (α-Fe) $\rightleftharpoons$ (γ-Fe) transformation. Dashed lines: martensitic transformation starting (M_s) and finishing (M_f) temperatures on cooling, and martensitic transformation starting (A_s) and finishing (A_f) temperatures on heating. Dashed-dotted line: order-disorder transition.

Crystal structure

Lattice parameters of the α phase are plotted in Fig. 4 (Zakharova et al. [64 Zak1]) and lattice constants of fcc (γ-Fe, Rh) solid solutions are given in Fig. 5 (Schwerdtfeger et al. [68 Sch2] and Chao et al. [71 Cha1]). The value of the lattice constant of bcc (α-Fe) at 296 K for 10 at% Rh is $a = 0.2899$ nm [64 Zak1] and that for the antiferromagnetic, CsCl-type, α'' phase at 50 at% Rh and 350 K amounts to $a = 0.2987$ nm, whereas, at the same concentration and temperature (50 at% Rh, 350 K) the value of the lattice constant of the ferromagnetic α' phase is $a = 0.2997$ nm [64 Zak1].

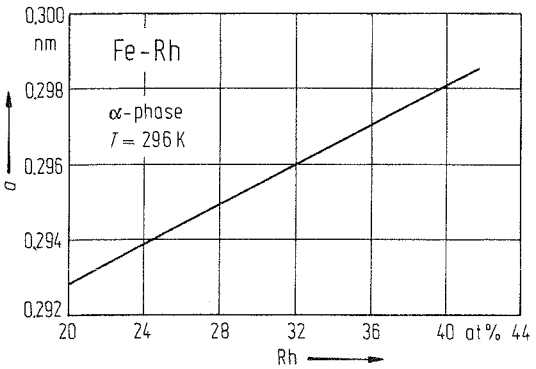

Fig. 4. Fe–Rh. Lattice parameter for cubic (bcc, CsCl-type) α-phase at 296 K.

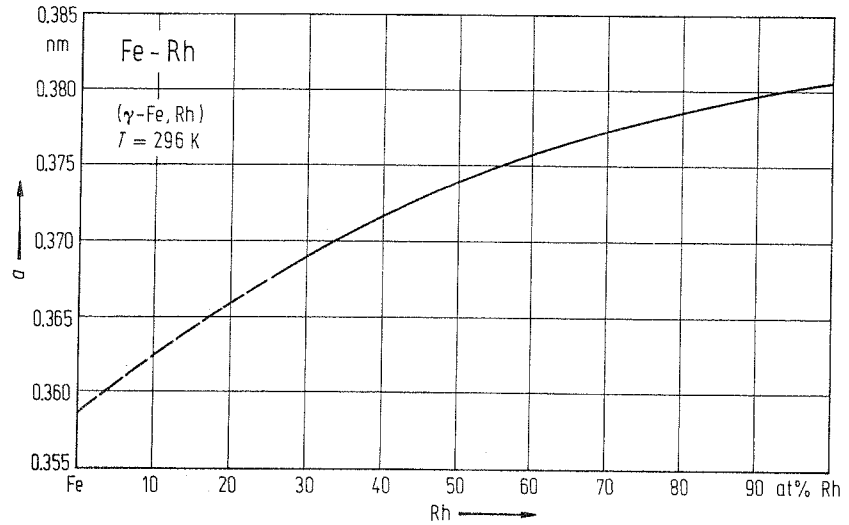

Fig. 5. Fe–Rh. Lattice parameter for fcc (γ-Fe, Rh) solid solution at 296 K.

Thermodynamics

Thermodynamic activities of Fe in solid Fe–Rh alloys at 1473 K have been determined by Schwerdtfeger et al. [68 Sch2] applying a method of equilibrating Fe–Rh alloys with iron oxide and a CO_2–CO gas mixture. The activity coefficient γ_{Fe} obtained for the Fe component is plotted in Fig. 6 as a function of concentration.

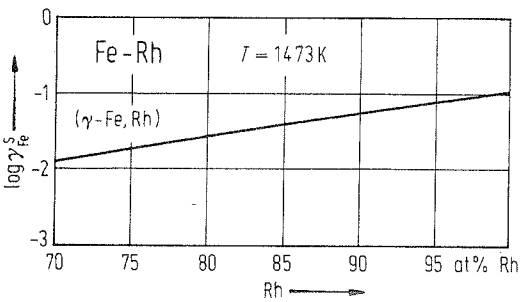

Fig. 6. Fe–Rh. Thermodynamic activity coefficient for Fe in Rh-rich (γ-Fe, Rh) solid solutions at 1473 K.

Fe–Ru (Iron–Ruthenium)

Phase diagram

At first the (α-Fe)-(γ-Fe) transition (Wever [28 Wev1, 29 Wev1]) and the ferromagnetic-paramagnetic transition at high Fe concentrations (Martelly [38 Mar2], Fallot [38 Fal1, 37 Fal1]) have been investigated. Further experimental work has been done by Gibson et al. [58 Gib1], Obrowski [59 Obr1] and Raub et al. [60 Rau1].

Adapting to the results obtained by Gibson et al. [58 Gib1] and using a thermodynamic model, Swartzendruber et al. [93 Swa4] have calculated phase equilibria of this system. The diagram thus obtained has been taken as a basis to draw Fig. 1.

In Fig. 2, a Fe-rich part of the phase diagram is shown on enlarged scale (see [93 Swa4]). Equilibria concerning the (α-Fe)-(γ-Fe) equilibria and the martensitic transition in the Fe-rich region are given in Fig. 3 ([93 Swa4, 38 Fal1, 37 Fal1]).

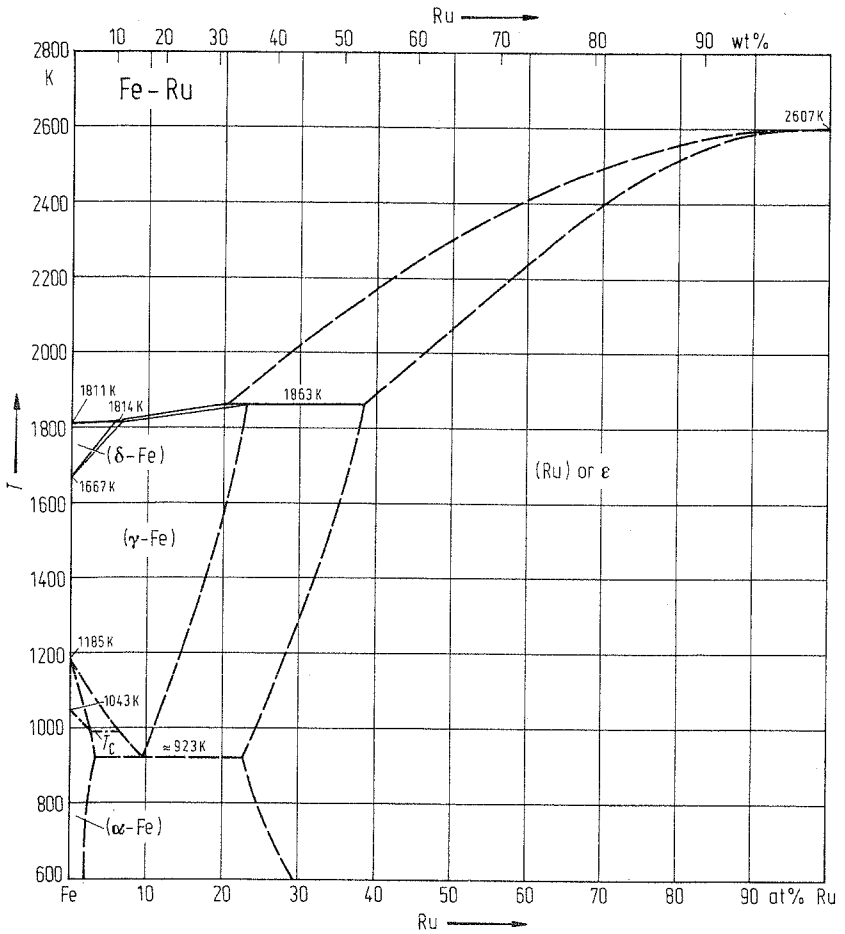

Fig. 1. Fe–Ru. Phase diagram.

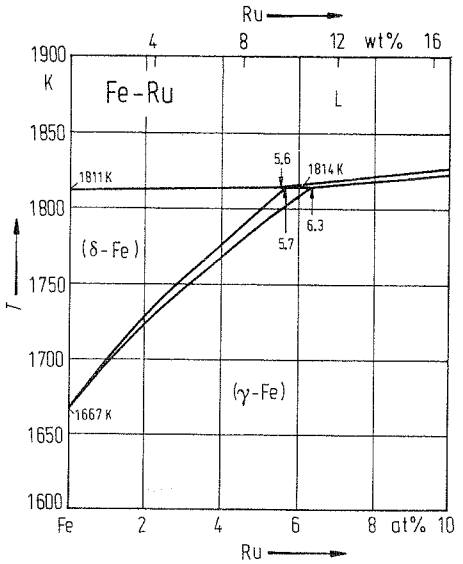

Fig. 2. Fe–Ru. Partial phase diagram (Fe-rich part): (δ-Fe) and (γ-Fe) equilibria.

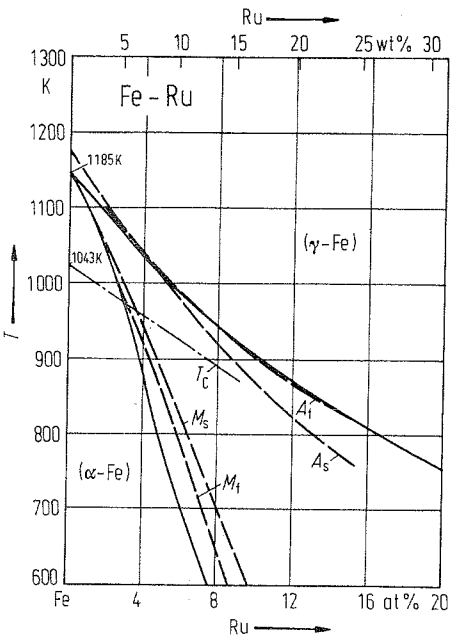

Fig. 3. Fe–Ru. Solid lines: equilibrium phase boundaries for the (α-Fe) $\rightleftharpoons$ (γ-Fe) transformation. Dashed lines: martensitic transformation starting (M_s) and finishing (M_f) temperatures on cooling, and martensitic transformation starting (A_s) and finishing (A_f) temperatures on heating. Dashed-dotted line: Curie temperature T_C.

Crystal structure

Some crystallographic data are given in Table 1. The data have been taken from the compilation by Swartzendruber et al. [93 Swa4].

Lattice parameters of bcc (α-Fe) solid solutions are plotted in Fig. 4 (Cotta et al. [60 Cot1]).

Table 1. Fe–Ru. Crystal structure and lattice parameters of intermediate phases at 293 K [60 Rau1].

Phase	at% Ru	Structure	Type	*a* [nm]	*c* [nm]
(γ-Fe)	9.2	fcc	Cu	0.3608	
	11.0	fcc	Cu	0.3605	
(ε-Fe)	23.4	hex	Mg	0.2574	0.1609
	30.0	hex	Mg	0.2583	0.1611

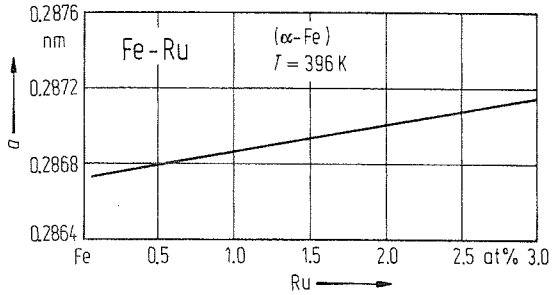

Fig. 4. Fe–Ru. Lattice parameter for bcc (α-Fe) solid solution at 396 K.

Thermodynamics

Measurements of the partial vapor pressure of Fe in solid Fe–Ru alloys at 1600 K have been done by Stepakoff et al. [68 Ste1] using a Knudsen effusion method. The thermodynamic activities thus obtained have been taken to draw Fig. 5.

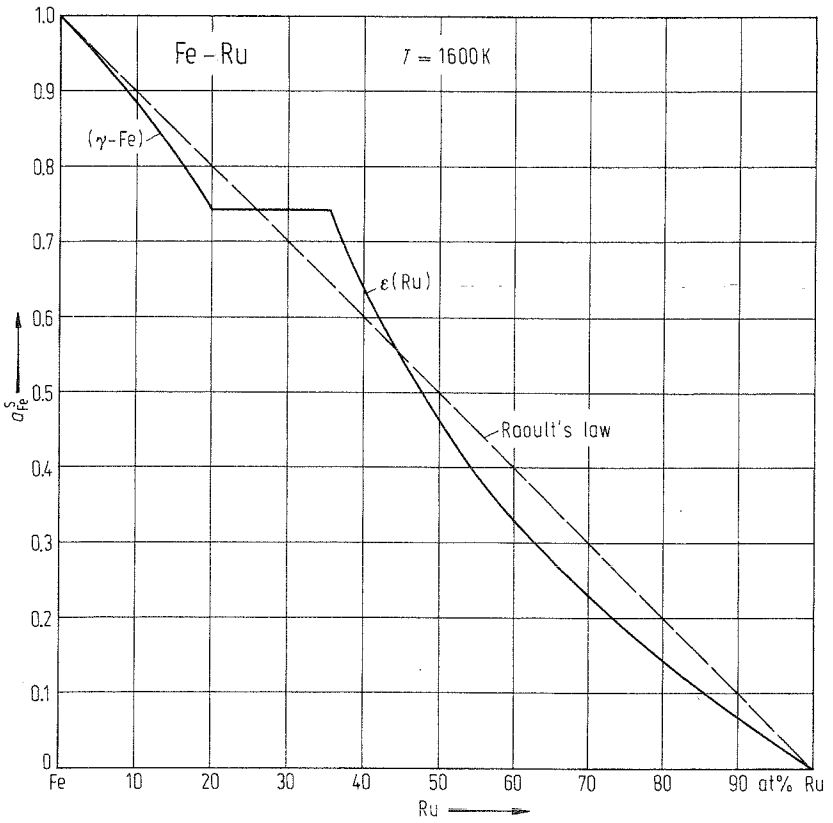

Fig. 5. Fe–Ru. Thermodynamic activity for solid solutions at 1600 K.

Fe–S (Iron–Sulfur)

Phase diagram

Many experimental investigations have been done to establish the phase diagram. Individual results were discussed in reviews like those reported by Hansen et al. [58 Han1] and Kubaschewski [82 Kub1, 93 Kub1]. Especially for the liquidus in the FeS–S part see Schürmann [72 Sch2] and Charma et al. [79 Cha1]. The assessed phase diagram reported by [93 Kub1] has been taken as a basis to construct Fig. 1. The Fe-rich region is given in Fig. 2 on enlarged scale (taken from Kubaschewski [82 Kub1, 93 Kub1]).

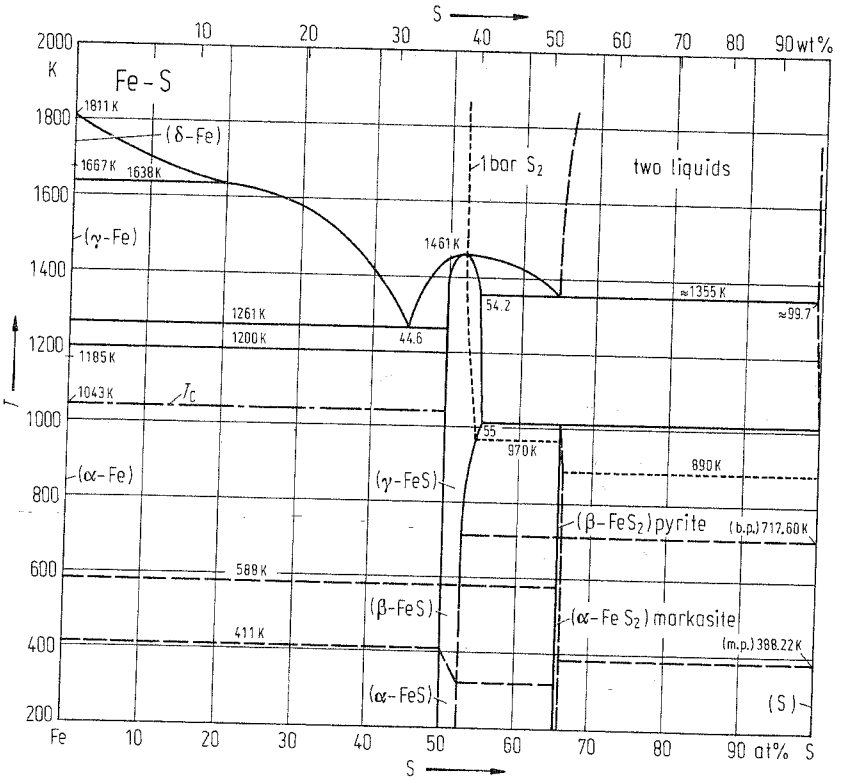

Fig. 1. Fe–S. Phase diagram.

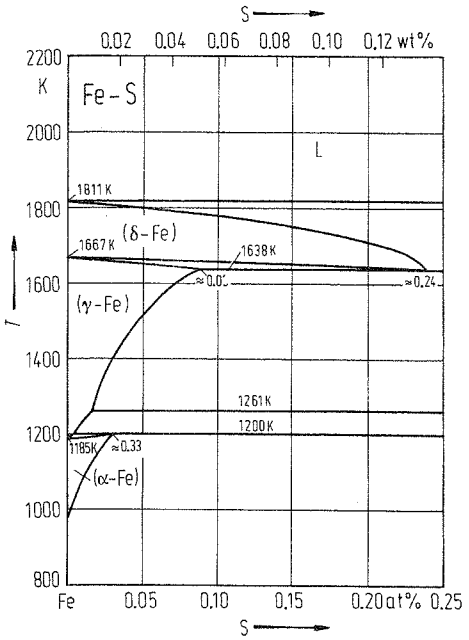

Fig. 2. Fe–S. Partial phase diagram (Fe-rich part).

Crystal structure

The crystal structure of (FeS) depends on concentration and temperature (and pressure). Between 50 and 51 at% S a hexagonal (NiAs-type) α' phase exists. Phase α" can be found between 51 and 52.4 at% S and phase β between 52.6 and 53.5 at% S. The structures of α" and β are similar to that of α' (see Pearson [58 Pea1]). These differentiations are not included in Fig. 1. For special information the reader is referred to reviews like those by [58 Pea1, 67 Pea1].

Another intermediate phase occurring in Fig. 1 is pyrite, FeS_2. Its structure is cubic (FeS_2-type). Lattice parameter: 0.5418 nm (Will et al. [84 Wil1]). The mineral markasite with the same stoichiometry (FeS_2) has an orthorhombic ($FeSb_2$-type) structure with lattice parameters: a = 0.4443 nm, b = 0.54245 nm and c = 0.3387 nm (Brostigen et al. [70 Bro1]).

Several other compounds between Fe and S have been found which do not fit the equilibrium diagram as given in Fig. 1. They are obviously metastable phases (Fe_2S_3, Fe_3S, Fe_3S_4, Fe_7S_8, Fe_9S_{10}, $Fe_{10}S_{11}$, $Fe_{11}S_{12}$; see Villars et al. [91 Vil1]).

Thermodynamics

Sharma et al. [79 Sha2] have discussed thoroughly thermodynamic activities of S in liquid Fe–S alloys in the concentration range up to 52 at% S. In this region they have calculated activity values, too, which are in good agreement with experimentally obtained ones. From there information was taken to draw ln a_S^L isotherms in Fig. 3.

Using an EMF method Schaefer [80 Sch1] has investigated the thermodynamic properties of solid $Fe_{0.9}S$. The resulting standard enthalpy of formation is: $\Delta H^S = -100.5(6)$ kJ / mol.

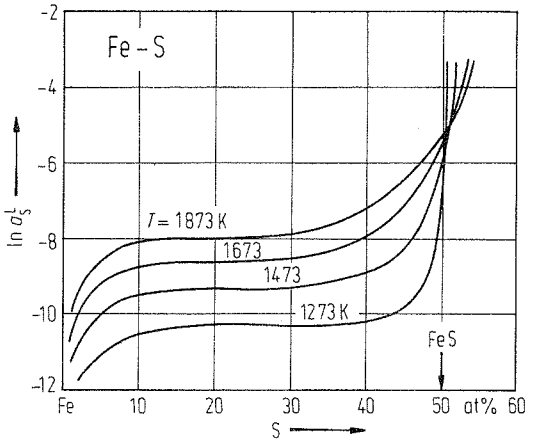

Fig. 3. Fe–S. Thermodynamic activity of S in liquid alloys at different temperatures.

Fe–Sb (Iron–Antimony)

The liquidus has been determined by Kurnakov et al. [08 Kur1], Vogel et al. [34 Vog1] and Geller [39 Gel1] using thermal analysis. α - γ equilibria have been investigated by Wever [28 Wev1, 29 Wev1] and Jones [34 Jon1]. Later on, Maier et al. [72 Mai1] by magnetic measurements, and Feschotte et al. [89 Fes1] by thermal analysis and X-ray diffractography, have very carefully reinvestigated the constitution. Of the reviews of this system those by Kubaschewski [82 Kub1], Bannykh et al. [86 Ban3] and Okamoto [93 Oka2] should be mentioned. From the latter author the assessed phase diagram was taken to construct Fig. 1.

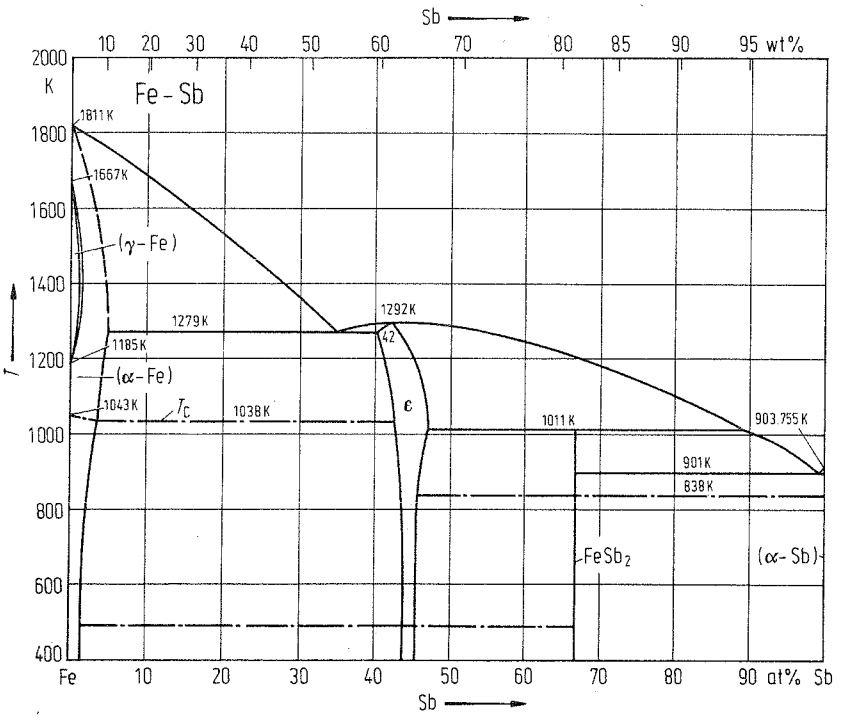

Fig. 1. Fe–Sb. Phase diagram. Dashed-dotted lines: Curie temperature T_C.

The (α-Fe) ⇌ (γ-Fe) equilibria are shown in Fig. 2 on enlarged scale (see Kubaschewski [82 Kub1]).

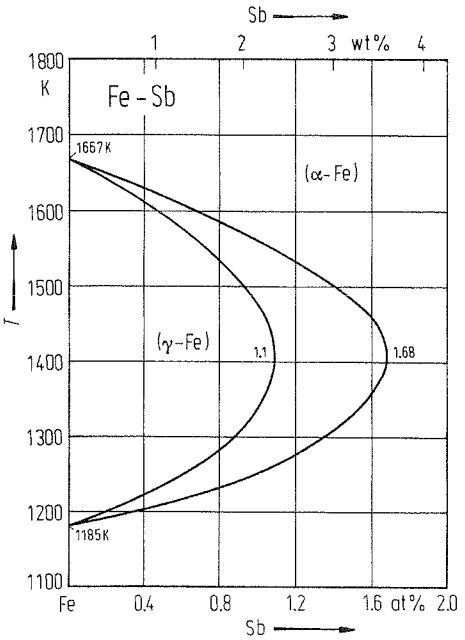

Fig. 2. Fe–Sb. (α-Fe) ⇌ (γ-Fe) phase equilibria.

Metastable phases

$FeSb_3$ has been found by Alekseevskii [48 Ale1]. Obviously, this phase is metastable and, therefore, could not be included in the equilibrium diagram.

$FeSb_4$ has been observed as a transient phase, which is found by crystallization of amorphous alloys and, obviously, is metastable (Chyczewski et al. [72 Chy1]).

Crystal structure

Lattice parameters of bcc (α-Fe) solid solutions have been obtained by Nageswararao et al. [74 Nag1]. The results are plotted in Fig. 3.

Crystallographic data of intermediate phases are listed in Table 1.

Table 1. Fe–Sb. Crystal structure and lattice parameters of intermediate phases.

Phase	Structure	Type	*a* [nm]	*b* [nm]	*c* [nm]	Ref.
ε (40 at% Sb)	hex	NiAs	0.4131		0.5178	27 Oft1
ε (50 at% Sb)	hex	NiAs	0.4072		0.5140	27 Oft1
$FeSb_2$	orth		0.5830	0.6535	0.3197	72 Ros1, 69 Hol1
$FeSb_4$	cub	α-Po	0.3039			72 Chy1

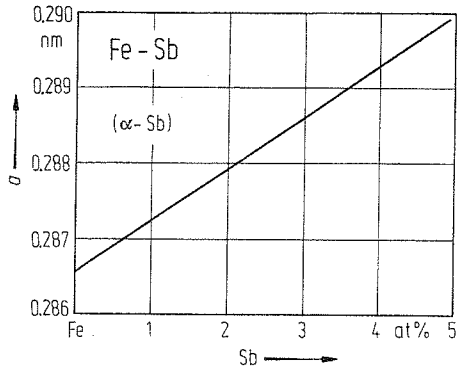

Fig. 3. Fe–Sb. Lattice parameter for bcc (α-Fe) solid solutions.

Thermodynamics

By Knudsen cell technique, Dynan et al. [75 Dyn1] have determined thermodynamic activities of Sb over the entire concentration range at 893 K. From primary results obtained, they calculated activities of Fe as well as enthalpies of formation and entropies of formation. The data published are plotted in Fig. 4, Fig. 5 and Fig. 6, respectively.

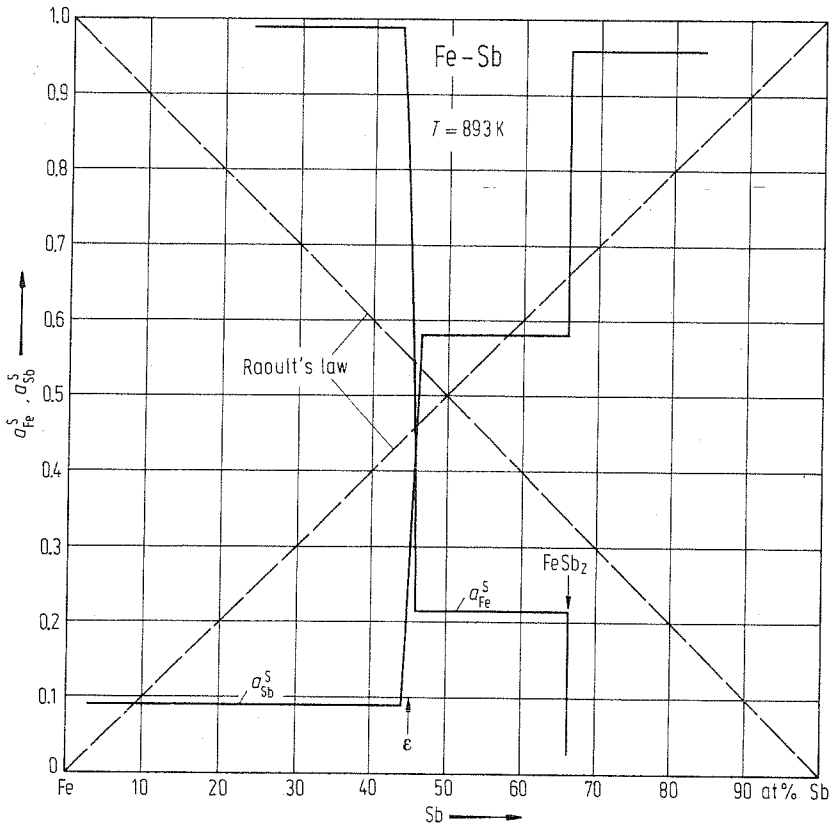

Fig. 4. Fe–Sb. Thermodynamic activities for solid solutions at 893 K.

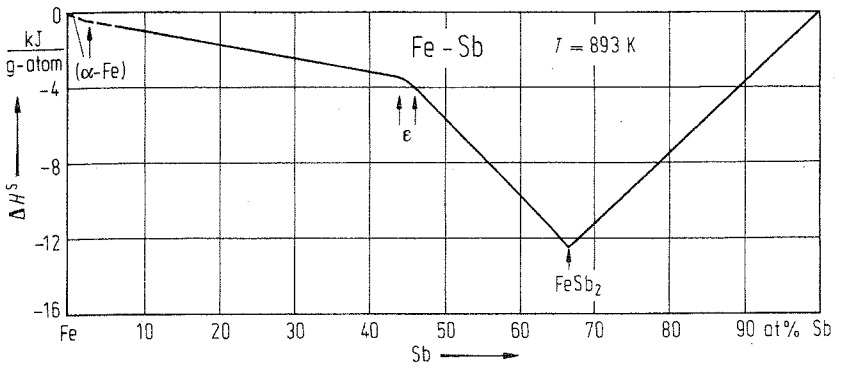

Fig. 5. Fe–Sb. Enthalpy of formation for solid solutions at 893 K.

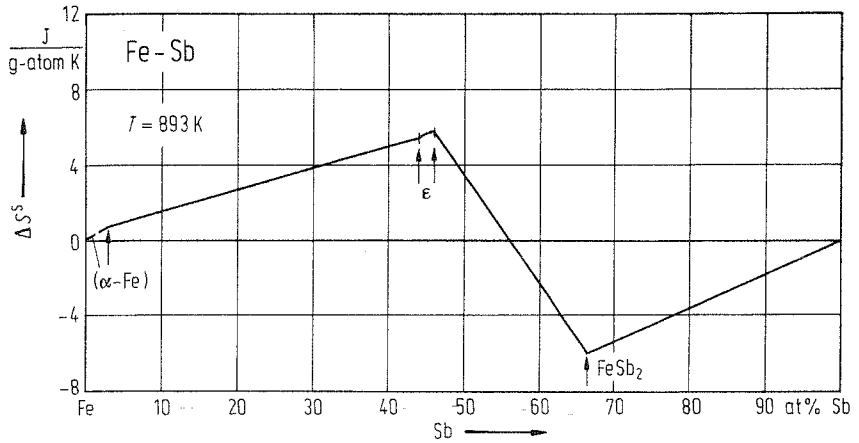

Fig. 6. Fe–Sb. Entropy of formation for solid solutions at 893 K.

Fe–Sc (Iron–Scandium)

Phase diagram

The phase diagram has been first investigated experimentally by Naumkin et al. [69 Nau1]. Bodak et al. [78 Bod1] have again determined phase equilibria, the results obtained are only in some parts similar to those reported by [69 Nau1]. An assessed diagram has been published by Kubaschewski [82 Kub1] and Okamoto [93 Oka2]. The assessed diagram from Okamoto, which is based mainly on the publication by Bodak et al. [78 Bod1], has been taken to construct Fig. 1.

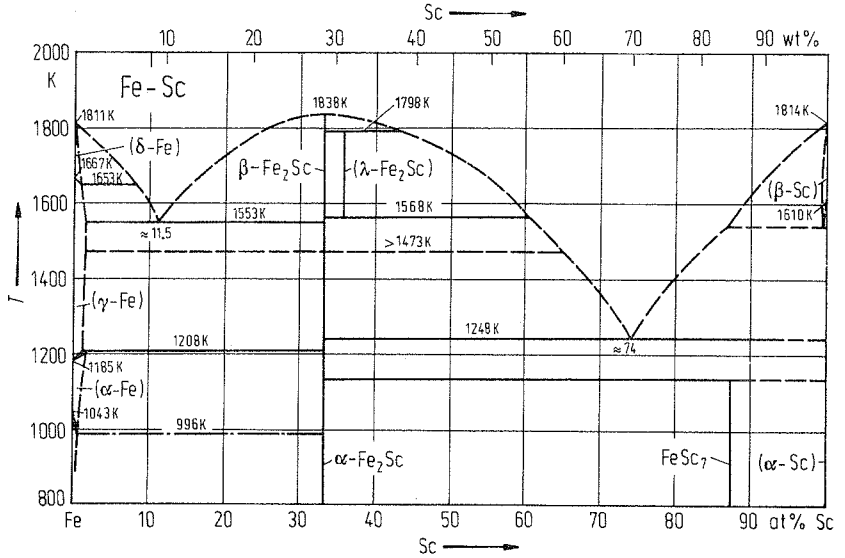

Fig. 1. Fe–Sc. Phase diagram. Dashed-dotted line: Curie temperature T_C.

Crystal structure

Crystallographic data of intermediate phases are listed in Table 1.

Table 1. Fe–Sc. Crystal structure and lattice parameters of intermediate phases.

Phase	Structure	Type	*a* [nm]	*c* [nm]	Ref.
α-Fe_2Sc	hex	$MgZn_2$	0.49370	0.80382	67 Pro1, 74 Ike1
β-Fe_2Sc	hex	$MgNi_2$	0.4972	1.6278	61 Dwi1
λ-Fe_2Sc	cub	Cu_2Mg	0.7039		64 Gla1, 78 Bod1

Thermodynamics

Integral enthalpies of mixing of liquid Fe–Sc alloys have been determined by Sudavtsova et al. [84 Sud1] at 1870 K up to 11 at% Sc and by Esin et al. [84 Esi1] up to 18 at% Sc. The results of the latter authors are given in Fig. 2.

Enthalpies of formation of Fe_2Sc have been determined calorimetrically at 1473 K by Selhaoui et al. [93 Sel1]. The value obtained amounts to $\Delta H^S = -11.2(12)$ kJ/g-atom.

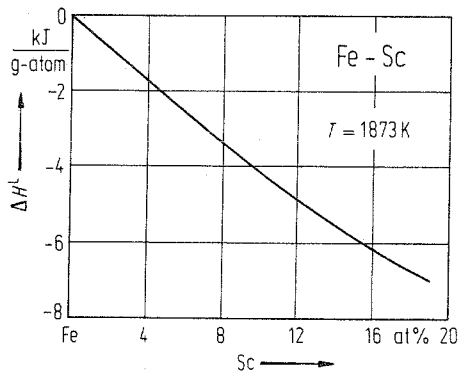

Fig. 2. Fe–Sc. Enthalpy of mixing for liquid alloys at 1873 K.

Fe–Se (Iron–Selenium)

Phase diagram

On the basis of experimental results reported by Dutrizak et al. [68 Dut1], Schuster et al. [79 Sch2], and Katayama et al. [90 Kat1], Okamoto [93 Oka2] has assessed the phase diagram, which has been taken to construct Fig. 1.

By codeposition of Fe and Se, a thin film consisting of a phase with cubic structure can be prepared (Srivastava et al. [75 Sri1]). On heating, this phase transforms to a hexagonal phase and at last, at about 520...570 K, to a tetragonal (AuCu-type) phase.

At high pressure and high temperature a pyrite-type FeS_2 is formed (6.5 10^9 Pa, 1070 K...1470 K; Bither et al. [66 Bit1]).

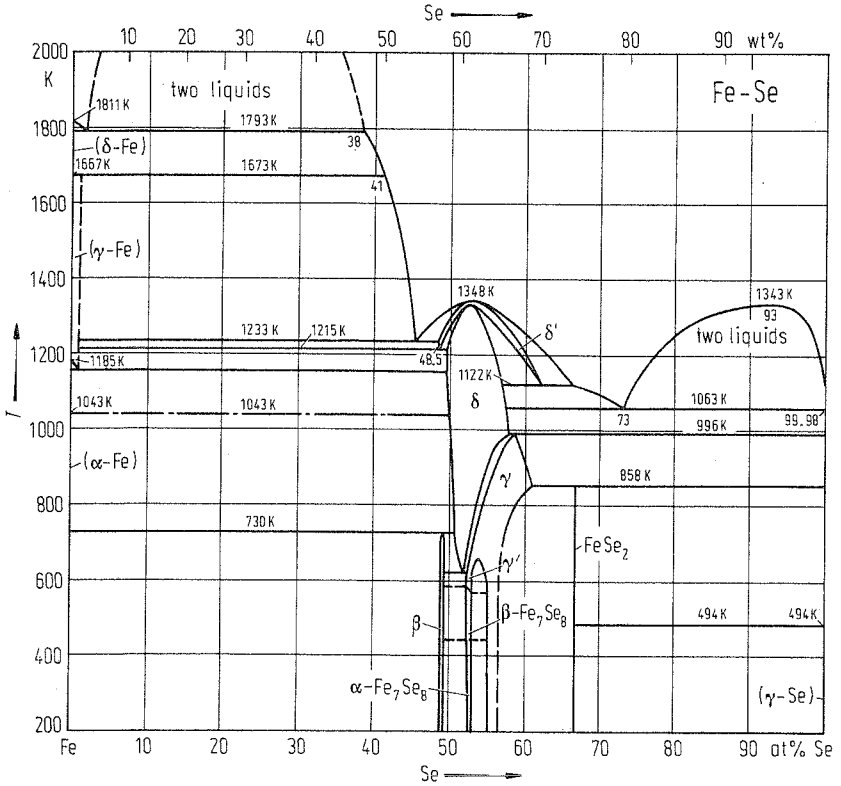

Fig. 1. Fe–Se. Phase diagram. Dashed-dotted line: Curie temperature T_C.

Crystal structure

Crystallographic data of intermediate phases are listed in Table 1.

It should be mentioned that the phase correlations between Fe_7Se_8, γ' and δ, obviously are not quite clear (see discussion by Okamoto [93 Oka2]).

Table 1. Fe–Se. Crystal structure and lattice parameters of intermediate phases.

Phase	at% Se	Structure	Type	*a* [nm]	*b* [nm]	*c* [nm]	Ref.
β		tetr	PbO	0.3773		0.5529	33 Häg1
δ	≈ 50	hex	NiAs	0.3644		0.5821	33 Häg1
	54.3			0.3619		0.5864	79 Sch3
γ'	54.3	mon		0.6269	0.3619 $\beta = 91°$	0.5964	33 Häg1, 79 Sch3
	60			0.626	0.359 $\beta = 90.98°$	0.582	75 Red1
γ	56.4	mon		0.6198	0.3540 $\beta = 92.0°$	1.1285	56 Oka1, 79 Sch3
	57.1 (372 K)			0.6208	0.3541 $\beta = 91.807°$	1.1281	70 And1
	58.5			0.6140	0.3531 $\beta = 91.0°$	1.1118	79 Sch3
Fe_7Se_8 (h)		hex	Fe_7Se_8	0.7236		1.766	59 Oka1
Fe_7Se_8 (l)		tricl.		1.253 $\alpha = 89.8°$	0.7236 $\beta = 89.4°$	2.354 $\gamma = 90°$	59 Oka1
$FeSe_2$		orth	FeS_2 marcasite	0.47890	0.57689	0.35755	38 Ten1, 58 Fis1
Metastable phases							
FeSe		cub		0.537			75 Sri1
		hex	NiAs	0.400		0.588	75 Sri1
		tetr	AuCu	0.418		0.473	75 Sri1
High-pressure phase							
$FeSe_2$		cub	FeS_2 pyrite	0.57859			66 Bit1, 68 Bit1

Thermodynamics

Using an isopiestic method, Schuster et al. [79 Sch2] have determined selenium vapor pressure of Fe–Se alloys at temperatures between 700 and 1200 K in the concentration range between 50 and 60 at% Se. From the results obtained thermodynamic activities have been calculated. The results for 873 K are plotted as ln a_{Fe} and ln a_{Se} as a function of concentration in Fig. 2.

From the temperature dependence of the thermodynamic activities, enthalpies of formation of the intermediate phases at 53.33 and 57.44 at% Se have been calculated and compared with results obtained by Svendsen [72 Sve1], who has determined the vapor pressure of selenium in the system, too. The ΔH^S values from both sources are given in Table 2. In this table calorimetrically determined ΔH^S values are also included, which have been determined by Gronvold [72 Gro1].

Table 2. Fe–Se. Enthalpy of formation of intermediate phases.

at% Se	ΔH^S [kJ g-atom^{-1}]	Ref.
53.33	– 40.8	79 Sch2
	– 35.0	72 Sve1
	– 30.9	72 Gro1
57.14	– 41.6	79 Sch2
	– 35.6	72 Sve1
	– 30.3	72 Gro1

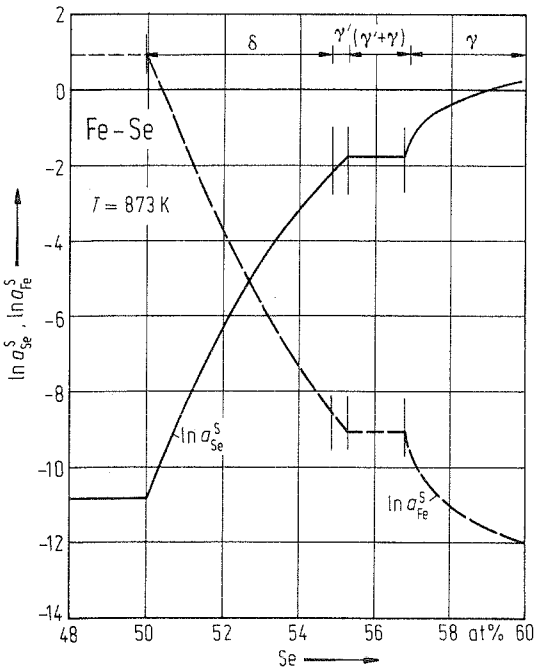

Fig. 2. Fe–Se. Thermodynamic activities for solid solutions at 873 K.

Fe–Si (Iron–Silicon)

Phase diagram

Phase equilibria of this system have been investigated very often. Reviews were given by Baraduc-Muller [10 Bar1], Guertler [17 Gue1], Hansen et al. [58 Han1], and Kubaschewski [82 Kub1, 93 Kub1]. Schürmann et al. [80 Sch3] and Chart [81 Cha1] again investigated the phase equilibria experimentally. On the basis of results reported in the literature, mainly using information from Schürmann et al. [80 Sch3] and Chart [81 Cha1], Kubaschewski [82 Kub1, 93 Kub1] has published an assessed phase diagram, which has been taken to draw Fig. 1.

In Fig. 2 the γ-loop is given as found by Übelacker [65 Übe1] and Fischer et al. [66 Fis1] (taken from Kubaschewski [82 Kub1, 93 Kub1].

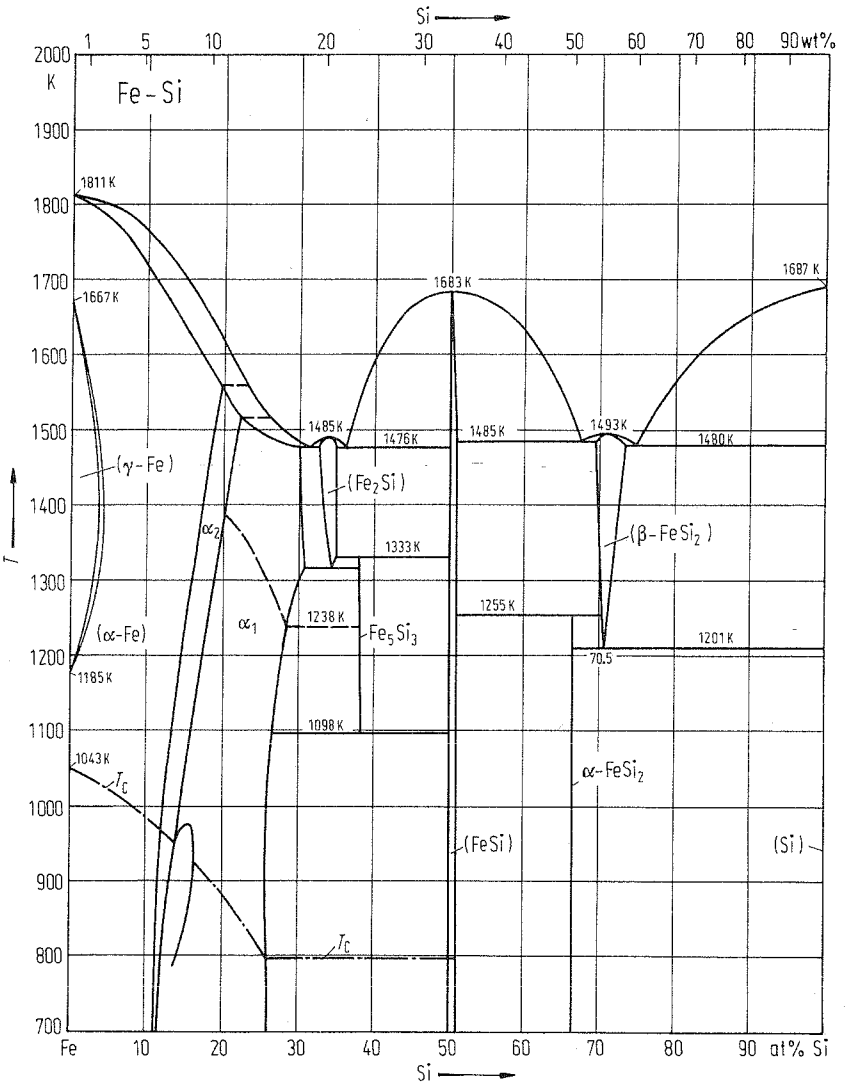

Fig. 1. Fe–Si. Phase diagram.

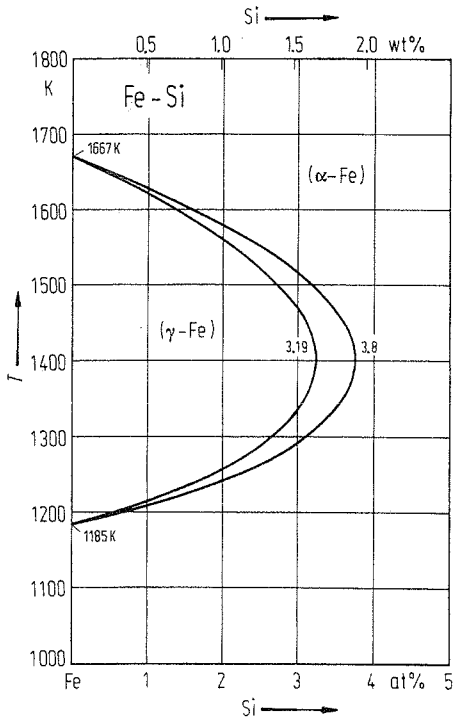

Fig. 2. Fe–Si. (α-Fe) ⇄ (γ-Fe) phase equilibria.

Crystal structure

At concentrations > 10at% Si order-disorder reactions occur in the (α-Fe) region (see Richter et al. [74 Ric1]). On cooling, at the critical temperature T_x the bcc (α-Fe) solid solution with random distribution of Fe and Si atoms became ordered in respect to nearest neighbours. The resulting phase α_2 corresponds to a CsCl-type superstructure. Continuing cooling, at T_y there occurs the phase α_1, with ordering in respect to a BiF_3-type superstructure. Remarkable is the region (α_1 + α_2), in which two phases, α_1 and α_2, are coherently coexisting (Schlatte [71 Sch1, 72 Sch1]). Lattice parameters determined by Richter et al. [74 Ric1] are plotted in Fig. 3. The X-ray analysis has been performed using samples slowly cooled to 293 K. It was shown that the degree of order is strongly dependent on cooling rate.

For (α-Fe) solid solutions a linear dependence of lattice parameter on Si-concentration has been found. The lattice parameters in Fig. 3 for alloys with more than 6 at% Si correspond to mean values of ordered Fe–Si solid solutions containing the CsCl-type superstructure as well as the BiF_3-type superstructure.

Crystallographic data of intermediate phases are compiled in Table 1.

Sandler et al. [85 San1] have prepared by flash-evaporation of a powder with 33 at% Si an amorphous alloy film, the crystallization mode of which has been studied.

Table 1. Fe–Si. Crystal structure and lattice parameters of intermediate phases.

Phase	Structure	Type	*a* [nm]	*b* [nm]	*c* [nm]	Ref.
Fe_2Si	cub	CsCl	0.281			74 Kha1
Fe_5Si_3	hex	Mn_5Si_3	0.67416		0.47079	43 Wei1
FeSi	cub	FeSi	0.4517			63 Wat1
$FeSi_2$	orth	$FeSi_2$	0.9863	0.7791	0.7833	71 Dus1

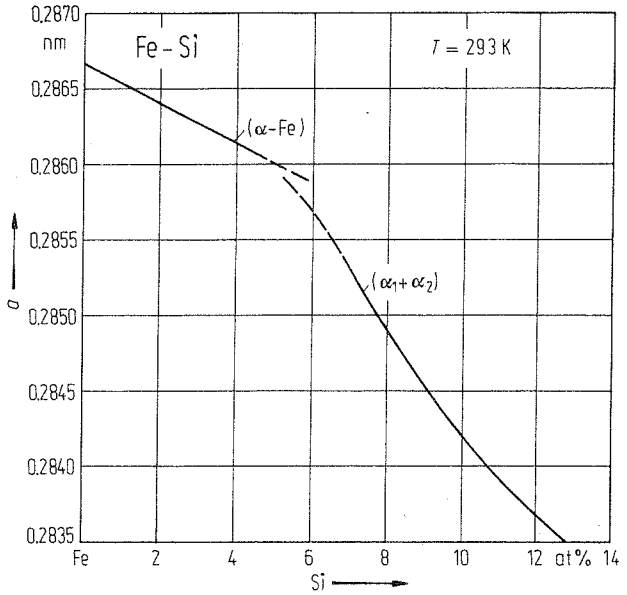

Fig. 3. Fe–Si. Lattice parameters for phases (α-Fe) and ($\alpha_1 + \alpha_2$) at 293 K.

Thermodynamics

The knowledge of thermodynamic properties of Fe–Si alloys is of interest for steelmaking. Therefore, a lot of experimental and theoretical work has been done in this field. One of the most informative analysis of melting equilibria and of thermodynamic properties has been reported by Schmid [80 Sch2], who has optimized all data available and has calculated a consistent set of values. The following figures have been taken from there.

Fig. 4 shows the enthalpies of mixing of liquid Fe–Si alloys. Integral excess entropies of mixing of liquid Fe–Si alloys are plotted in Fig. 5. The logarithm of the activity coefficients of Si in liquid alloys is given in Fig. 6. At last, the integral enthalpies of formation of solid Fe–Si alloys are shown in Fig. 7.

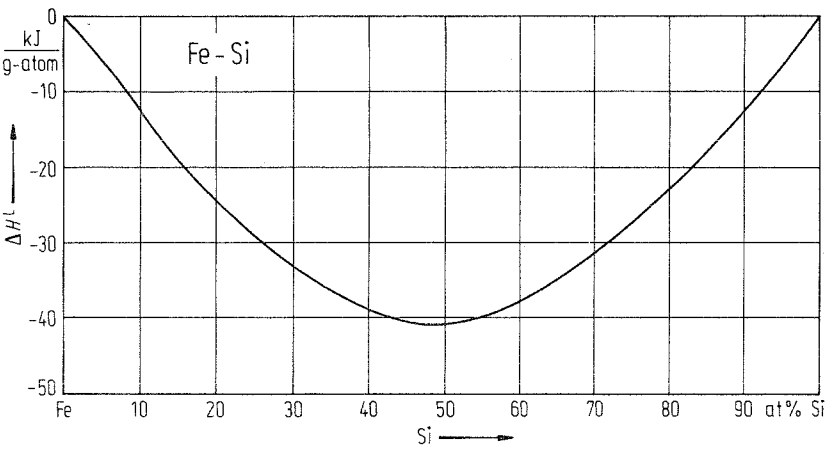

Fig. 4. Fe–Si. Enthalpy of mixing for liquid alloys.

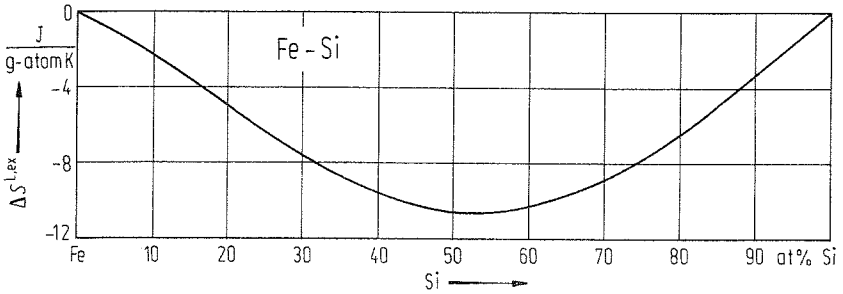

Fig. 5. Fe–Si. Excess entropy of mixing for liquid alloys.

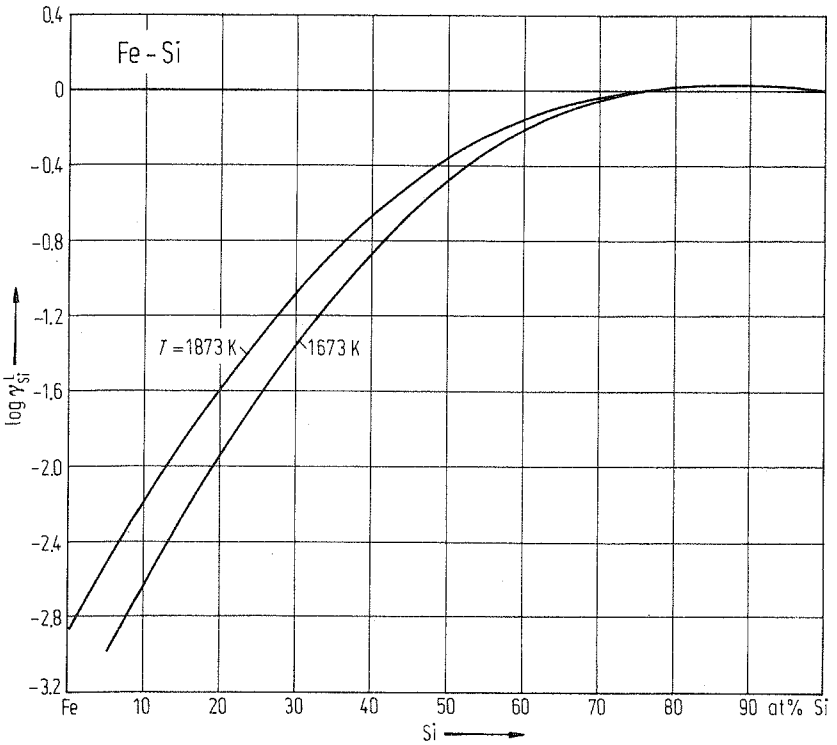

Fig. 6. Fe–Si. Thermodynamic activity coefficient for Si in liquid alloys at 1673 K and 1873 K.

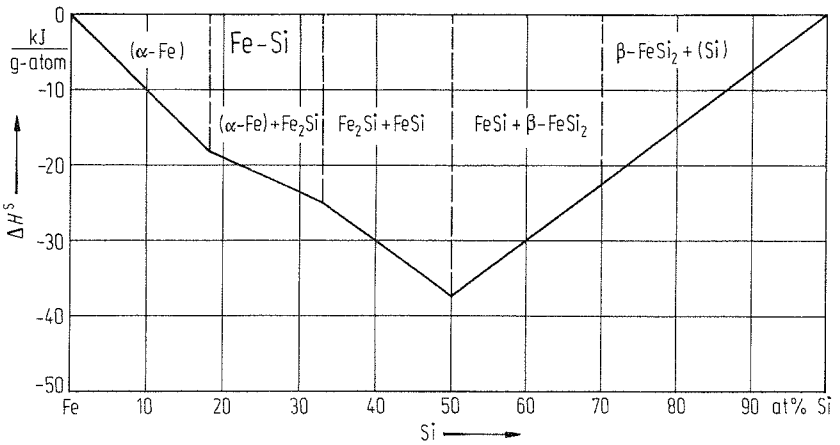

Fig. 7. Fe–Si. Enthalpy of formation for solid alloys.

Fe–Sm (Iron–Samarium)

Phase diagram

By thermal analysis, X-ray diffractography and metallographic methods, Buschow [71 Bus2] has investigated the phase diagram. The results were taken by Okamoto [93 Oka2] to construct an assessed diagram, which was used as a basis for Fig. 1.

Nassau et al. [60 Nas1] have found an intermediate phase Fe_5Sm, which is not included in Fig. 1 as it has not been confirmed by other authors (see Okamoto [93 Oka2]).

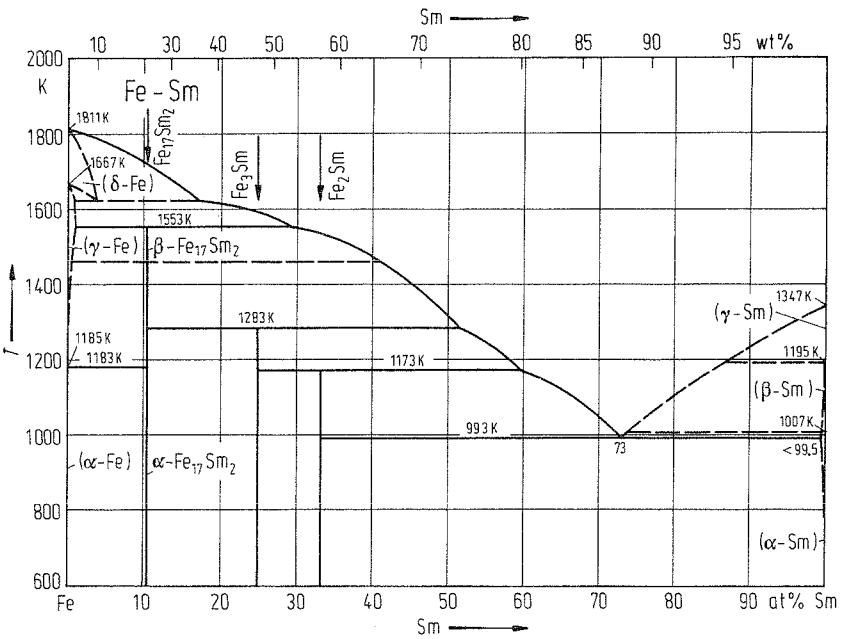

Fig. 1. Fe–Sm. Phase diagram.

Crystal structure

Crystallographic data of intermediate phases are compiled in Table 1.

Table 1. Fe–Sm. Crystal structure and lattice parameters of intermediate phases.

Phase	Structure	Type	a [nm]	c [nm]	Ref.
α-$Fe_{17}Sm_2$	hex	Th_2Zn_{17}	0.8553	1.2425	66 Bus2
β-$Fe_{17}Sm_2$	hex	$Ni_{17}Th_2$	0.849	0.830	89 Gle1
Fe_3Sm	hex	Ni_3Pu	0.5187	2.4910	71 Bus2
Fe_2Sm	cub	Cu_2Mg	0.74164		60 Nas1, 68 Man2
Questionable phase					
Fe_5Sm	hex	$CaCu_5$	0.496	0.415	60 Nas1

Fe–Sn (Iron–Tin)

Phase diagram

First work to establish the phase equilibria by thermal analysis and metallographic observations has been done by Isaac et al. [07 Isa1]. Later on, frequently and by several authors, investigations have been performed. Also, reviews have been published several times, at first by Romig [42 Rom1], and, besides others, at last by Kubaschewski [82 Kub1], Bannykh et al. [86 Ban2] and Okamoto [93 Oka2]. The phase diagram assessed by Okamoto [93 Oka2] was the basis to draw Fig. 1.

The γ-loop and the Sn-rich part of the phase diagram are given on enlarged scale in Fig. 2 and Fig. 3, respectively.

The phase "Fe_3Sn" mentioned in some publications (for instance by Nial [43 Nia1]) is in reality an oxygen-stabilized phase (Singh et al. [86 Sin1]).

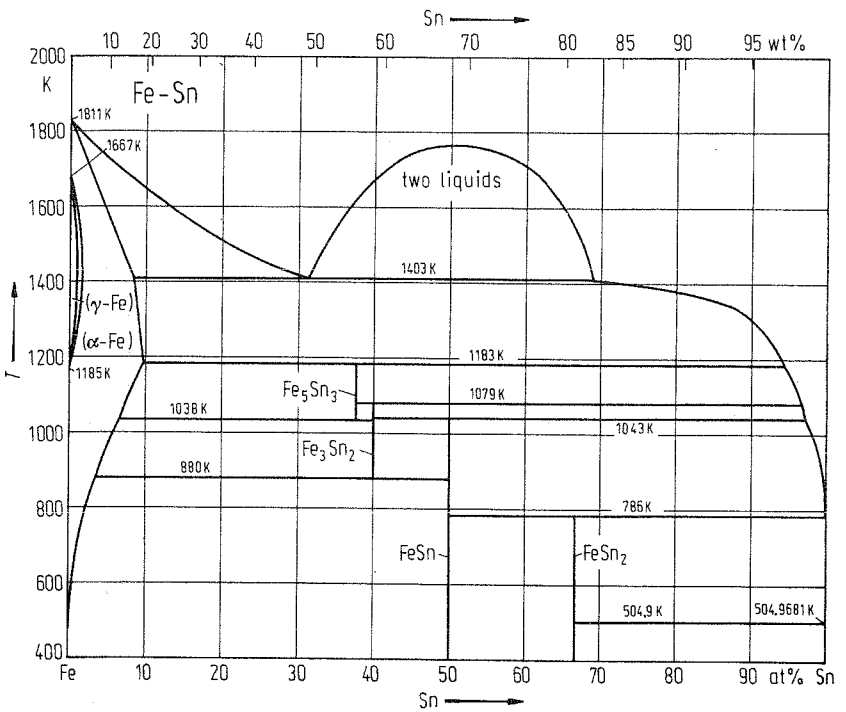

Fig. 1. Fe–Sn. Phase diagram.

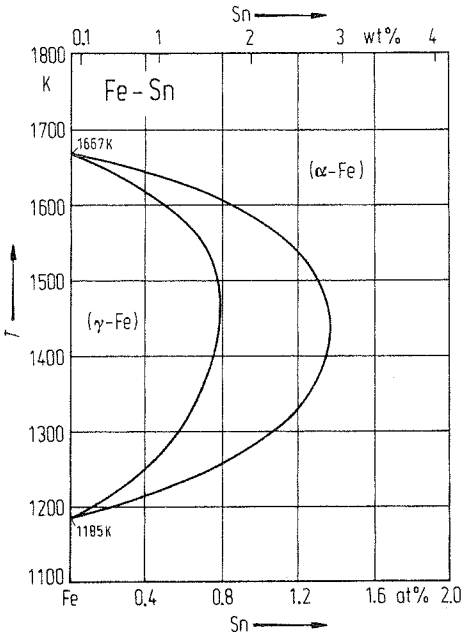

Fig. 2. Fe–Sn. (α-Fe) ⇌ (γ-Fe) phase equilibria.

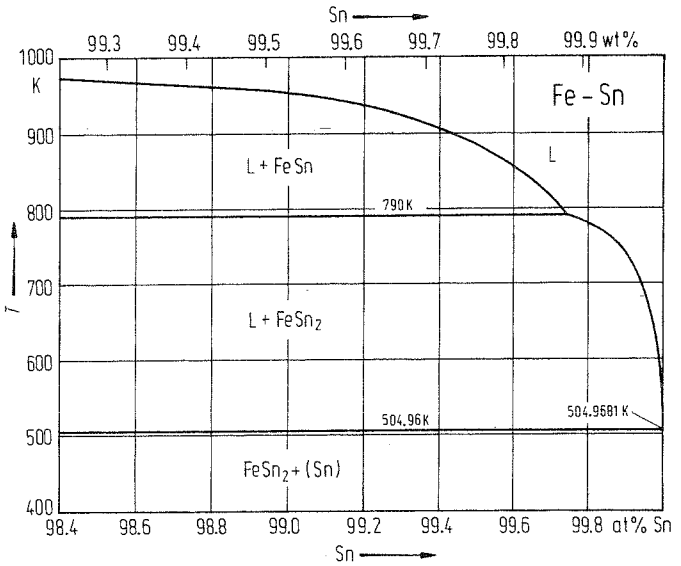

Fig. 3. Fe–Sn. Partial phase diagram (Sn-rich part).

Crystal structure

Lattice parameters of (α-Fe) solid solutions published by different authors are in good agreement. As shown by Okamoto [93 Oka2] they are depending linearly on concentration. From there information was taken to draw Fig. 4.

Crystallographic data of intermediate phases are listed in Table 1.

Table 1. Fe–Sn. Crystal structure and lattice parameters of intermediate phases.

Phase	Structure	Type	a [nm]	c [nm]	Ref.
"Fe_3Sn"	hex	Ni_3Sn	0.5460	0.4362	33 Ehr1
Fe_5Sn_3 (37.5 at% Sn)	hex	Ni_2Sn	0.4203	0.5217	70 Dje1, 66 Yam1
Fe_3Sn_2	hex		0.5344	1.9845	76 Mal1
FeSn	hex	CoSn	0.5303	0.4449	33 Ehr1
$FeSn_2$	tetr	Al_2Cu	0.6533	0.5323	43 Nia1

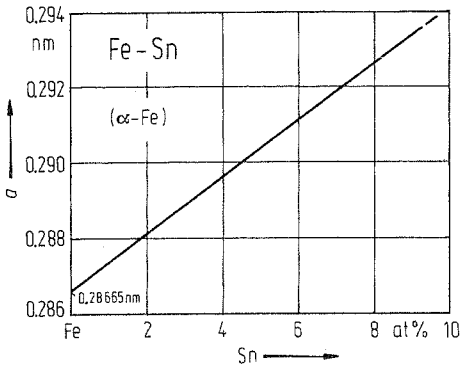

Fig. 4. Fe–Sn. Lattice parameter for bcc (α-Fe) solid solution.

Thermodynamics

At T = 1820 K, Lück et al. [85 Lüc1] have determined by high-temperature calorimetry the enthalpy of mixing of liquid Fe–Sn alloys for concentrations < 23 at% Sn. By modelling, ΔH^L-values have been calculated for the whole concentration range. The results are given in Fig. 5.

Using a vapor pressure method, Onillon [67 Oni1] has determined thermodynamic activities of the components. The results obtained have been taken by Hultgren et al. [73 Hul1] to propose assessed values for 1820 K. These values are plotted as activity isotherms in Fig. 6.

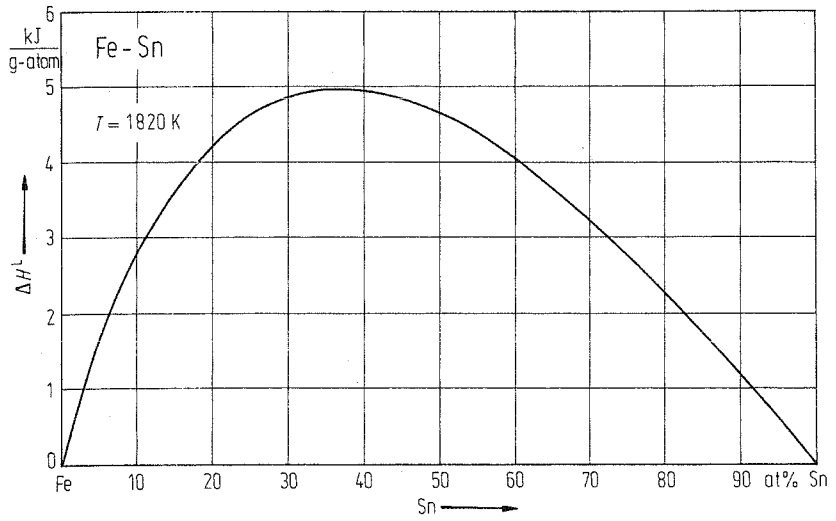

Fig. 5. Fe–Sn. Enthalpy of mixing for liquid alloys at 1820 K.

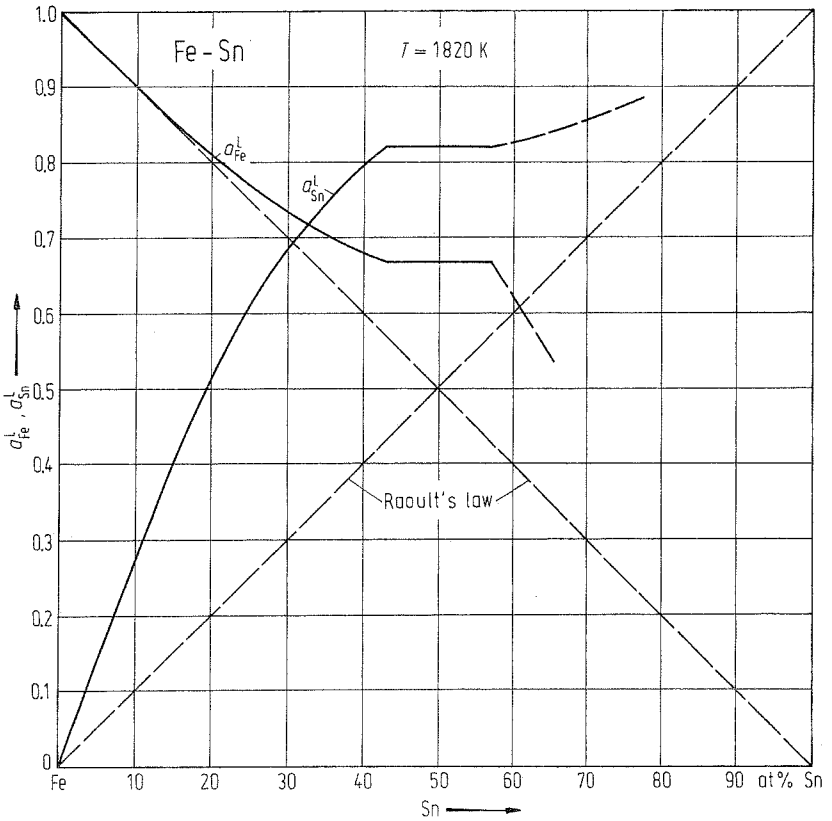

Fig. 6. Fe–Sn. Thermodynamic activities for liquid alloys at 1820 K.

Fe–Sr (Iron–Strontium)

Phase diagram

According to theoretical considerations, Wever [29 Wev1, 28 Wev1] does not expect any solubility between Fe and Sr.

By a semiempiric model, Niessen et al. [83 Nie1] have estimated the Gibbs free enthalpy of mixing. Using these thermodynamic values Okamoto [93 Oka2] has calculated the phase diagram, which was taken to draw Fig. 1.

The experimentally determined solubility of Sr in liquid Fe found by Ageev et al. [85 Age1] (analytical method: atomic absorption spectroscopy) is in rather good agreement with calculated solubilities by Okamoto [93 Oka2]. The former authors obtained 1.78 10^{-3} at% Sr at 1873 K (calculated: 1 10^{-3} at% Sr).

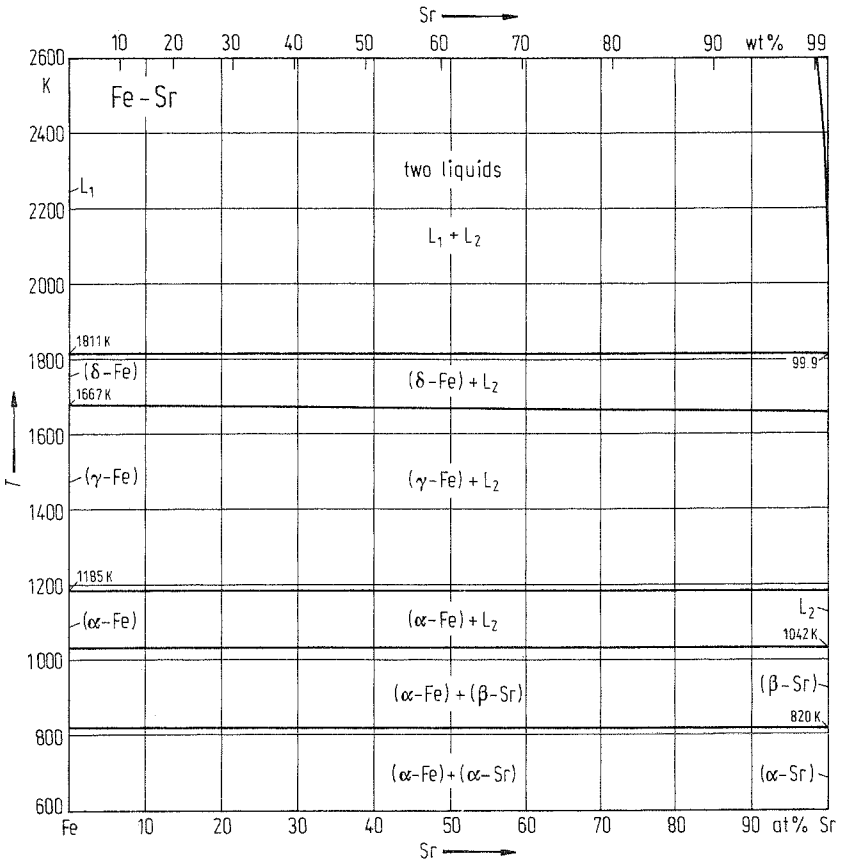

Fig. 1. Fe–Sr. Phase diagram.

Fe–Ta (Iron–Tantalum)

Phase diagram

Genders et al. [36 Gen1], Nemilov et al. [38 Nem1], Abrahamson et al. [66 Abr1], Sinha et al. [67 Sin3] and Fischer et al. [70 Fis1] have investigated the iron-rich part of the system (thermal analysis, magnetic and X-ray diffraction analysis). From the experimental results obtained, Swartzendruber et al. [93 Swa3] have constructed an assessed phase diagram, which has been taken as a basis for Fig. 1. The region of the interrupted γ-loop is given in Fig. 2 on enlarged scale.

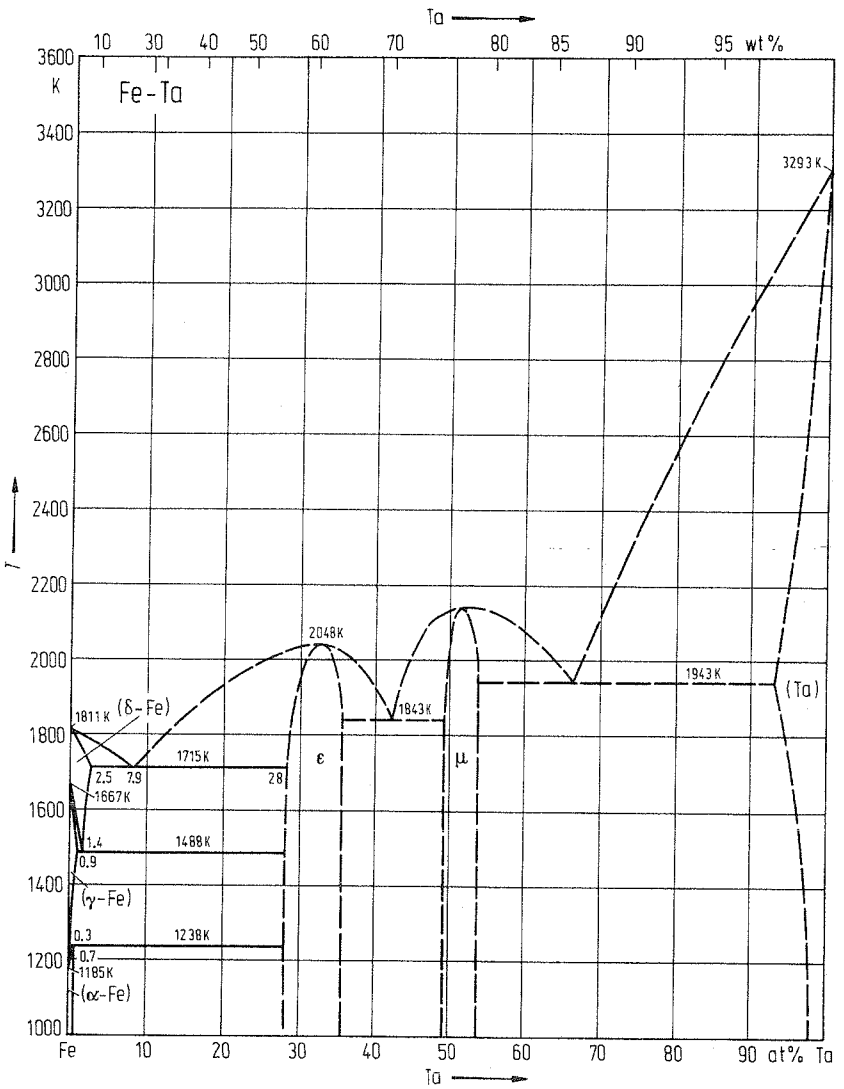

Fig. 1. Fe–Ta. Phase diagram.

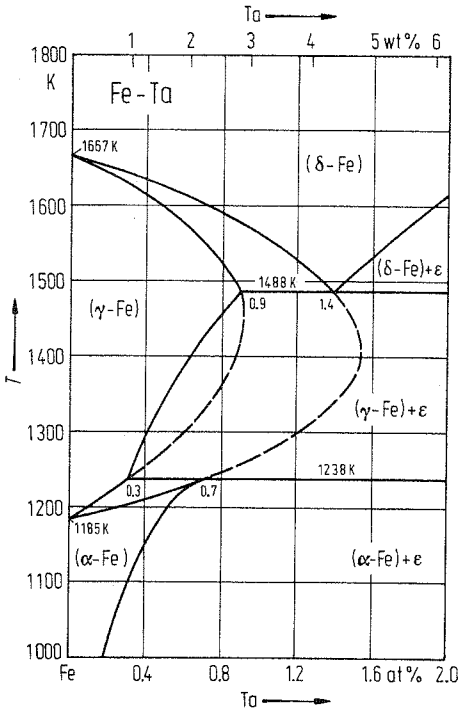

Fig. 2. Fe–Ta. Partial phase diagram (Fe-rich part).

Crystal structure

Crystallographic data of intermediate phases are listed in Table 1.

By sputtering, Naoe et al. [81 Nao1] have prepared thin films (1 μm) in the range between 5 and 25 at% Ta. At concentrations > 14 at% Ta these films were amorphous with crystallization temperatures between 900 and 1100 K.

Table 1. Fe–Ta. Crystal structure and lattice parameters of intermediate phases.

Phase	Structure	Type	*a* [nm]	*c* [nm]	Ref.
ε (Fe_2Ta)	hex	$MgZn_2$	0.4806	0.7846	72 Jon1
μ (FeTa) 49 at% Ta	hex	W_6Fe_7	0.4911	2.698	66 Ram1, 83 Ahm1

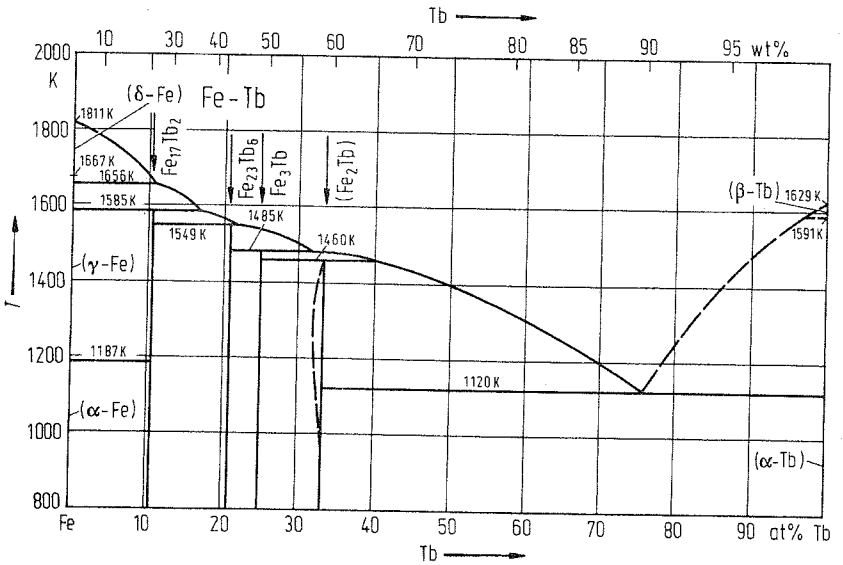

Fig. 1. Fe–Tb. Phase diagram.

Crystal structure

Crystallographic data of intermediate phases are listed in Table 1.

By quenching of a liquid alloy with ≈ 50 at% Tb, a phase of $MgZn_2$-type has been prepared (cooling rate ≈ 10^3 K/s; p = 7.7 GPa), which is metastable under normal conditions.

By sputtering, thin amorphous films with stoichiometry $Fe_{81}Tb_{19}$ have been prepared and investigated by Tanaka et al. [92 Tan1]. Especially, the magnetic anisotropy has been investigated by Harris et al. [92 Har1].

Table 1. Fe–Tb. Crystal structure and lattice parameters of intermediate phases.

Phase	Structure	Type	a [nm]	c [nm]	Ref.
α-$Fe_{17}Tb_2$	hex	Th_2Zn_{17}	0.8467	0.8309	66 Bus2
β-$Fe_{17}Tb_2$ (Tb-rich)	hex	$Ni_{17}Th_2$	0.8504	1.2413	65 Kri3, 76 Dar1
Fe_3Tb_6	cub	$Mn_{23}Th_6$	1.2007		65 Kri3, 77 Orl1
Fe_3Tb	hex	Ni_3Pu	0.5122	2.4745	66 Bus2
Fe_2Tb	cub	Cu_2Mg	0.7369		62 Skr1, 65 Kri2
Metastable phase					
≈ 50 at% Tb	hex	$MgZn_2$	0.527	0.864	85 Tsv1

Thermodynamics

Recently, Landin et al. [94 Lan1] have assessed the phase diagram by thermodynamic modelling. The result is similar to that given in Fig. 1.

Fe–Tc (Iron–Technetium)

Phase diagram

Thermal analysis of Fe-rich alloys has been performed by Buckley et al. [63 Buc1]. Only one intermediate phase is existing in this system, as Darby et al. [62 Dar2, 62 Dar1] found (σ-phase). Moffatt [76 Mof1] has constructed a provisional phase diagram, which seems feasible to Kubaschewski [82 Kub1]. This diagram, also accepted by Okamoto [93 Oka2], has been taken to draw Fig. 1.

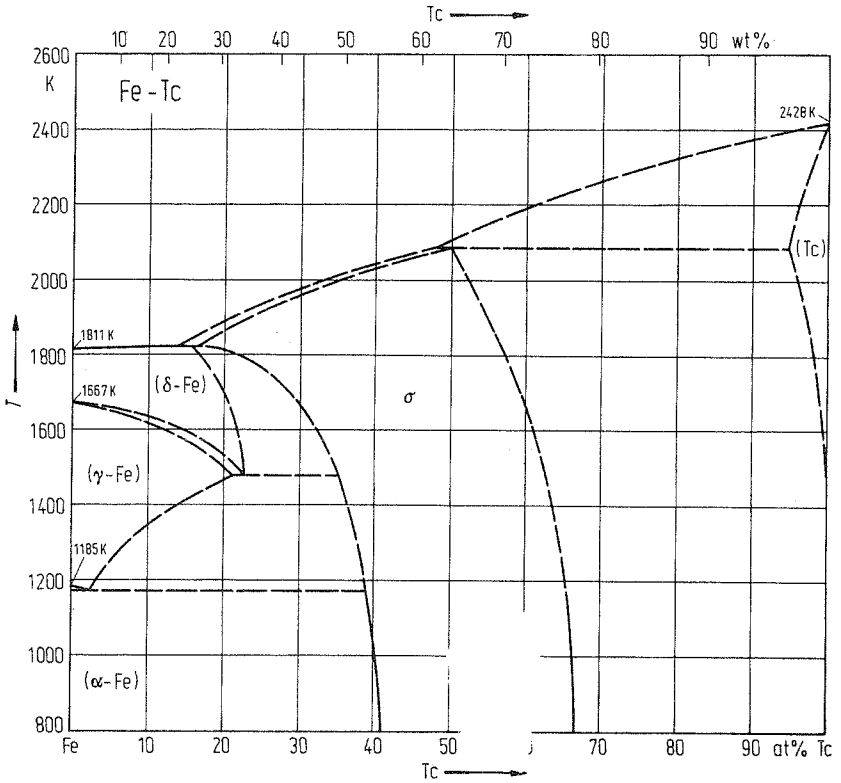

Fig. 1. Fe–Tc. Tentative phase diagram.

Crystal structure

Crystallographic data of the tetragonal σ-phase are given in Table 1.

Table 1. Fe–Tc. Lattice parameters of intermediate phases.

at% Tc	*a* [nm]	*c* [nm]	Ref.
40	0.9010	0.4713	62 Dar2
50	0.9077	0.4756	62 Dar1
60	0.9130	0.4788	62 Dar1

Fe–Te (Iron–Tellurium)

Phase diagram

More or less complete investigations of the phase equilibria have been done by Chiba [55 Chi1], Llewellyn et al. [59 Lle1], Geiderikh et al. [61 Gei1] and Abrikosov et al. [70 Abr1]. At last, comprehensive work using thermal analysis, X-ray diffractography and isopiestic measurements have been performed by Ipser et al. [74 Ips2, 74 Ips1]. This information, especially that published by [74 Ips2] and [74 Ips1], has been used by Okamoto et al. [93 Oka3] to construct an assessed phase diagram, which has been taken as a basis to draw Fig. 1. For the concentration range between 40 and 56 at% Te the phase equilibria are demonstrated on enlarged scale in Fig. 2.

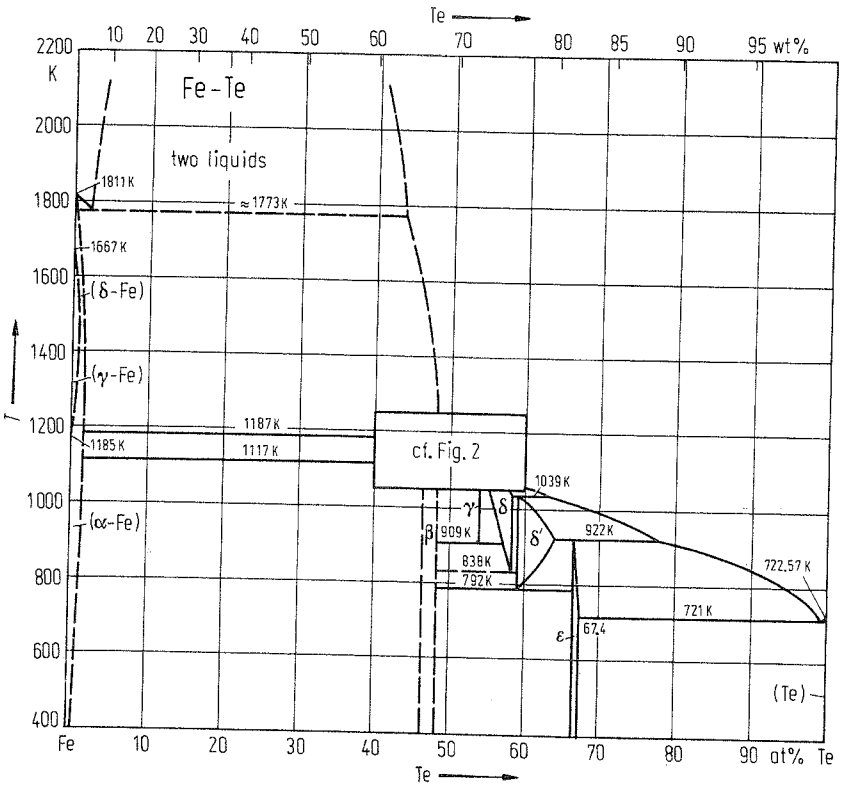

Fig. 1. Fe–Te. Phase diagram.

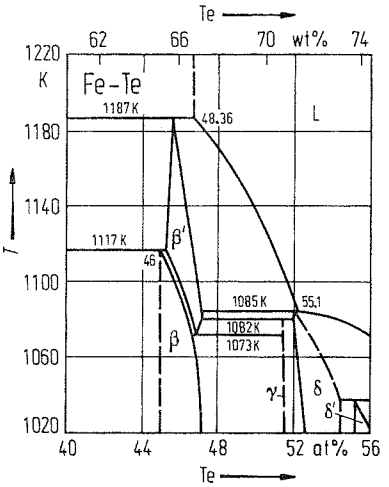

Fig. 2. Fe–Te. Partial phase diagram (40...56 at% Te).

Crystal structure

Crystallographic data of intermediate phases are compiled in Table 1.

Table 1. Fe–Te. Crystal structure and lattice parameters of intermediate phases.

Phase	at% Te	T [K]	Structure	Type	*a* [nm]	*b* [nm]	*c* [nm]	Ref.
β'			hex					74 Ros1
	44.4	1108			0.4031		2.113	
	47.4	1108			0.4013		2.096	
β			tetr	Cu_2Sb				54 Gro1
	47.2				0.38230		0.62767	
	47.5				0.38198		0.62805	
β_1			mon					75 Fru1
	47.1	4.2			0.3843	0.3791	0.6264	
						$\beta =$		
						89.254°		
δ			mon					64 Che1
	54.5				0.386		0.563	76 Red1
					(only small monoclinic distortion)			
	58.3				0.3846	0.6661	0.5641	54 Gro1
						$\beta = 90.20°$		
δ'			hex	NiAs				54 Gro1
	59.7				0.3827		0.5642	74 Ips1
	60.4				0.3813		0.5653	74 Ips1
	62.6				0.3775		0.5673	74 Ips1
ε			orth					70 Bro1
	66.1				0.62650	0.52639	0.38759	57 Lle1
	66.7				0.62655	0.52619	0.38743	57 Lle1
	67.7				0.6276	0.5280	0.3864	57 Lle1

Thermodynamics

At concentrations up to 67 at% Te the vapor pressure of Te of Fe–Te alloys at temperatures between 823 and 1173 K has been determined by Ipser et al. [74 Ips2] using an isopiestic method. From the results obtained, thermodynamic activities of the components were calculated. In Fig. 3 $\log a_{Fe}$ and $\log a_{Te}$ are plotted as a function of concentration. Standard states hereby are solid Fe and liquid Te.

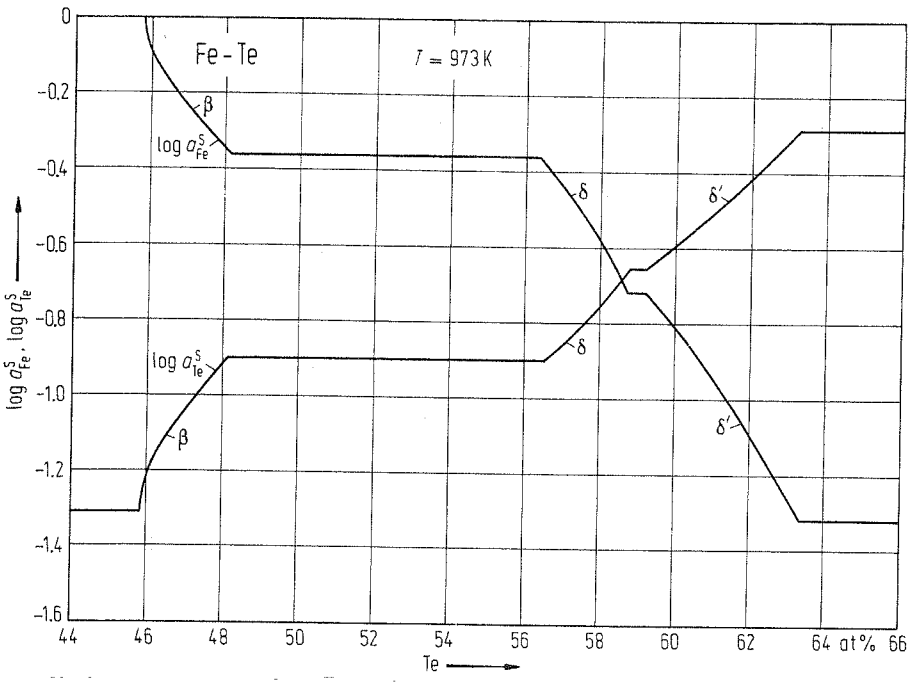

Fig. 3. Fe–Te. Thermodynamic activities for solid alloys at 973 K. Standard states: solid Fe and liquid Te.

Fe–Th (Iron–Thorium)

Phase diagram

At first, Thomson [65 Tho1, 66 Tho2], investigating the entire concentration range, has proposed a phase diagram, which, later on, has been modified regarding newer results obtained by Johnson et al. [69 Joh2], Smith et al. [65 Smi1], Matthias et al. [61 Mat1], Chiotti et al. [81 Chi1], Buschow et al. [71 Bus1], Cirafici et al. [90 Cir1], Palenzona et al. [89 Pal1], and at last by Laabs et al. [91 Laa1]. Using the knowledge of all the results obtained by the above mentioned authors, Okamoto [93 Oka2] has constructed an assessed phase diagram (similar to that published by [89 Pal1]), which was used as a basis to draw Fig. 1.

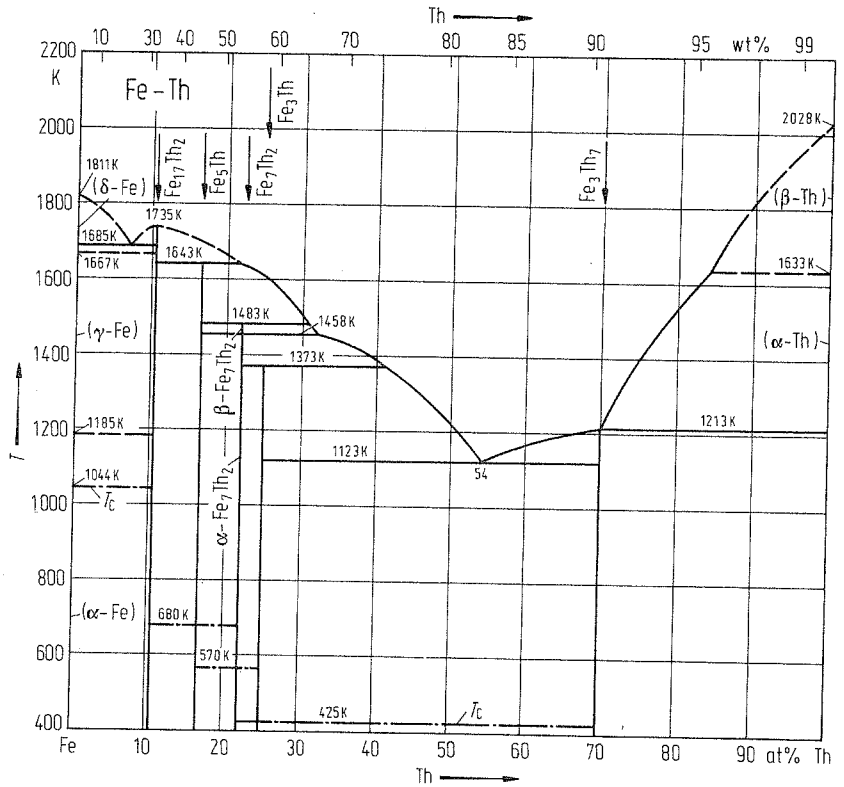

Fig. 1. Fe–Th. Phase diagram. Dashed-dotted lines: Curie temperature T_C.

Crystal structure

Crystallographic data of intermediate phases are summarized in Table 1.

Van der Kraanen et al. [76 Kra1] have determined the temperature dependence of the lattice parameters of Fe_3Th. The results are plotted in Fig. 2.

Table 1. Fe–Th. Crystal structure and lattice parameters of intermediate phases.

Phase	Structure	Type	a [nm]	c [nm]	Ref.
$Fe_{17}Th_2$	hex	Th_2Zn_{17}	0.8565	1.2469	69 Joh2
Fe_5Th	hex	$CaCu_5$	0.5121	0.4052	66 Tho2
α-Fe_7Th_2	hex	Ce_2Ni_7	0.5188	2.4774	89 Pal1
β-Fe_7Th_2	hex	Gd_2Co_7	0.5195	3.7133	89 Pal1
Fe_3Th	hex	$PuNi_3$	0.5207	2.518	66 Tho2
Fe_3Th_7	hex	Fe_3Th	0.9830	0.6214	66 Tho2

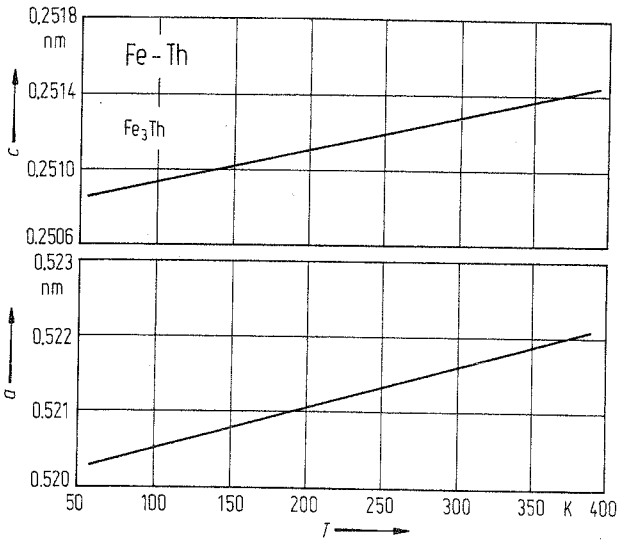

Fig. 2. Fe–Th. Lattice parameters vs. temperature for hexagonal Fe_3Th.

Thermodynamics

Skelton et al. [73 Ske1] have determined thermodynamic functions using the EMF method. The evaluation of the results by Chiotti et al. [81 Chi1] yields thermodynamic values of intermediate phases at 1000 K, which are given in Table 2.

Table 2. Fe–Th. Integral values of formation of intermediate phases (from Chiotti et al. [81 Chi1]). Reference states are γ-Fe and α-Th.

Phase	at% Th	ΔH^S [kJ g-atom^{-1}]	ΔS^S [J g-atom^{-1} K^{-1}]
$Fe_{17}Th_2$	10.5	− 14.0	− 5.9
Fe_5Th	16.7	− 20.6	− 9.4
Fe_7Th_2	22.2	− 24.5	− 12.0
Fe_3Th	25.0	− 26.2	− 13.3
Fe_3Th_7	70.0	− 12.3	− 5.3

Fe–Ti (Iron–Titanium)

Phase diagram

Basic results of experimental investigations of phase equilibria have been published by Hellawell et al. [57 Hel1], Murakami et al. [59 Mur1], Kornilov et al. [56 Kor1], Raub et al. [67 Rau1], Matyka et al. [79 Mat1], Abrahamson et al. [66 Abr1], and several others. Assessments of the phase diagram have been performed by Kubaschewski [82 Kub1] and Murray [93 Mur1]. The diagram proposed by the latter author has been taken to construct Fig. 1. Fig. 2 and Fig. 3 give the α-Ti solvus and the γ-loop at the iron side, respectively.

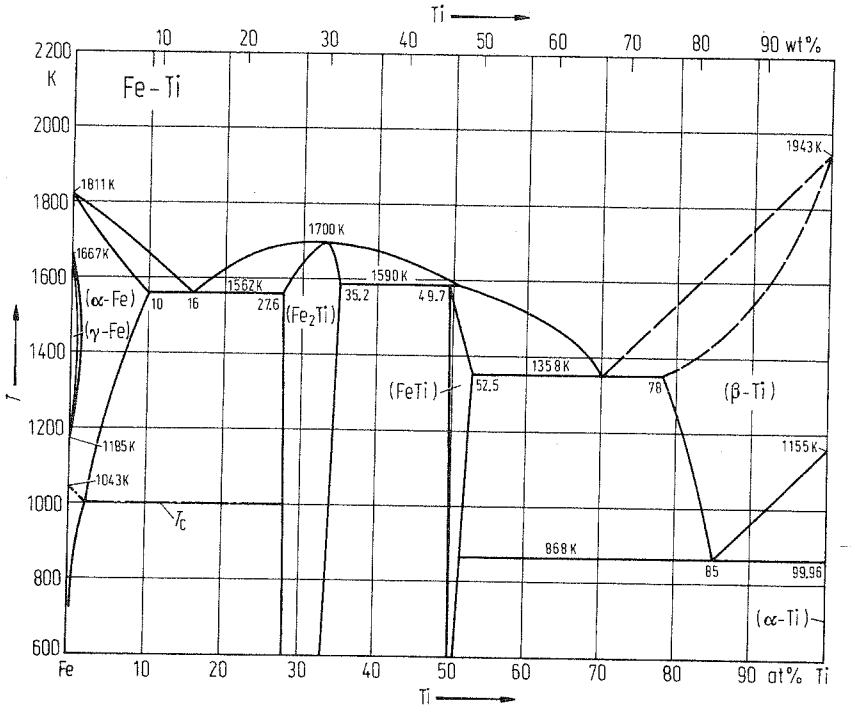

Fig. 1. Fe–Ti. Phase diagram.

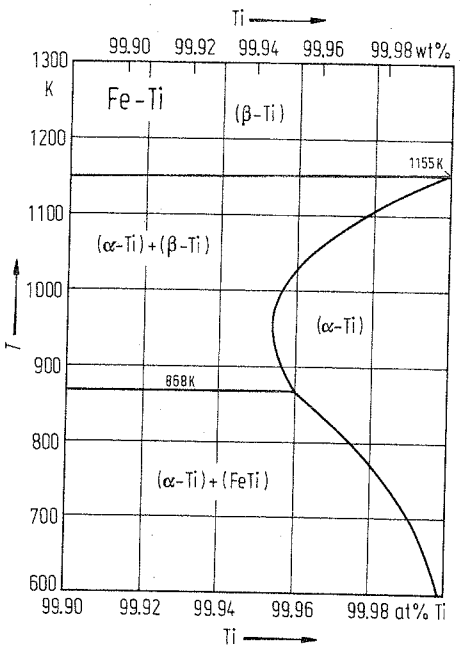

Fig. 2. Fe–Ti. Partial phase diagram (Ti-rich part).

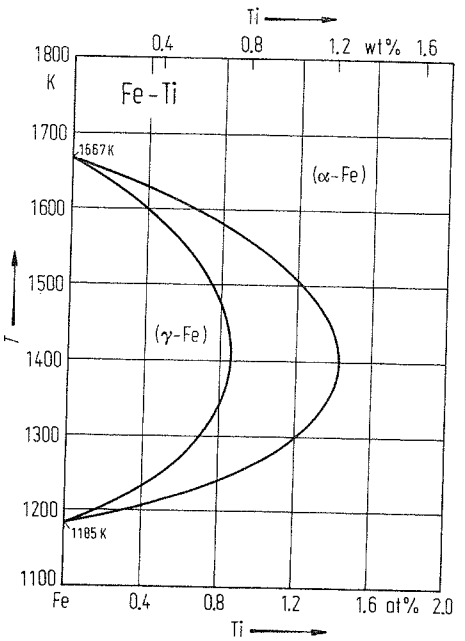

Fig. 3. Fe–Ti. (α-Fe) $\rightleftharpoons$ (γ-Fe) phase equilibria.

Metastable phases

Hexagonal (α-Ti), on quenching, can be formed by martensitic reaction from (β-Ti) at concentrations < 4 at% Fe (Stupel et al. [76 Stu1]). The start temperature of martensitic reaction, M_s, and that of the reverse reaction (A_s), are plotted in Fig. 4 (see [60 Gri1, 63 Kan1, 80 Yam1, 93 Mur1]).

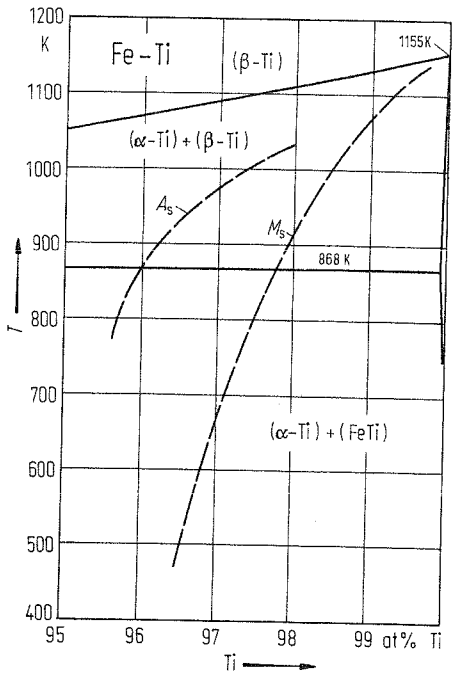

Fig. 4. Fe–Ti. Martensitic transformation starting temperatures on cooling (M_s) and on heating (A_s) of Ti-rich alloys. Solid lines: equilibrium phase boundaries.

Along the transition of metastable (β-Ti) into the equilibrium mixture (α-Ti) + (β-Ti) there occurs a metastable hexagonal (ω-MnTi-type) phase ω (Oshio et al. [69 Osh1]). For a comprehensive discussion of formation conditions see Murray [93 Mur1].

Fe_2Ti transforms martensitically at 265 K (at stoichiometric composition) possibly forming a variant of the $MgZn_2$-type Laves phase (Ikeda et al. [72 Ike1]).

Ray et al. [72 Ray1], by splat-cooling of liquid Fe-Ti alloys, succeeded in preparing (β-Ti) solid solutions up to 35 at% Fe and (FeTi) in the range from 35 to 50 at% Fe.

At concentrations near that of the Ti-rich eutectic, Polesya et al. [73 Pol1] prepared amorphous alloys with 70 to 72 at% Ti. In the neighbourhood of the Fe-rich eutectic (13 to 23 at% Ti) no amorphous alloys could be obtained by melt-spinning (Inoue et al. [80 Ino1]). By vapor-quenching, Sumiyama et al. [86 Sum1] could prepare amorphous alloys in the range between 20 and 75 at% Ti. Mechanical alloying enables the production of amorphous alloys, too. Eckert et al. [91 Eck1] prepared such alloys with concentrations from 30 to 70 at% Ti.

Crystal structure

Lattice parameters of bcc (α-Fe) and of bcc (β-Ti) are plotted in Fig. 5 and Fig. 6, respectively, as a function of concentration (see Murray [93 Mur1]).

FeTi has a bcc ordered structure (CsCl-type), as Pietrokovsky et al. [60 Pie1] and Ray et al. [72 Ray1] (X-ray diffractography) as well as Doroshenko et al. [67 Dor1] and Huthmann et al. [75 Hut1] (neutron scattering) have stated. Lattice parameters were plotted in Fig. 7 (determined by [72 Ray1]).

Lattice parameters of (Fe_2Ti) determined by Ray et al. [72 Ray1] are given in Fig. 8.

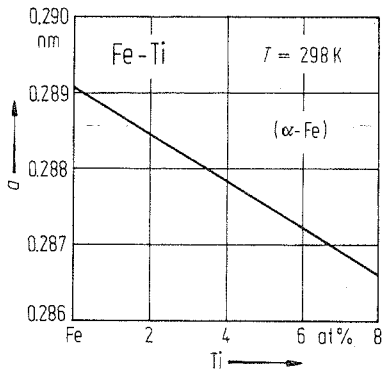

Fig. 5. Fe–Ti. Lattice parameter for bcc (α-Fe) solid solution at 298 K.

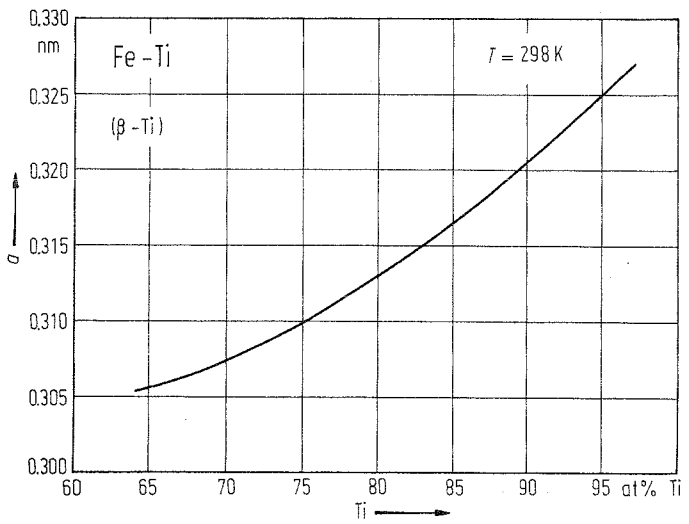

Fig. 6. Fe–Ti. Lattice parameter for bcc (β-Ti) solid solution at 298 K.

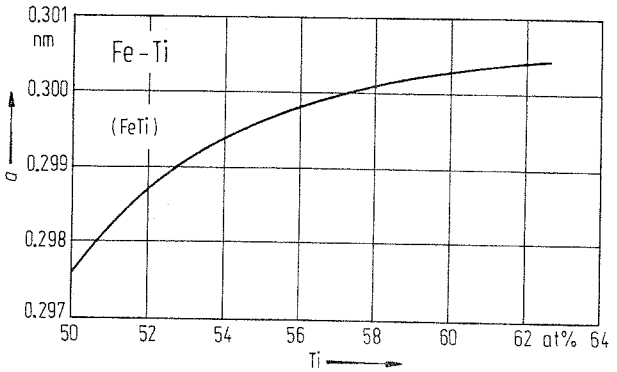

Fig. 7. Fe–Ti. Lattice parameter for cubic (CsCl-type) solid solution (FeTi).

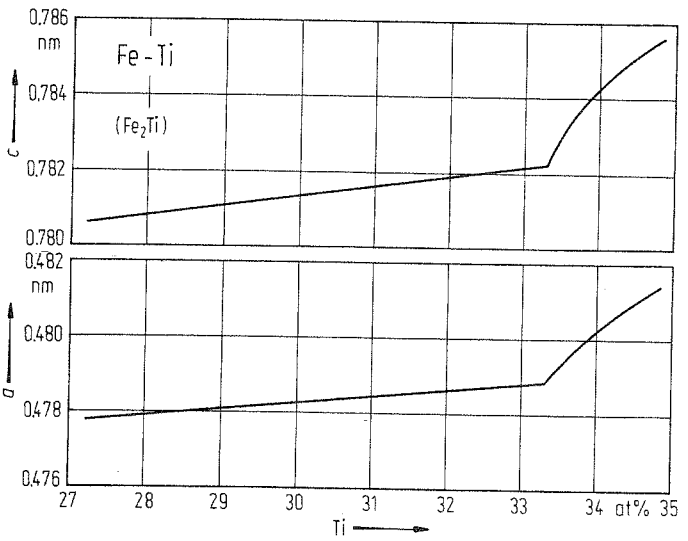

Fig. 8. Fe–Ti. Lattice parameters for hexagonal ($MgZn_2$-type) solid solution (Fe_2Ti).

Thermodynamics

By high-temperature reaction calorimetry, Gachon et al. [83 Gac1] have determined the enthalpies of formation of the intermediate phases of this system. The results are given in Table 1.

Enthalpies of mixing of liquid alloys have been determined experimentally up to 40 at% Ti (Esin et al. [81 Esi1], Batalin et al. [84 Bat1] and Wang et al. [91 Wan1]). Hari Kumar et al. [94 Har1] have calculated assessed ΔH^L values, which are in good agreement with the experimental data from the works mentioned above. These ΔH^L values are plotted in Fig. 9.

Experimentally determined thermodynamic activities are in rather good agreement with those obtained by an assessment (Fruchan [70 Fru1], Wagner et al. [74 Wag1], Furukama et al. [75 Fur2], Hari Kumar et al. [94 Har1]). The results from the latter assessment were taken to draw Fig. 10.

Table 1. Fe–Ti. Enthalpies of formation of intermediate phases (Gachon et al. [83 Gac1]).

Phase	at% Ti	ΔH^S [kJ g-atom^{-1}]
FeTi	50	– 31.0(13)
Fe_2Ti	33	– 27.6(10)

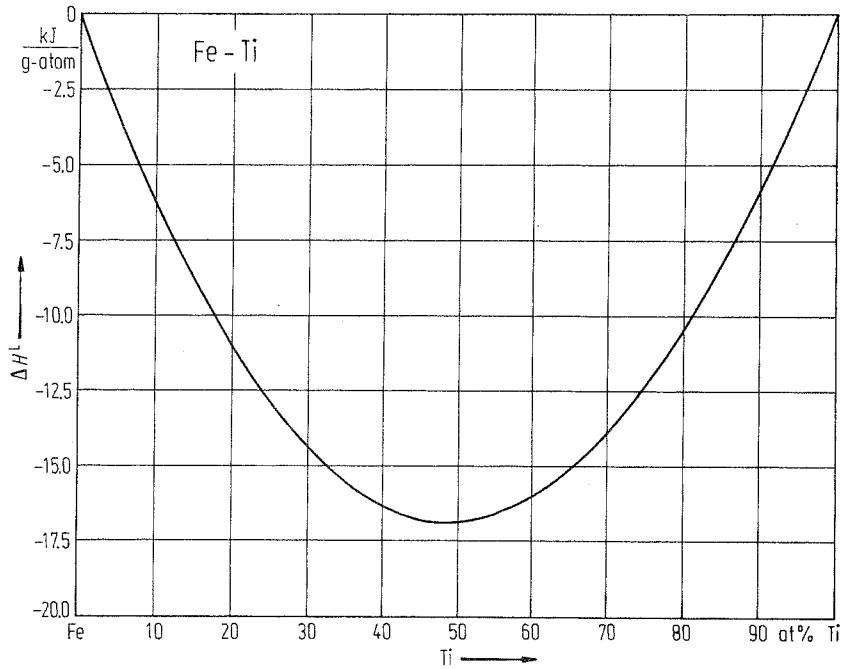

Fig. 9. Fe–Ti. Enthalpy of mixing for liquid alloys.

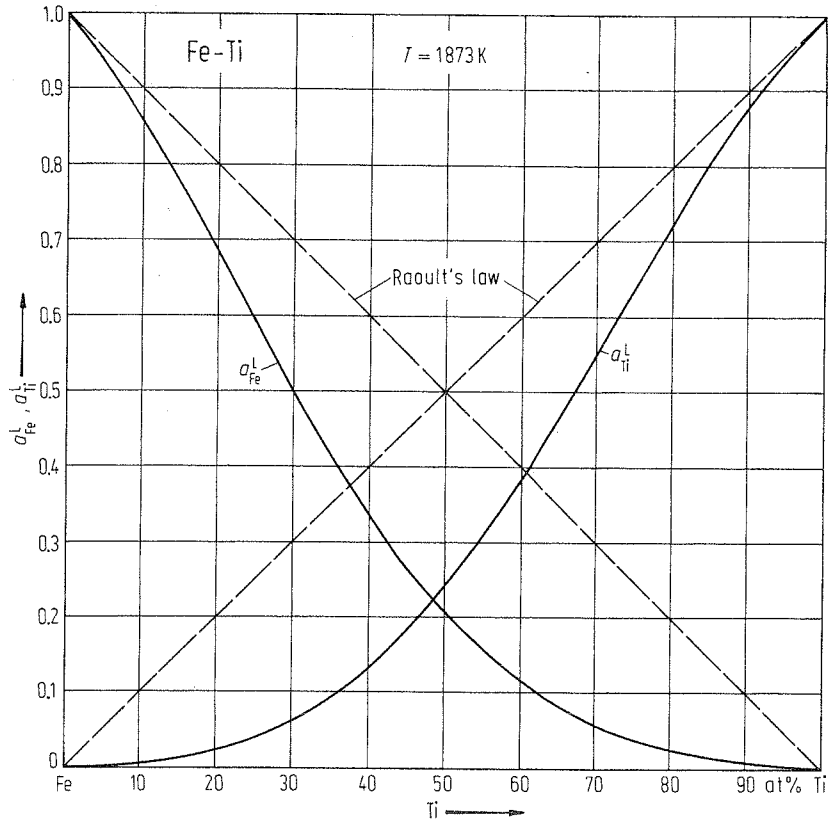

Fig. 10. Fe–Ti. Thermodynamic activities for liquid alloys at 1873 K.

Fe–Tl (Iron–Thallium)

Isaak et al. [07 Isa2] stated that there is no mutual solubility of the components, even not at the boiling point of Tl (1746 K). Grzhimalskiy et al. [68 Grz1], however, found a certain diffusion of the elements in each other (see Kubaschewski [82 Kub1]).

Fe–Tm (Iron–Thulium)

Phase diagram

The phase equilibria have been determined by Kolesnichenko et al. [72 Kol1]. From there information was taken by Kubaschewski [82 Kub1] and Okamoto [93 Oka2] to construct an assessed phase diagram. The results of the latter author were taken to draw Fig. 1.

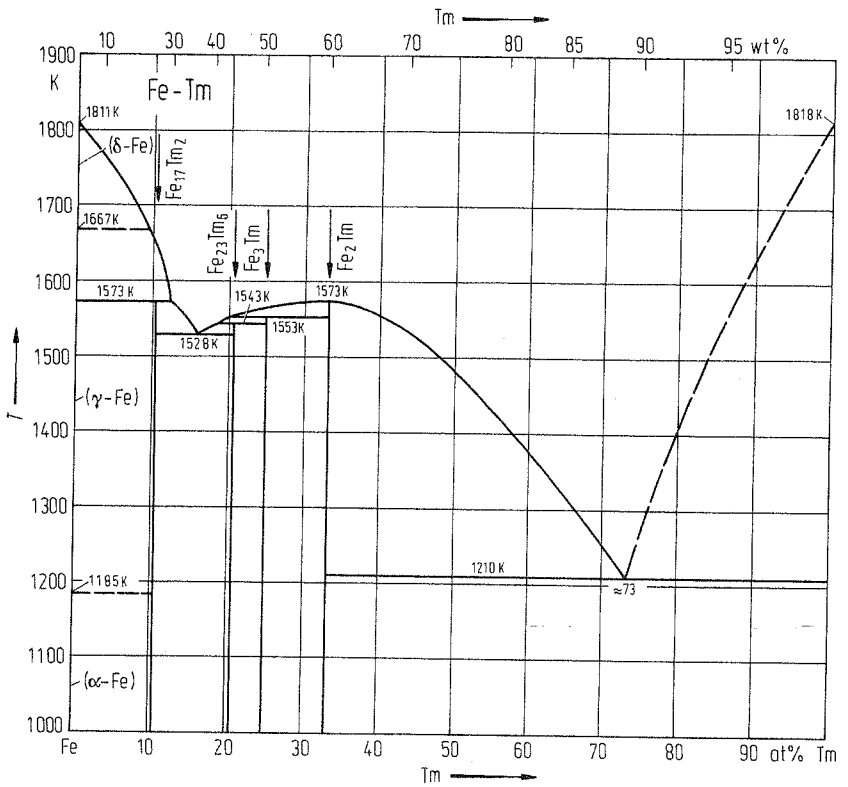

Fig. 1. Fe–Tm. Phase diagram.

Crystal structure

Crystallographic data of intermediate phases are listed in Table 1.

By rapid solidification of a melt with 50 at% Tm at a pressure of 7.7 GPa Tsvyashenko et al. [85 Tsv1] succeeded in preparing a metastable phase with hexagonal Laves-type structure.

Table 1. Fe–Tm. Crystal structure and lattice parameters of intermediate phases.

Phase	Structure	Type	a [nm]	c [nm]	Ref.
$Fe_{17}Tm_2$	hex	Th_2Ni_{17}	0.8417	0.8293	72 Kol1, 89 Gub1, 80 Chr1
$Fe_{23}Tm_6$	cub	Th_6Mn_{23}	1.198		72 Kol1, 65 Kri2, 65 Kri3
Fe_3Tm	hex	Be_3Nb	0.5063	2.4621	72 Kol1, 83 Mal1
Fe_2Tm	cub	$MgCu_2$	0.724		72 Kol1, 60 Has1, 62 Skr1
Metastable phase					
50 at% Tm	hex	$MgZn_2$	0.529	0.854	85 Tsv1

Fe–U (Iron–Uranium)

Phase diagram

Experimental determination of the phase diagram has been performed by Kutaytsev et al. [62 Kut1] (see Lebedev et al. [73 Leb1] and Kubaschewski [82 Kub1]), as well as Gordon et al. [50 Gor1], Grogan et al. [50 Gro1], Clews [50 Cle1], Michaud [66 Mic1] and Chapman et al. [84 Cha1] (thermal analysis). Assessments of the diagram were published by Hultgren et al. [73 Hul1], Chiotti et al. [81 Chi1], Kubaschewski [82 Kub1] and Okamoto [93 Oka2].

Fig. 1 has been constructed on the basis of information given by Okamoto [93 Oka2].

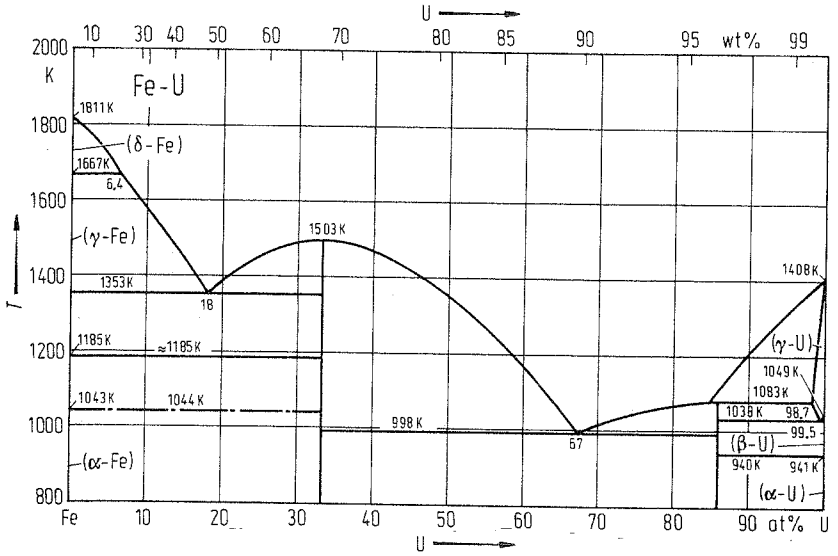

Fig. 1. Fe–U. Phase diagram. Dashed-dotted line: Curie temperature T_C.

Crystal structure

Crystallographic data of intermediate phases of this system are listed in Table 1.

Table 1. Fe–U. Crystal structure and lattice parameters of intermediate phases.

Phase	Structure	Type	a [nm]	c [nm]	Ref.
Fe_2U	cub	$MgCu_2$	0.70629		86 Iti1
FeU_6	tetr	MnU_6	1.02499	0.52500	85 Kim1

Thermodynamics

Using the EMF method Yoshihara et al. [74 Yos1] have determined the enthalpy of formation of Fe_2U. It amounts to $\Delta H^S = -20.6$ kJ/g-atom.

Also from EMF measurements, Lebedev et al. [73 Leb1] and Gardie et al. [92 Gar1] have determined thermodynamic activities of liquid Fe–U alloys in a narrow concentration range.

At 60.6 at% U Lebedev et al. [73 Leb1] found $a_U = 0.579$, and Gardie et al. $a_U = 0.601$ at the same concentration and temperature (1148 K) (see Okamoto [93 Oka2]).

Fe–V (Iron–Vanadium)

Phase diagram

The optimal information on solid-liquid equilibria is that obtained by calculation (Hack et al. [79 Hac1], Andersson [83 And1]). The γ-loop has been determined experimentally by Fischer et al. [70 Fis1]. The results are in agreement with calculations by Andersson [83 And1]. The field of the σ-phase has been investigated by Büth [83 Büt1]. Using this information Smith [93 Smi1] has constructed an assessed phase diagram, which was the basis for Fig. 1.

Hanneman et al. [65 Han1] have found that the expansion of the γ-loop depends on pressure. Results obtained up to 5.0 GPa are plotted in Fig. 2.

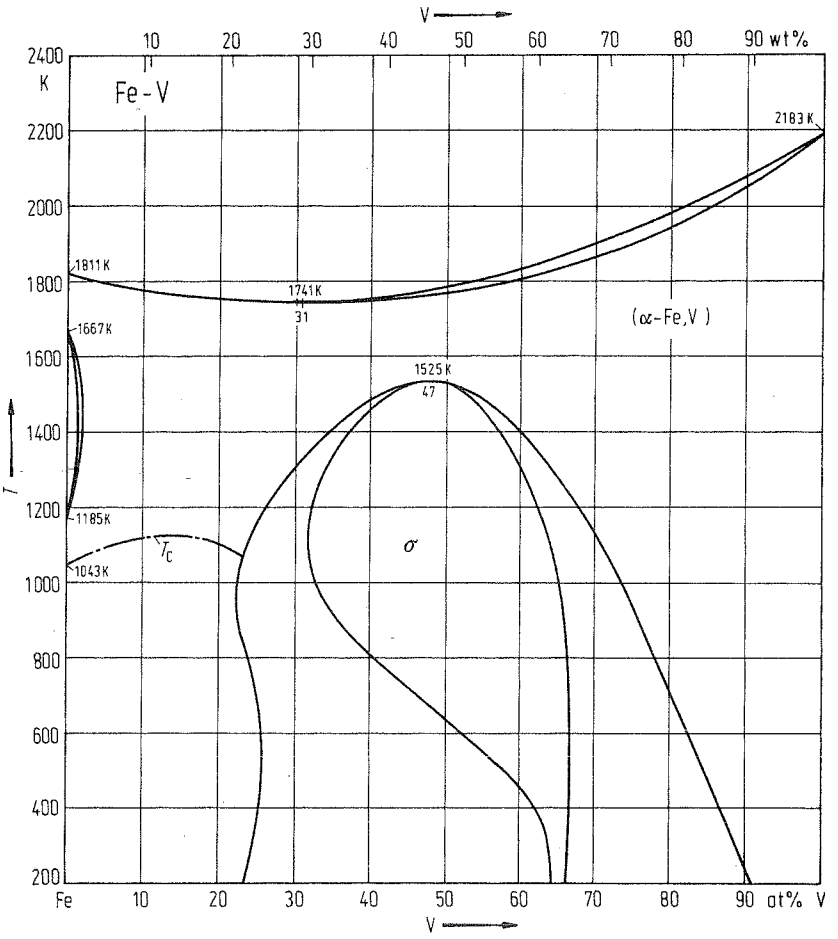

Fig. 1. Fe–V. Phase diagram.

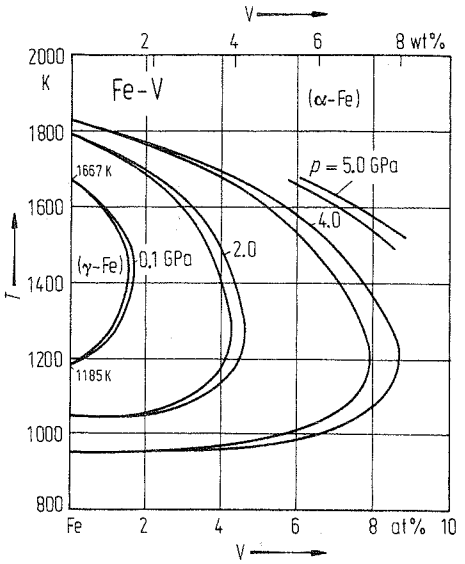

Fig. 2. Fe–V. (α-Fe) ⇌ (γ-Fe) phase equilibria at different pressure.

Crystal structure

Lattice parameters of (α-Fe, V) solid solutions are plotted in Fig. 3. Data to draw this figure have been taken from Smith [93 Smi1].

Lattice parameters of the tetragonal (α-Fe, Cr)-type intermediate phase σ are given in Fig. 4 as a function of concentration (from values given by Smith [93 Smi1]).

By quenching the (α-Fe, V) phase in the concentration range near 50 at% V this phase can be retained at room temperature. The reaction $\alpha \rightarrow \sigma$ is rather sluggish. As an intermediate product of this reaction, before σ is formed on heating, the phase α' with bcc (CsCl-type) structure is produced (Wever [30 Wev1], Bungardt et al. [59 Bun1], see Smith [93 Smi1]). Its lattice parameter is $a = 0.2910$ nm at 50 at% V (Philip et al. [57 Phi1]).

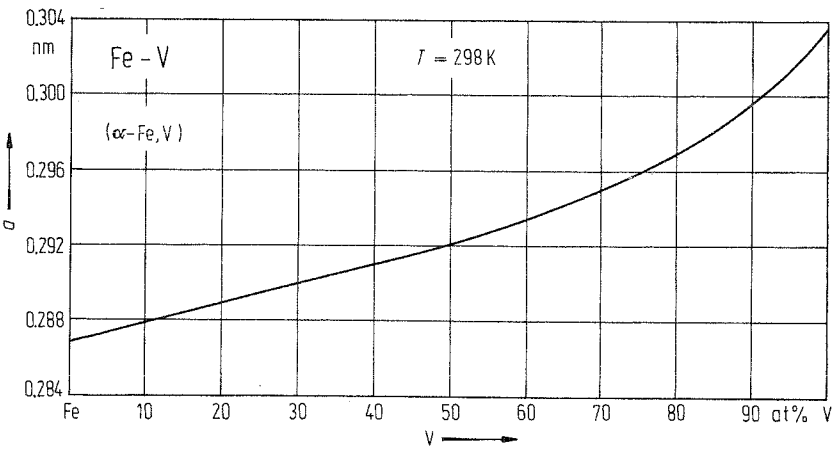

Fig. 3. Fe–V. Lattice parameter for bcc (α-Fe, V) solid solution at 298 K.

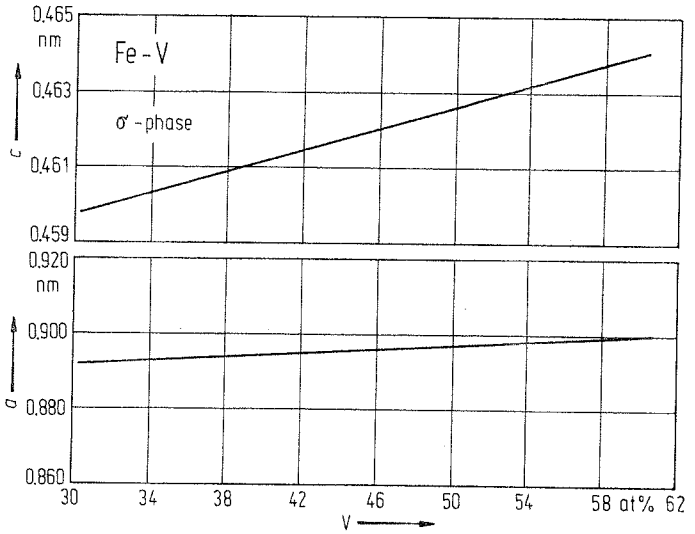

Fig. 4. Fe–V. Lattice parameters for tetragonal (α-FeCr-type) solid phase σ.

Thermodynamics

Thermodynamic activities of liquid alloys have been determined experimentally by Kubaschewski et al. [77 Kub2] and Furukawa et al. [75 Fur1]. The results are in rather good agreement with optimized data published by Hari Kumar [91 Har1]. The latter data have been taken to draw Fig. 5.

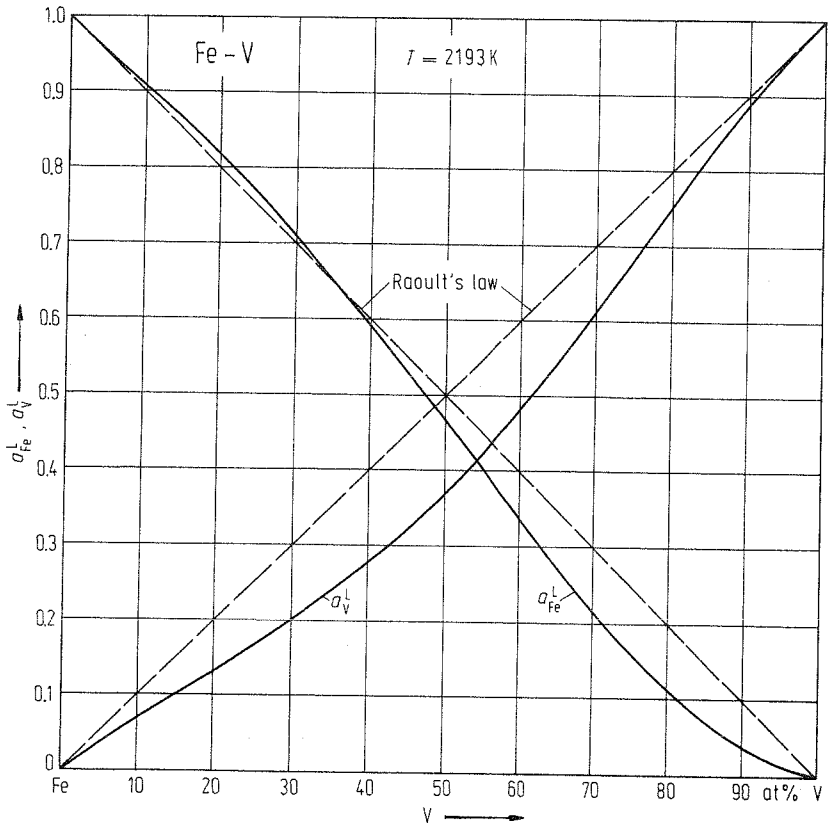

Fig. 5. Fe–V. Thermodynamic activities for liquid alloys at 2193 K.

Enthalpies of mixing of liquid Fe–V alloys have been determined by Batalin et al. [81 Bat1, 82 Bat1], Iguchi et al. [82 Igu1] and Schaefers et al. [93 Sch1]. Hari Kumar et al. [91 Har1] optimized the results known to them and constructed a ΔH^L-concentration diagram, which has been taken to draw Fig. 6.

Determinations of thermodynamic activities of solid Fe–V alloys have been performed by Saxer [62 Sax1], Myles et al. [64 Myl1], Weidner [71 Wei1], Furukawa et al. [75 Fur1], Robinson et al. [76 Rob1], and Kubaschewski et al. [77 Kub2]. Optimized activity coefficients of vanadium, γ_V, taken from Smith [93 Smi1] are plotted in Fig. 7 (at 1600 K).

Enthalpies of formation of solid alloys have been determined by Spencer et al. [73 Spe2] using an adiabatic high-temperature calorimeter. The results are plotted in Fig. 8. The data of ΔH^S for (α-Fe, V) solid solutions are similar to those obtained by assessment by Hari Kumar et al. [91 Har1].

Entropies of formation of (α-Fe, V) solid solutions published by Spencer et al. [73 Spe2] are given in Fig. 9. Reference states for the data in Fig. 8 and Fig. 9 are (γ-Fe) and (α-V).

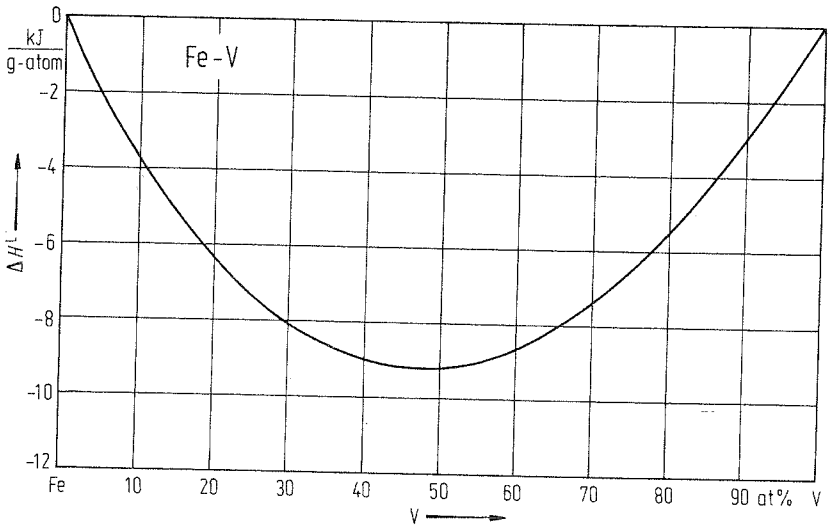

Fig. 6. Fe–V. Enthalpy of mixing for liquid alloys.

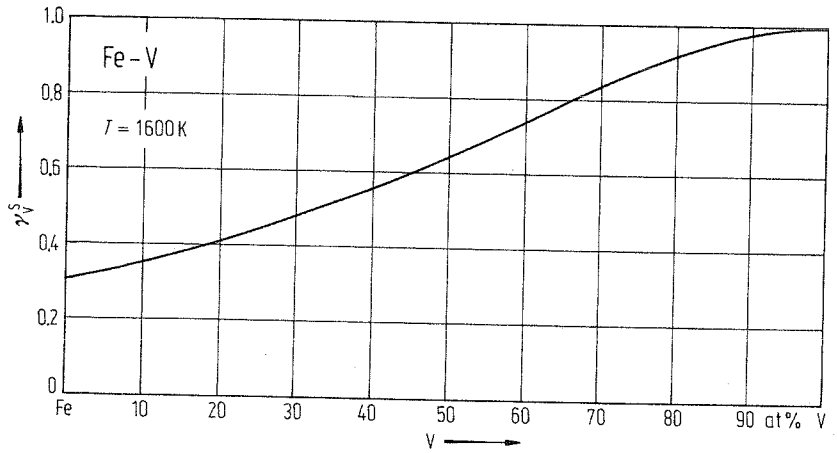

Fig. 7. Fe–V. Thermodynamic activity coefficient of V in solid solutions at 1600 K.

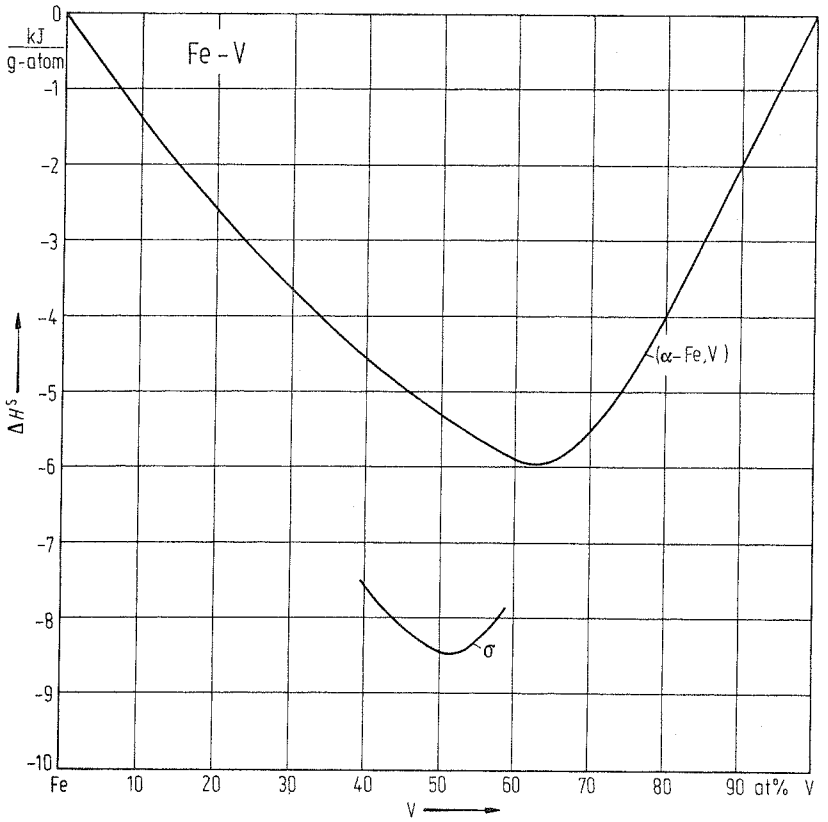

Fig. 8. Fe–V. Enthalpy of formation for (α-Fe, V) solid solution and the σ-phase at 1623 K.

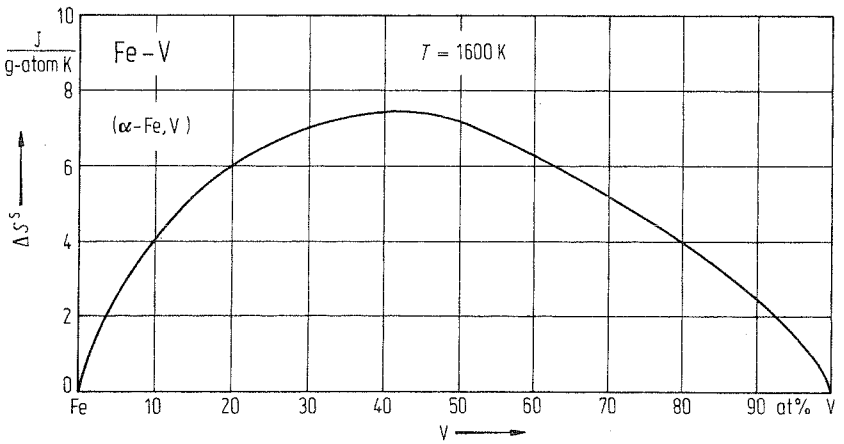

Fig. 9. Fe–V. Entropy of formation for (α-Fe, V) solid solution at 1600 K.

Fe–W (Iron–Tungsten)

Phase diagram

Reviews of this system have been published by Hansen et al. [58 Han1], Kubaschewski [82 Kub1] and Nagender Naidu et al. [93 Nag1]. In the phase diagram proposed by the latter authors the phase δ-FeW is regarded, which has been found and investigated by Henig et al. [81 Hen1]. This newer phase diagram has been taken as a basis to draw Fig. 1.

For thorough discussion of the phase equilibria and the possible metastable phases the reader is referred to Nagender Naidu et al. [93 Nag1].

The solid-liquid equilibria at concentrations < 18 at% W are given on enlarged scale in Fig. 2.

Solid-solid equilibria at the Fe-rich side are shown in Fig. 3 in more detail.

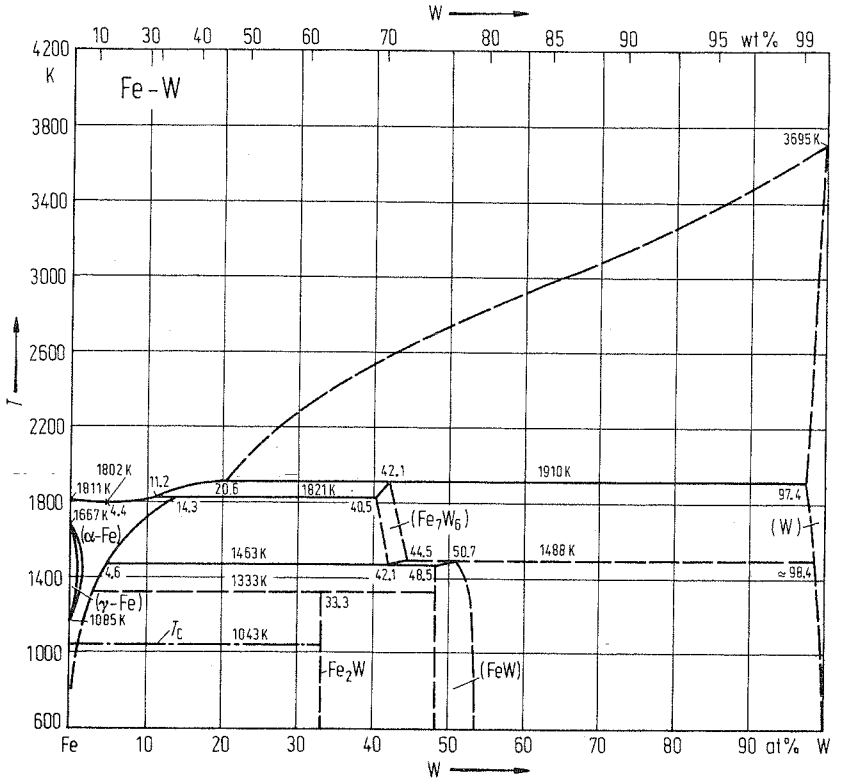

Fig. 1. Fe–W. Phase diagram. The phase Fe_2W is metastable.

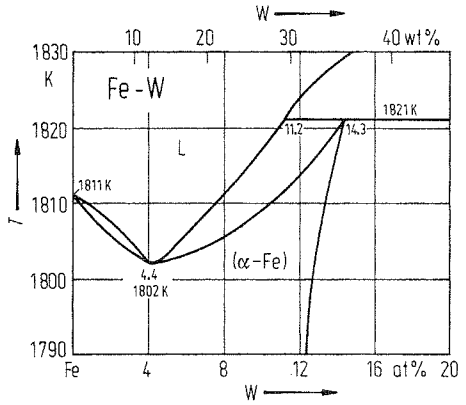

Fig. 2. Fe–W. Solid-liquid phase equilibria for Fe-rich alloys.

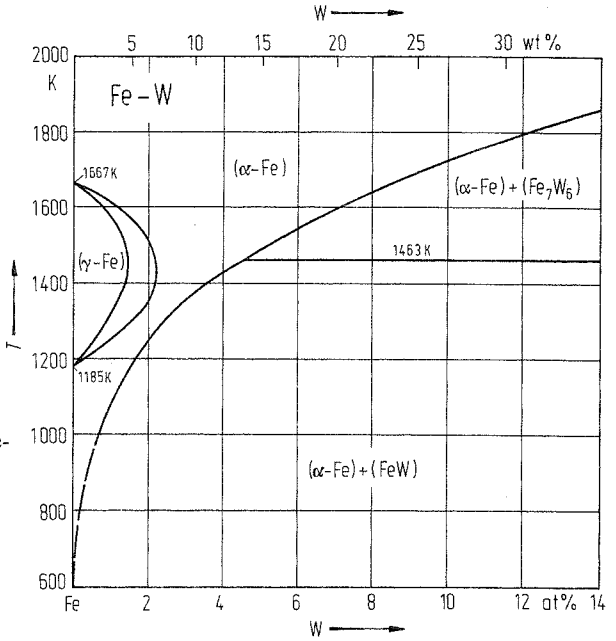

Fig. 3. Fe–W. Solid-solid phase equilibria for Fe-rich alloys.

Crystal structure

Lattice parameters of (α-Fe) as a function of concentration (mean of the data given by Nagender Naidu et al. [93 Nag1]) are plotted in Fig. 4.

Crystallographic data for intermediate phases are listed in Table 1.

In earlier phase diagrams there appears Fe_2W (or λ) as a stable phase (see Hansen et al. [58 Han1], Kubaschewski [82 Kub1] and Kostakis [85 Kos1]). However, Henig et al. [81 Hen1] has stated that λ is metastable. This phase decomposes very sluggishly into the equilibrium phases (after more than 2000 h by tempering at 1273 K). Therefore, in Fig. 1 it is included using dashed lines (see Sinha et al. [67 Sin2]).

Table 1. Fe–W. Crystal structure and lattice parameters of intermediate phases.

Phase	Structure	Type	*a* [nm]	*b* [nm]	*c* [nm]	Ref.
μ-Fe_7W_6	hex	Fe_7W_6	0.4755		2.5830	36 Wes1, 67 Sin2
δ-FeW (50.7 at% W)	orth	MoNi	0.776	1.248	0.710	81 Hen1
Metastable phase						
λ-Fe_2W	hex	Zn_2Mg	0.4737		0.7719	28 Arn1, 67 Sin2

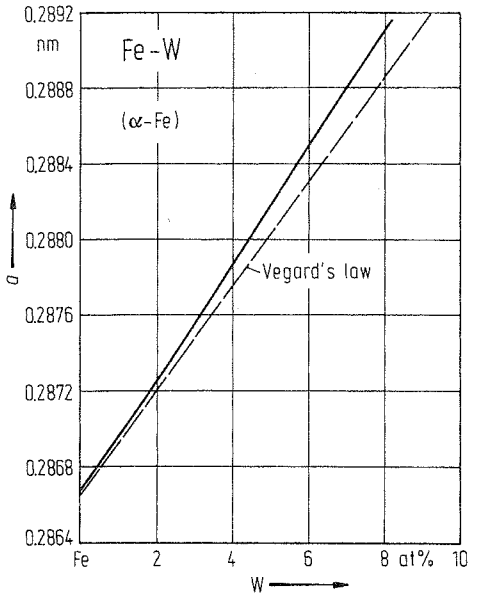

Fig. 4. Fe–W. Lattice parameter for bcc (α-Fe) solid solution.

Thermodynamics

Some experimental thermodynamic data have been obtained for Fe–W alloys. The results are compiled in Table 2.

Table 2. Fe–W. Thermodynamic data for some Fe–W alloys (Nagender Naidu et al. [93 Nag1]).

Phase	at% W	T [K]	ΔH^S [kJ g-atom^{-1}]	ΔS^S [J g-atom^{-1} K^{-1}]	Ref.
liquid	2.5		0.38		82 Igu1
	5.0		0.42		
	7.5		0.800		
(α-Fe)	4	1325...1400	− 0.4(80)	− 0.5(60)	76 Rez1
μ-Fe_7W_6	40	1200...1300	− 16.8(53)	5(3)	76 Rez1
	40	1180...1300	5.8	11	80 Kle1
λ (metastable)	33	1200...1300	− 22.9(24)	− 13.2	76 Rez1
	33	1180...1300	− 0.3	4	80 Kle1

Fe–Y (Iron–Yttrium)

Phase diagram

Experimental investigations of the phase equilibria have been performed by Farkas et al. [59 Far1] and Domagala et al. [61 Dom1]. Assessed phase diagrams have been published by Gschneidner [61 Gsc2], Kubaschewski [82 Kub1], and at last by Zhang et al. [93 Zha1]. From the latter authors information has been taken to draw Fig. 1.

By splat-cooling of a Fe–Y liquid with 32 at% Y, Tenhover [81 Ten1] has prepared an amorphous alloy. He has shown that the crystallization of this glassy alloys occurs in two different steps.

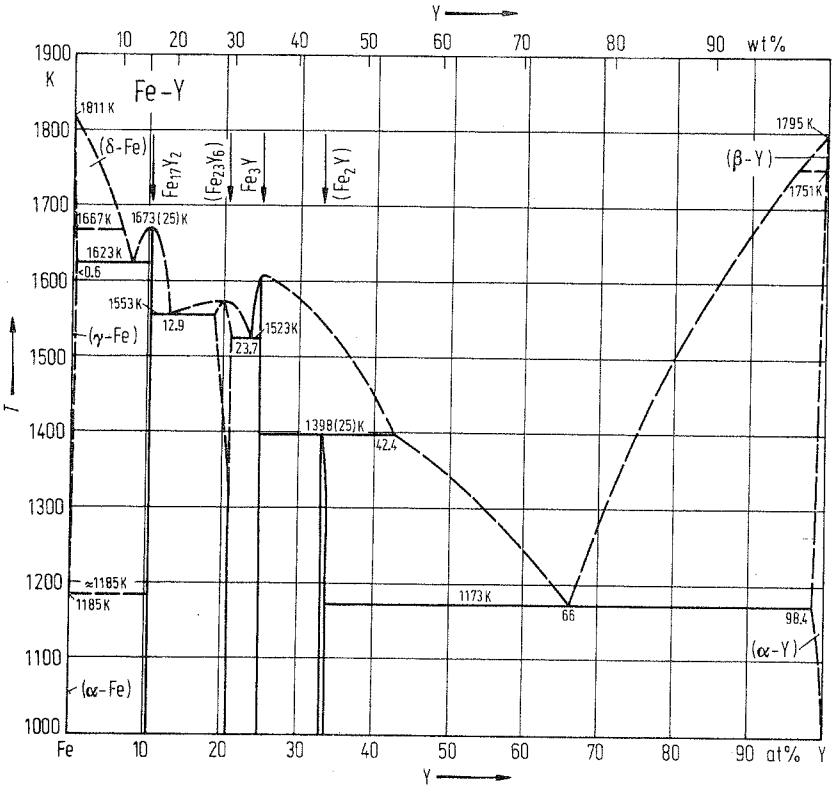

Fig. 1. Fe–Y. Phase diagram.

Crystal structure

Crystallographic data of intermediate phases are listed in Table 1.

Table 1. Fe–Y. Crystal structure and lattice parameters of intermediate phases.

Phase	Structure	Type	*a* [nm]	*c* [nm]	Ref.
α-$Fe_{17}Y_2$	hex	$Ni_{17}Th_2$	0.8463	0.8282	77 Bus1, 86 Chu1
β-$Fe_{17}Y_2$	hex	Th_2Zn_{17}	0.8460	1.2410	82 Kub1
$Fe_{23}Y_6$	cub	$Mn_{23}Th_6$	1.2084		65 Kri2, 77 Bus1, 84 Bay1
Fe_3Y	hex	$PuNi_3$	0.5137	2.461	65 Vuc1, 77 Bus1
Fe_2Y	cub	Cu_2Mg	0.7363		77 Bus1, 82 Kra1

Thermodynamics

Using the EMF method with solid electrolyte, Subramanian et al. [84 Sub1] have determined thermodynamic properties of intermediate phases. The results obtained are listed in Table 2.

Enthalpies of mixing of liquid Fe–Y alloys have been measured by high-temperature calorimetry (at 1873 K) by Ryss et al. [76 Rys1]. The results are plotted in Fig. 2.

Table 2. Fe–Y. Thermodynamic properties of intermediate phases at 973 K, determined by Subramanian et al. [84 Sub1].

Phase	ΔH^S [kJ g-atom^{-1}]	ΔS^S [J g-atom^{-1} K^{-1}]
$Fe_{17}Y_2$	– 6.38(31)	– 1.90(28)
$Fe_{23}Y_6$	– 8.09(49)	– 2.24(44)
Fe_3Y	– 8.97(54)	– 3.03(48)
Fe_2Y	– 7.09(61)	– 0.96(55)

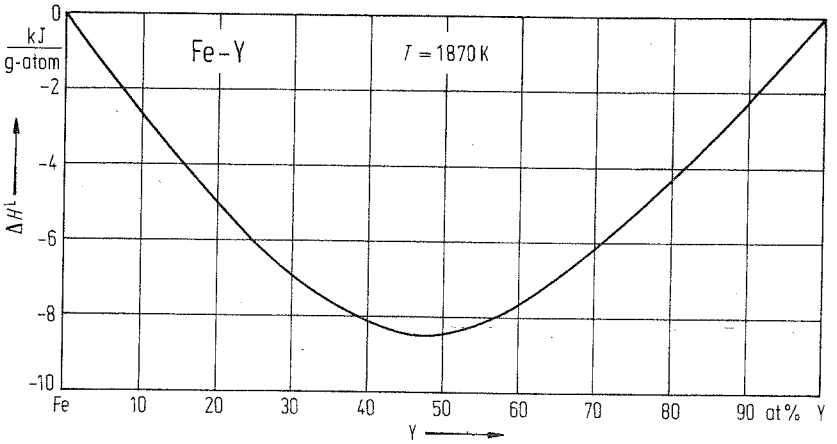

Fig. 2. Fe–Y. Enthalpy of mixing for liquid alloys at 1870 K.

Fe–Yb (Iron–Ytterbium)

Phase diagram

Phase equilibria of this system have been investigated by Iandelli et al. [76 Ian1]. The phase diagram published on the basis of this work has been redrawn by Okamoto [93 Oka2], and also has been taken to construct Fig. 1.

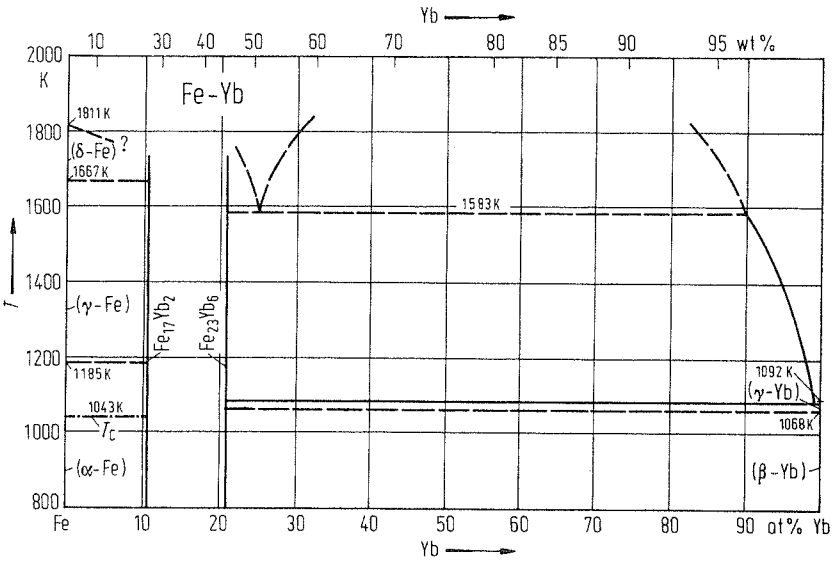

Fig. 1. Fe–Yb. Phase diagram.

High-pressure phases

Fe_2Yb with cubic structure (Cu_2Mg-Laves-type) has been produced at 1273 K and < 0.6 GPa by Cannon et al. [72 Can1]. Meyer et al. [77 Mey1] has prepared this phase at 1473 K and 8.0 GPa. Tsvyashchenko et al. [85 Tsv1] succeeded to form Fe_2Yb quenching liquid alloys containing 20 and 33 at% Yb (cooling rate $10^2 \ldots 10^3$ K/s, constant pressure 7.7 GPa). The latter authors [85 Tsv1] were able to prepare at 31 and 48 at% Yb the hexagonal $MgZn_2$-Laves-type phase (at the same forming conditions as before).

Crystal structure

Crystallographic data of intermetallic compounds are listed in Table 1.

Table 1. Fe–Yb. Crystal structure and lattice parameters of intermediate phases.

Phase	Structure	Type	*a* [nm]	*c* [nm]	Ref.
$Fe_{17}Yb_2$	hex	$Ni_{17}Th_2$	0.8414	0.8249	72 Bus1
$Fe_{23}Yb_6$	cub	$Mn_{23}Th_6$	1.945		72 Bus1
Metastable high-pressure phases					
Fe_2Yb (19at% Yb)	cub	Cu_2Mg	0.7211		72 Can1
Fe_2Yb (31 at% Yb)	hex	$MgZn_2$	0.5131	0.834	85 Tsv1

Fe–Zn (Iron–Zinc)

Phase diagram

Phase equilibria have been investigated several times. An assessed phase diagram was proposed recently by Kubaschewski [82 Kub1] and Burton et al. [93 Bur2]. The diagram published by [93 Bur2] has been taken to draw Fig. 1.

The positive deviations of thermodynamic activities from Raoult's law in the range of (α-Fe) solid solutions published by Wriedt [67 Wri1] indicate the existence of a metastable miscibility gap in this phase. Kirchner et al. [73 Kir1] and Nishizawa et al. [79 Nis1] have calculated the miscibility gap using the above mentioned activity data. The results are given in Fig. 2 (dashed lines). In this calculation, Kirchner et al. [73 Kir1] have not regarded the magnetic effects, whereas Nishizawa et al. [79 Nis1] did.

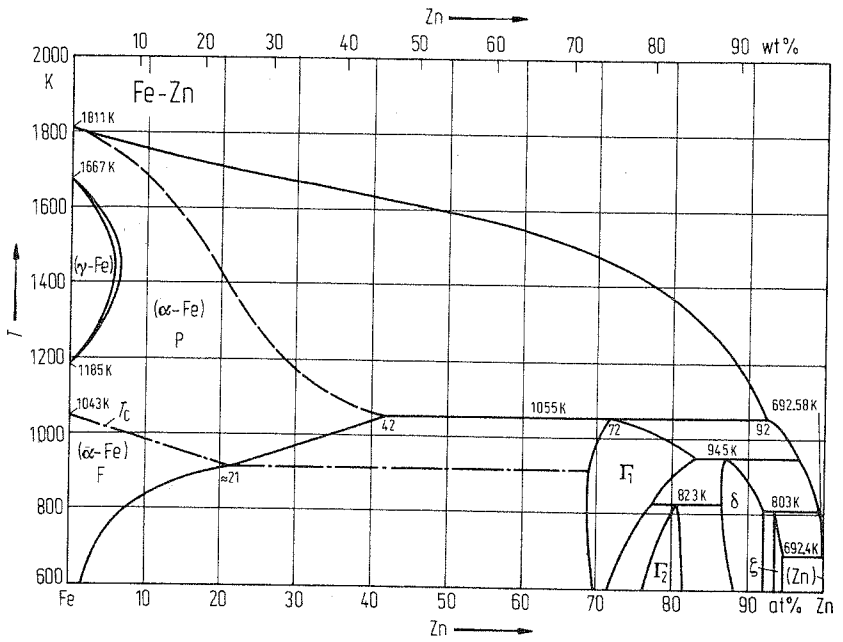

Fig. 1. Fe–Zn. Phase diagram. P: paramagnetic, F: ferromagnetic.

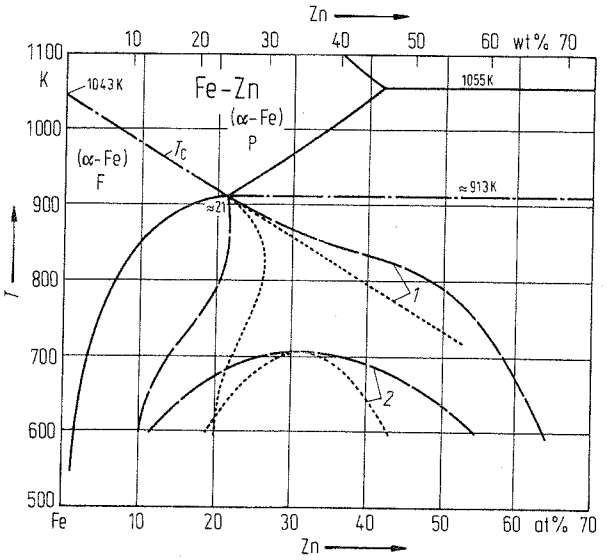

Fig. 2. Fe–Zn. (α-Fe) phase equilibria. Solid lines: stable equilibria, dashed lines: metastable equilibria, dotted lines: spinodal. The calculation of the miscibility gap has been performed by [79 Nis1] taking into account magnetic effects (*1*), and by [73 Kir1] disregarding such effects (*2*). P: paramagnetic, F: ferromagnetic.

Crystal structure

Lattice parameters of (α-Fe) are plotted in Fig. 3.

Crystallographic data of intermediate phases are listed in Table 1.

Table 1. Fe–Zn. Crystal structure and lattice parameters of intermediate phases.

Phase	Structure	Type	*a* [nm]	*b* [nm]	*c* [nm]	Ref.
Γ_1 (Fe_3Zn_{10})	cub	Cu_5Zn_8	0.89823			74 Bra1, 68 Joh1
Γ_2 ($Fe_{11}Zn_{40}$)	cub	$Fe_{11}Zn_{40}$	1.7963			74 Bas1, 81 Kos1
δ ($FeZn_{10}$)	hex	$FeZn_{10}$	1.27812		5.72532	80 Gel1, 93 Ang1
ζ ($FeZn_{13}$)	mon	$CoZn_{13}$	1.3424	0.76080 $\beta = 127.30°$	0.5061	62 Bro1, 79 Gel1

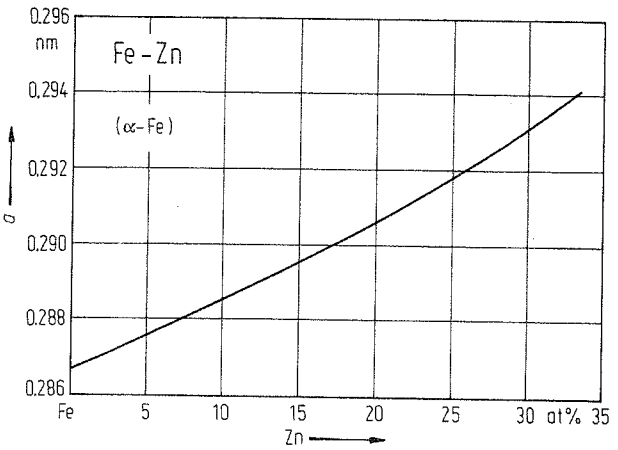

Fig. 3. Fe–Zn. Lattice parameter for bcc (α-Fe) solid solution.

Thermodynamics

Vapor pressure measurements over solid Fe–Zn alloys have been done by Wriedt [67 Wri1] and Gellings et al. [80 Gel2]. From the results obtained, Gellings et al. [80 Gel2] have calculated thermodynamic activities, which are presented in Fig. 4 as isotherms for $T = 617$ K. These authors have also estimated enthalpies of formation of solid alloys using the model developped by Miedema et al. [75 Mie1]. The results are given in Table 2.

From data published by Wriedt [67 Wri1], Hultgren [73 Hul1]has calculated integral enthalpies of formation and integral excess entropies of formation of (α-Fe) solid solutions. The results are plotted in Fig. 5 and Fig. 6, respectively.

Table 2. Fe–Zn. Enthalpy of formation of solid alloys estimated using Miedema's model (Gellings et al. [80 Gel2]).

Stoichiometry	ΔH^S [kJ g-atom^{-1}]
$FeZn_3$	– 3.80
Fe_3Zn_{10}	– 4.00
$FeZn_4$	– 2.67
$FeZn_7$	– 1.94
$FeZn_{10}$	– 1.42
$FeZn_{13}$	– 1.12

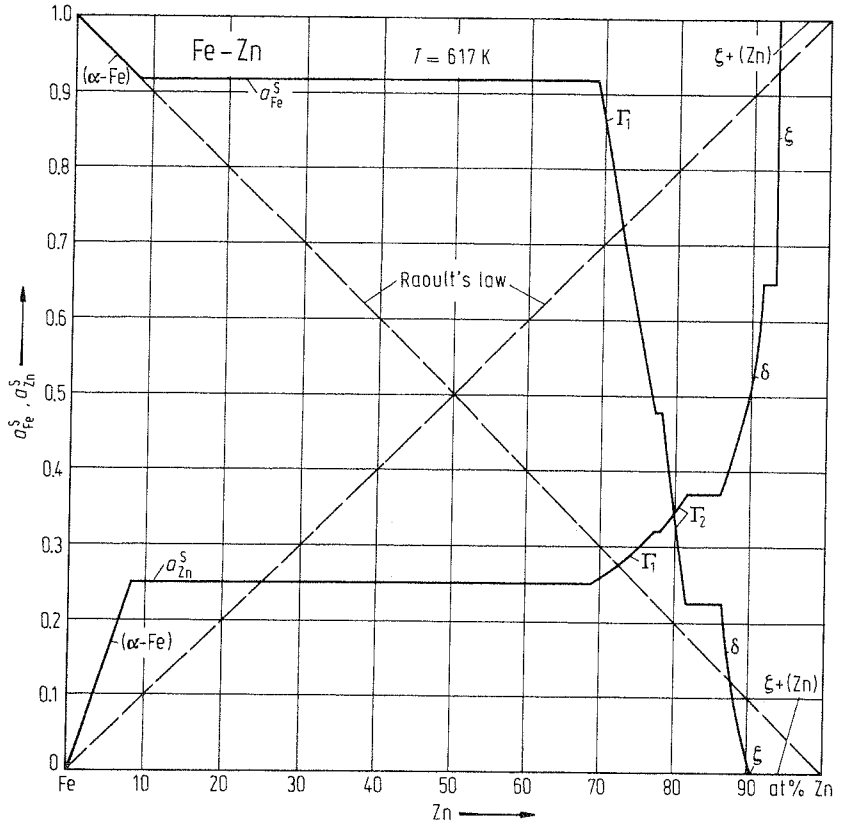

Fig. 4. Fe–Zn. Thermodynamic activities for solid alloys at 617 K.

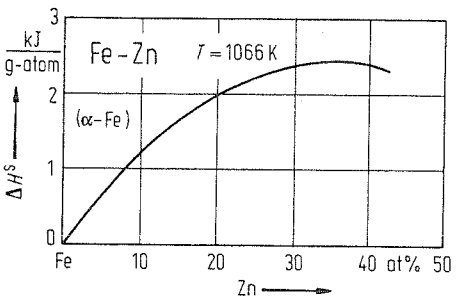

Fig. 5. Fe–Zn. Enthalpy of formation for (α-Fe) solid solutions at 1066 K.

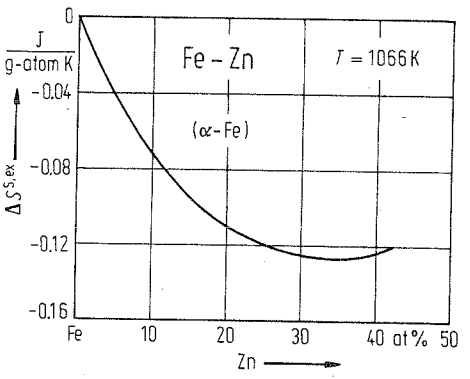

Fig. 6. Fe–Zn. Excess entropy of formation for (α-Fe) solid solutions at 1066 K.

Fe–Zr (Iron–Zirconium)

Phase diagram

The phase equilibria have been investigated rather often. A review is given by Kubaschewski [82 Kub1] and Arias et al. [93 Ari1]. The latter authors have published an assessed phase diagram, basing mainly on the works of Hayes et al. [51 Hay1], Svechnikov et al. [62 Sve1, 63 Sve1], Malakhova et al. [81 Mal1] and Aubertin et al. [85 Aub1]. The diagram published by Arias et al. [93 Ari1] was taken to draw Fig. 1.

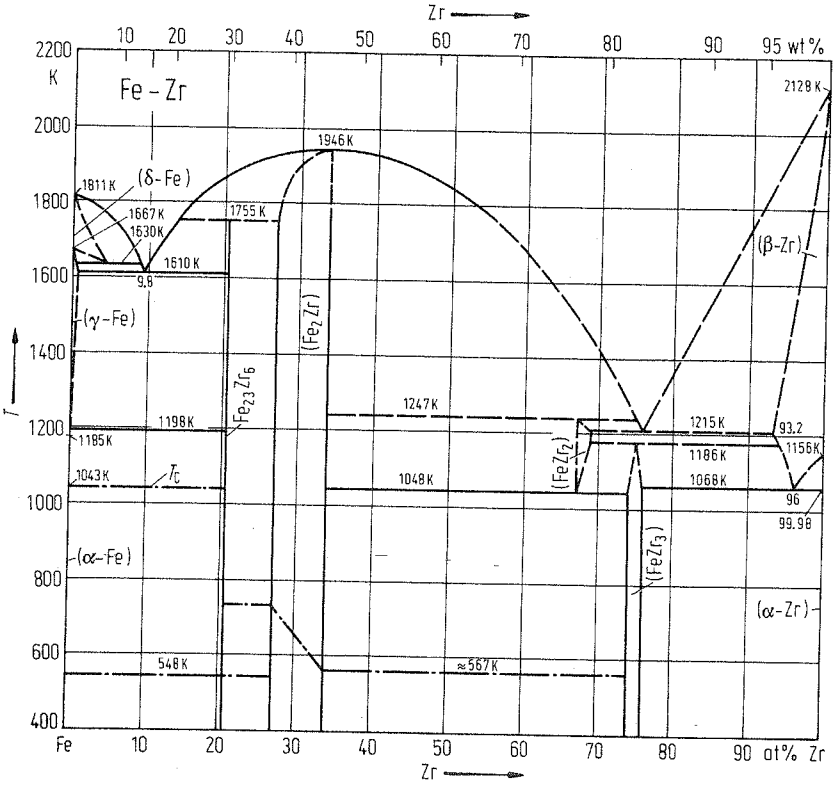

Fig. 1. Fe–Zr. Phase diagram. Dashed-dotted lines: Curie temperature T_C.

Metastable phases

If alloys with 80...98 at% Zr were quenched from temperatures between 1073 K and 1148 K, an ω phase has been found (Malakhov et al. [82 Mal1]). Also, on crystallization of amorphous Fe–Zr alloys, ω was found as an intermediate phase(Buschow et al. [83 Bus1]). The latter authors found the following lattice parameters for the tetragonal ω at 80 at% Zr: $a = 0.502$ nm; $c = 0.300$ nm.

In the concentration range between 7 and 80 at% Zr, amorphous alloys were obtained by splat-cooling (Masumoto et al. [80 Mas1], Chi et al. [82 Chi1], Fukamichi et al. [82 Fuk1], Batalla et al. [85 Bat1], and many others).

As an intermediate phase during the crystallization process of amorphous alloys with 80 at% Zr, Buschow [83 Bus1] detected metastable $FeZr_3$ (m) with orthorhombic crystal structure. The lattice parameters are $a = 0.3959$ nm; $b = 0.6139$ nm; $c = 0.6846$ nm as Altounian et al. [85 Alt1] reported. This metastable $FeZr_3$ (m) phase transforms rapidly into the stable $FeZr_3$ phase above 723 K [85 Alt1].

At concentrations between 57.5 and 76.0 at% Zr, amorphous alloys transform into the metastable $FeZr_2$(m) phase with cubic structure of Fe_3W_3C-type (Altounian et al. [85 Alt1]). In a following reaction this latter modification transforms into stable phases.

Crystal structure
Crystallographic data of intermediate phases are compiled in Table 1.

Table 1. Fe–Zr. Crystal structure and lattice parameters of intermediate phases.

Phase	Structure	Type	a [nm]	b [nm]	c [nm]	Ref.
$Fe_{23}Zr_6$	cub	$Mn_{23}Th_6$	1.169056			65 Kri5, 63 Sve1
Fe_2Zr (at 34.3 at% Zr)	cub	Cu_2Mg	0.70702			63 Sve1
$FeZr_2$	tetr	Al_2Cu	0.6385		0.5596	72 Hav1
$FeZr_3$	orth	BRe_3	0.3324	1.0990	0.8810	83 Bus1, 81 Bus1

Thermodynamics
Colinet et al. [85 Col1] have published enthalpies of formation of intermediate phases. The results are given in Table 2.

Using high-temperature calorimetry Lück et al. [90 Lüc1] have measured the enthalpy of mixing of liquid Fe–Zr alloys in the range up to 25 at% Zr. By modelling, the ΔH^L-concentration curve has been calculated for higher Zr content, too. The results are given in Fig. 2.

Table 2. Fe–Zr. Enthalpies of formation calculated by Colinet et al. [85 Col1].

Phase	ΔH^S [kJ g-atom^{-1}]	Phase	ΔH^S [kJ g-atom^{-1}]
Fe_5Zr	– 16.0	$FeZr_2$	– 20.0
Fe_2Zr	– 23.0	$FeZr_3$	– 12.0
FeZr	– 24.0		

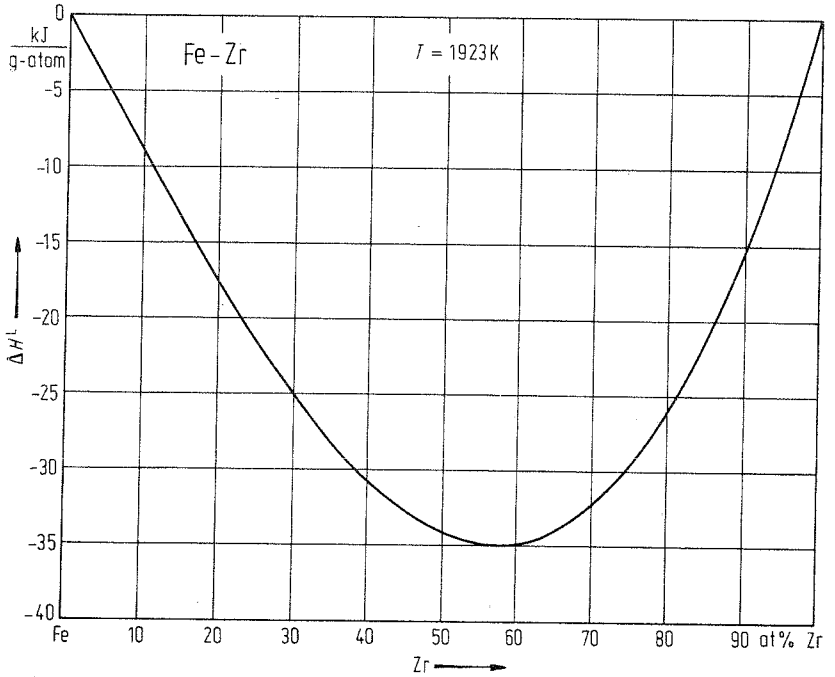

Fig. 2. Fe–Zr. Enthalpy of mixing for liquid alloys at 1923 K.